Closing the Loop: Exploring the Use of Sacral Level Dorsal Root Ganglia Signals for Adaptive Neuromodulation of Bladder Function

by

Zhonghua Ouyang

A dissertation submitted in partial fulfillment
of the requirements for the degree of
Doctor of Philosophy
(Biomedical Engineering)
in the University of Michigan
2020

Doctoral Committee:

Associate Professor Tim M. Bruns, Chair
Associate Professor Cynthia A. Chestek
Associate Professor Parag G. Patil
Associate Professor William C. Stacey

Zhonghua Ouyang

ailеenou@umich.edu

ORCID iD: 0000-0002-6371-4321

Dedication

This dissertation is dedicated to my mom and dad. Thank you for your unconditional love, trust, and support.

Acknowledgements

Getting to this point of my PhD journey is more rewarding than I had expected because of the people I have met and learned from along the way. As I conclude this chapter of my career, I would like to acknowledge everyone who played a very important role in it.

First, I would like to thank Dr. Tim Bruns, my PhD advisor, for both supporting my research and serving as a role model. He is instrumental in developing my research interest in the peripheral nervous system. Through observing and learning from him, I improved my critical thinking, attention to detail, research skills, communication skills, and most importantly, sense of empathy for others. He created a diverse group of students and an inclusive lab culture, which made a non-US student like me feel welcome. With his willingness to share his professional network, I am able to establish a strong connection in the field of neural engineering that greatly helps with my career after PhD. Finally, I want to thank him for helping me improve my English writing, word by word, phrase by phrase, throughout the past 5 and a half years. He has made a significant impact in my life, and for this I will forever be grateful.

My deep gratitude also goes to all the pNEURO lab alumni, who guided me when I first joined the lab. Dr. Shani Ross helped me start my first project and taught me how to conduct in-vivo experiments, from which all my major projects in this dissertation were based on. Abeer Khurram led me into the real-world of CAD and helped me develop my first hardware with experimental application. Dr. Zach Sperry, who is also a dear friend outside of work, showed me

the ropes when I joined the lab and was always there to provide ideas and help with enthusiasm. Seeing him graduate allowed me to witness a great example of how a PhD degree is done. Dr. Ahmad Jiman and Dr. Lauren Zimmerman not only volunteered countless hours to help with my experiments but also showed me that it is possible to have an amazing social life and family life while successfully pursuing a PhD.

I am grateful to be supported by the current members of pNEURO lab as I am crossing this finish line, especially Elizabeth Bottorff and Lauren Madden, who are some of the most fun, sassy, and dedicated PhD students I have ever seen. While they are much younger than me, they keep me humble. Our lab manager, Eric Kennedy, is always someone I can always rely on, and he is an amazing example of work-life harmony, as he always seems unfazed juggling work, family, and hobbies. I am also very lucky to have forged a friendship with Dr. Jessica Xu, DVM, our vet resident and rotating post-doc. Her deep passion for research, animals, and new adventure profoundly influenced me. I am honored to mentor some of the best undergrad and grad students, Nikolas Barrera, Vlad Marcu, Alec Socha, Jake Schwartz, Alexa Rybicki, Josie Stalmack, Richard Liu, Maeve Willen, and more. Finally, I want to thank Dr. Elisabeth Steel, Vanessa Pruitt, and Dr. Po-Ju Chen, for being amazing role models, and everyone else in the Bruns lab, for creating this great experience in my PhD journey.

This dissertation would not have happened without my other dissertation committee members: Dr. Cindy Chestek, Dr. Parag Patil, and Dr. William Stacey. They helped me grow as a researcher in both technical and methodological aspects. While my peers in the TNE community come and go, they are the ones who have witnessed my growth, mentored me, and made sure I succeed from the beginning to the end.

I would like to thank the veterinary staff, technicians, and husbandry staff at ULAM for providing technical support, including Dr. Tara Martin, Dr. Patrick Lester, Dr. Shayne Ballou, and Dr. Lauren Kruger, Taryn Hetrick, Micaleah Newman, who also helped me adopt Dubs, my best animal friend in the world. Outside of Bruns lab, I am grateful to be surrounded by a wonderful translational neural engineering community. I learned so much from everyone, including Dr. Paras Patel, Elissa Welle, Bobby Graham, Hans Zander, Muru Zhou, Charles Lu, and many more. I would especially like to thank Dr. Jim Weiland, for trusting me enough to give me a lecturing opportunity in his BIOMEDE 599 class, and all the other PIs who went to my journal club presentations and provided valuable insights.

I was incredibly fortunate to be a part of some amazing collaborations throughout my PhD journey. I would like to thank Dr. Lance Zirpel, Dr. Katie Bittner, and other people at Medtronic for their effort on our two collaborative projects. I would like to thank my collaborators Dr. Margot Damasor, Dr. Dennis Bourbeau, Dr. Robert Karam at Cleveland FES Center and University of South Florida. Last but not least, I would like to thank Dr. Simon Schultz and Dr. Carl Lubba from Imperial College London, who used my data to conduct an important DRG signal study and demonstrated the importance of data sharing.

The College of Engineering Communication and Marketing team will always have a special place in my heart. They are the ones who picked me out from the crowd and told me that I have a special story to tell. They encouraged me to pursue an amazing vlog journey, and since then I have overcome the fear of showing my true self to others. Through this process, I have discovered so much about myself, and I am also grateful to have this amazing platform to contribute to the community.

Most importantly, I would not have been motivated to achieve any of my successes if I had not had a strong family and friend support. Whether they are in the US or all the way across the ocean, they keep me protected and loved, so I have the strength to help others through my work.

Finally, thank you Camerron, my rock and my best friend, for always being there for me.

Table of Contents

List of Tables

List of Figures

Abstract

Overactive bladder (OAB) is a highly prevalent condition which negatively affects the physical and mental health of millions of people worldwide. Sacral neuromodulation (SNM) is a third-line therapy that provides improved efficacy and less adherence issues as compared to conventional treatments. There have been ~300,000 SNM implants since the therapy was first introduced over 20 years ago. While SNM is delivered in an open-loop fashion, the therapy could have improved clinical efficacy by adopting a closed-loop stimulation paradigm that uses objective physiological feedback. One promising approach to obtain such feedback is by tapping into the nervous system that innervates the bladder. This dissertation focuses on using sacral level dorsal root ganglia (DRG) neural signals to provide sensory feedback for adaptive SNM a feline model.

This work began with exploring machine learning algorithms and feature selection methods for bladder pressure decoding in an offline analysis of DRG signals. A Kalman filter delivered the highest performance based on correlation coefficient between the pressure measurements and algorithm estimation. Additionally, firing rate normalization significantly contributed to lowering the normalized error, and a correlation coefficient-based channel selection method provided the lowest error compared to other channel selection methods.

Following algorithm optimization, this work implemented the optimized algorithm and feature selection method in real-time in anesthetized healthy bladder and simulated OAB feline models. A 0.88 ± 0.16 decoding correlation coefficient fit was achieved by the algorithm across

35 normal and simulated OAB bladder fill sequences in five experiments. Additionally, closed-loop neuromodulation was demonstrated using the estimated pressure to trigger pudendal nerve stimulation, which increased bladder capacity by 40% in two trials.

Finally, closed-loop SNM with the DRG sensory feedback algorithm was performed in anesthetized experiments. Our approach increased bladder capacity by 13.8% over no stimulation ($p < 0.001$). While there was no statistical difference in bladder capacity between closed-loop and continuous stimulation ($p = 0.80$), closed-loop stimulation reduced stimulation time by 57.7%. Interestingly, clearly-identified bladder single units had a reduced sensitivity during stimulation, suggesting a potential mechanism of SNM.

This dissertation also developed a method for chronic behavioral monitoring and neuromodulation of bladder function in a feline model. We tracked urodynamic parameters across multiple week testing intervals. We observed that animals could tolerate pudendal nerve stimulation above motor threshold. Interestingly, stimulation at 5 and 33 Hz appeared to have a modulatory effect on voiding interval and efficiency in line with prior work under anesthesia.

Overall, this work demonstrated that sacral level DRG are a viable sensory feedback target for adaptive SNM. This dissertation also investigated a behavioral paradigm that will be useful for system validation in awake and chronic experiments. Behavioral experiments such as these, as well as development of low-power systems for adaptive monitoring and feedback, are a crucial step prior to clinical translation of this method. Ultimately, implementation of closed-loop adaptive SNM will lead to an improved therapy and greater potential benefit for the millions of individuals with OAB.

Chapter 1 Introduction

1.1 Overactive Bladder (OAB)

1.1.1 Definition and Impact

Overactive bladder (OAB) is a symptom-based bladder dysfunction, and it is officially defined by the International Continence Society as "urinary urgency, usually accompanied by frequency and nocturia" [1]. OAB has a high prevalence of 16.5% among the US population [1]. OAB is estimated to have affected 548 million adults over 20 years old globally in 2018 [2]. Risk factors for OAB include age, gender, body mass index, neurological diseases (stroke, Parkinson's disease, depression etc.), pregnancy, heart diseases, and other non-bladder-related causes [3]. Regardless of risk factors, OAB causes symptoms primarily by affecting sensory pathways, leading to urge sensation at a low bladder volume. An urge sensation can be a result of (1) neurogenic dysregulation: a reduction in the inhibitory neural impulses and increase in excitatory afferent impulses due to neurological conditions or (2) myogenic dysfunction: an increase in detrusor muscle sensitivity to cholinergic stimulation [1].

OAB can have a profound impact on one's physical and mental health. While mild symptoms include a sudden uncontrollable onset of urgency and discomfort, severe cases can cause varied degrees of incontinence, leading to urinary tract infections (UTIs) if not properly managed [3]. This directly limits patients' daily activities including exercising, traveling, and sexual functions. Psychological burden ranges from social embarrassment to anxiety, depression,

and an overall low quality of life [4]. Each year, OAB management directly and indirectly costs ~$13 billion of economic burden in the US alone [3].

1.1.2 Diagnosis and Conventional Treatments

OAB is diagnosed with a combination of a bladder diary, physical exams, and urinalysis [1]. Current treatments aim to control the symptoms if the root cause cannot be identified or addressed in the short-term. Non-neurogenic OAB and some cases of neurogenic OAB are primarily managed with three levels of treatments ranked by invasiveness (the fourth level involves cystoplasty which is uncommon as an OAB treatment). The first-line treatment is behavioral therapy, including bladder and pelvic floor muscle training to address mild cases by strengthening the pelvic muscle tone. The second-line treatment is pharmacological therapy, including anticholinergic and beta-3 agonist drugs to target and relax the bladder smooth muscles [5]. One option in third-line therapy is intravesical Botox® injections, delivered with a cystoscope and an embedded needle through the urethra into the detrusor wall. Botox® is US Food and Drug Administration (FDA) approved for refractory OAB patients when medication fail to work. It relaxes the bladder by blocking excitatory neurotransmitters released from pelvic nerves into the bladder wall [6]. Both medication and Botox® injections are recurrent long-term therapies and are associated with a high percentage of chronic adverse effects (dry mouth, dizziness from drugs [7]; urinary tract infections, urinary retention from Botox® [6]) and high dropout rates due to logistic and tolerability issues [8], [9]. Studies show that roughly two thirds of the patients dropped out of Botox repeated treatments after one or two injections, mostly due to tolerability issues, and the 6-month OAB medication persistence rate is only 28% [8], [10]. In addition, OAB medication is associated with an increased risk of dementia [11].

1.2 Neural Control of LUT and Neuromodulation

Neuromodulation is a third-line therapy that modulates nerve activities by delivering electrical stimulation (or less commonly pharmaceutical agents) to a target location. Like Botox®, neuromodulation is used primarily in refractory OAB that cannot be properly managed by first- or second- line solutions. For both neurogenic and non-neurogenic OAB, neuromodulation works by electrically stimulating peripheral nerves to reduce the urge sensation at low bladder volume through mechanisms that are currently not well understood.

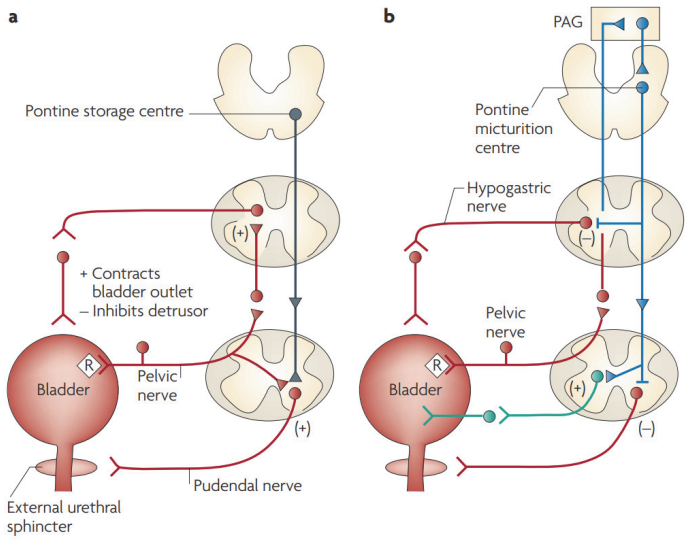

Figure 1. Neural control of the lower urinary tract involves the pudendal, pelvic, and hypogastric nerves. (a) storage phase (b) emptying phase. [12]

Neuromodulation targets depend on the neural control of the lower urinary tract, which involves the brain, the spinal cord, and the peripheral ganglia [12]. While the bladder emptying phase involves voluntary cortical control, the storage phase is entirely maintained by the brain stem (pontine storage center), the spinal cord, and the peripheral ganglia/nerves (Figure 1). OAB mainly affects the bladder storage function, making the spinal cord and peripheral nerves common therapeutic targets. While progressive neurological conditions such as Parkinson's Disease and Alzheimer's Disease [13] cause OAB in part due to the reduced inhibition activity of the pontine micturition center (PMC) in the brain stem, the PMC has not become a common target possibly due to its difficulty of access.

Among peripheral nerves, the pudendal, pelvic, and hypogastric nerves directly innervate the lower urinary tract (Figure 1 [12]). During the storage phase, sympathetic hypogastric nerves maintain a relaxed bladder, and the somatic pudendal nerve maintains urethral sphincter closure, while the pelvic nerve generally stays quiescent. Both the pudendal and the pelvic nerve branch out from sacral nerves, which are a popular stimulation target for managing OAB [14], [15]. Stimulating the dorsal genital nerves, a branch of the pudendal nerve that carries sensory information from the penis and clitoris, has also shown positive patient outcomes [16]–[18], potentially due to activation of sensory pathways in the pudendal nerve that suppress the parasympathetic micturition reflex [18]. Stimulating the tibial nerve or saphenous nerve has also shown to improve bladder function. The mechanisms of these approaches are less well understood, and include possible pathway crosstalk and other interacting mechanisms through the sacral plexus [19], since both nerves either share spinal levels with pudendal and pelvic nerves.

According to the AUA guidelines in 2019 [20], sacral neuromodulation (SNM, e.g. InterStim®, Medtronic,and Axonics®, Axonics Modulation Technologies) and percutaneous tibial nerve stimulation (PTNS, e.g., Urgent® PC) are the two neuromodulation treatments recommended for OAB. Other therapies such as targeting the spinal cord [21] epidural space and various other nerves (e.g. saphenous nerves, dorsal genital nerves) [18], [22], implantable tibial nerve stimulation (e,g., eCoin, BlueWind RENOVA iStim™) [23], and intravaginal electrical stimulation [24], are still in investigative stages [17].

Both PTNS and SNM provide improved clinical efficacy and lower complication rates compared to Botox® [25]; however, both therapies are currently delivered in an open-loop fashion or on an intermittent schedule with very limited control given to the patient and no real-

time adaptation of stim parameter to the state of the patients. Below the pros and cons of current PTNS and SNM treatments are discussed.

1.2.1 Percutaneous Tibial Nerve Stimulation (PTNS)

Approved by the FDA in 2000 [26], PTNS is an in-office procedure for OAB that requires 12 weekly treatment sessions of 30 minutes and follow-up maintenance treatment sessions once per month or as needed. During each treatment, a needle electrode is placed near the posterior tibial nerve by the ankle while a surface return electrode is place on the foot on the same side distal to the needle electrode. A collection of clinical trials showed the therapeutic success, indicated by a $\geqslant$50% decrease in urge or urge urinary incontinence and a 25% reduction in frequency, was between 33% and 71% [27]. The adverse effects of PTNS are minimal, including bruising (0.9%), discomfort (1.8%), and slight bleeding [27]. While Peters et al. showed that 28% patients dropped out after 1 year [28], 42% withdrew after 3 years [29], the level of adherence is considerably improved compared to OAB medication and Botox® injection therapy. Patients who pursued maintenance treatment more often reported improvements in nocturia. Interestingly, transportation, distance, and time commitment did not play a significant role in the decision to pursue maintenance therapy [30]. Several companies and groups are working on implantable tibial nerve stimulators (e.g., eCoin, BlueWind RENOVA iStim™) to reduce the need for clinic visits [23], [31]. PTNS is suitable for patients who prefer not receiving medical implants and who can keep up with regular clinical visits; however, SNM provides improved clinical efficacy and more convenience to responding patients [25].

1.2.2 Sacral Neuromodulation

Sacral neuromodulation therapy applies constant electrical stimulation to the S3 (or the less commonly S4) nerve root of the patient unilaterally. There have been ~300,000 SNM implants since the therapy was first introduced over 20 years ago (Medtronic sales data on file. Current as of May 2020). The stimulation is driven by an implantable pulse generator (IPG), which can either be powered by a primary cell or an external rechargeable coil (Figure 2). The device implantation is performed through a minimally invasive surgery, during which a tined quadripolar lead is inserted through the S3 foramen and placed near the S3 spinal nerve, with the guidance of intra-operative fluoroscopy. A pocket is created under the lower back skin on the same or opposite side of the lead implant to hold the IPG. Bipolar constant voltage or current stimulation is delivered through two of the four stimulation electrodes at 14Hz frequency, 210μs pulse width, and a comfortable amplitude.

The overall therapeutic success rate of SNM ranges from 61% to 90% [32], which is comparable to PTNS success rate. The largest and longest clinical trial (InSite) to date shows that 80% out of 340 patients who participated the study responded to trial stimulation and were implanted with the InterStim system [14]. The therapeutic success rate for OAB was 82% and 67% at 12-month and 5-year follow-up (from a clinical study published as [14]). Adverse effects include an undesirable change in stimulation (22%) and implant site pain (15%). Similarly, the most

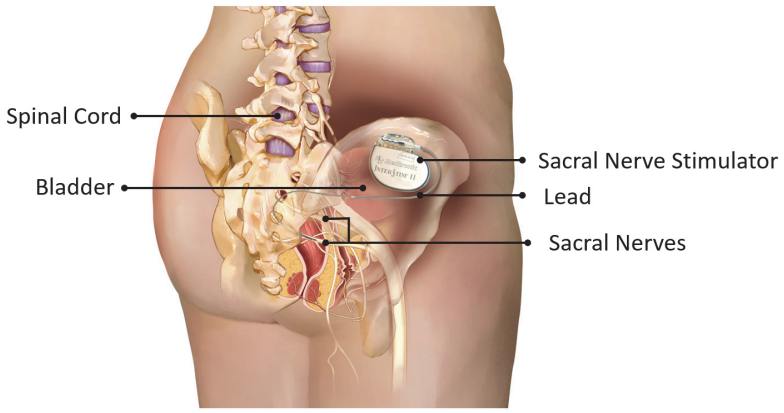

Figure 2. Sacral neuromodulation implantation diagram. Modified from [139]

recent clinical study using the rechargeable Axonics system showed a 71% responding rate to SNM, with 98% of the participants still responding after a year [15]. While SNM serves as an alternative therapy after medication fails, it has the potential to replace medication, as one study shows that 82% of patients discontinued OAB medication after SNM treatment for over 22 months [33]. Compared with Botox® and PTNS, SNM resulted in the highest reduction in voiding frequency and incontinence episodes [25]. While SNM therapy is more costly [34] compared to Botox® , it shows a lower rate of complications [35], and because SNM therapy is delivered through an implantable device, there are minimal compliance issues. A study showed that SNM improved symptoms in patients who did not respond to transcutaneous PTNS [36]. SNM is also shown to be effective in treating OAB across different ages [37].

1.3 Motivation for Closed-loop Neuromodulation

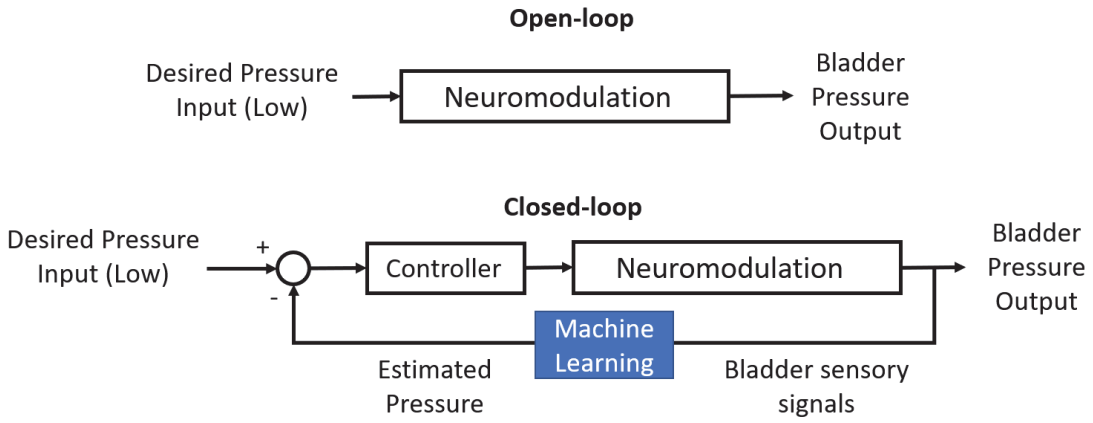

Figure 3. Open-loop (top) and closed-loop (bottom) neuromodulation for overactive bladder. Open-loop stimulation is fixed regardless of the bladder state, while closed-loop stimulation changes based on the bladder state estimate, which, in this dissertation work, can be estimated from neurosensory signals. The controller determines the stimulation parameters based

While SNM is a standard treatment for refractory OAB symptoms compared to conventional treatments, the clinical efficacy is shown to attenuate over time [38], [39]. Blok et al. showed that SNM efficacy delivered by a rechargeable device stabilized three months into the

treatment and could last up to at least one year [15] in the number of leaks, large leaks, voids, and urgency. However, the InSite study and Peters et al., with a longer study period, both reported relapse of symptoms in the course of 5- and 2- year treatment [38], [39]. Besides lead migration, nerve desensitization is the leading theory as to why SNM loses therapeutic efficacy over time, which has been shown in other somatosensory nerves and reflexes in response to electrical stimulation [40]–[42]. Electrical stimulation should be minimized as much as possible to preserve the health and sensitivity of the nerve target. It is possible that SNM can be reduced or even eliminated when it is not needed, such as during the initial bladder filling phase when the spinal reflex for storage is not active, to help deliver better and longer clinical outcomes. Therefore, a bladder sensory feedback-based, or closed-loop, stimulation paradigm might offer greater clinical benefit.

Prior animal and human work have suggested the superiority of closed-loop stimulation in both improving effectiveness and reducing stimulation time over open-loop stimulation. More specifically, stimulating peripheral nerves during non-voiding contractions or the latter parts of a bladder fill cycle have been shown to increase bladder capacity significantly higher than or at the same level as compared to continuous stimulation [43], [44]. Potts et al. found that in rats, SNM only in the second half of the bladder fill cycle increased bladder capacity significantly, while stimulating the first half did not [43]. Wenzel et al. found that pudendal nerve stimulation at the beginning of bladder contractions increased bladder capacity twice as much as continuous stimulation [44]. Among several on-demand dorsal genital nerve clinical studies [16]–[18], one suggested that stimulation only after the urge to void, for as short as 30 seconds in duration, can lead to mean subjective improvements of 73% in the incontinence score [17]. While these studies

have shown promising preliminary results, the use of direct pressure measurement or patient self-sensing as feedback is not ideal for clinical long-term use.

The source of sensory feedback is critial for closed-loop neuromodulation. Bladder state signals can be recorded from the bladder and nerves that innervate the bladder. Current development efforts in implantable bladder sensors focus on wireless implementation using varied measuring mechanisms [45], none of which, however, has received FDA clearance yet. One major concern with such device is the risk for lower urinary tract infections [46]. Bladder state-related signals can also be recorded from electromyogram (EMG) signals from the external urethral sphincter (EUS), providing indirect indication of bladder activity. Horvath et al. showed that conditional dorsal genital nerve (DGN) stimulation with EUS EMG signals reduced the total stimulation time to 21% while maintaining the same bladder capacity compared to continuous stimulation in spinal cord injury patients who presented with neurogenic detrusor overactivity [47]. Similarly, Opisso et al. also showed that EUS EMG signals can be used to successfully identify bladder contractions in neurogenic detrusor overactivity patients [48]. Both studies where performed in a controlled environment, in which the patients were immobile. Translating this method to a chronic bladder application might be challenging due to suseptability to motion artifacts, despite the fact that EMG has been extensively used in closed-loop motor control applications [49]. But more importantly, EMG is a motor signal that only reflects the timings of contractions and not urgency. Finally, afferent LUT signals can be recorded from sacral, pudendal, and pelvic nerves that directly innervate the LUT (Figure 1). The pelvic nerve is challenging to identify and access in humans due to its highly convoluted network struture. In comparison, the pudendal nerve is much easier to access and has already been used as a stimulation target for managing chronic pelvic pain [50]. Whole sacral or pudendal nerve

electroneurogram (ENG) recordings are not ideal because both nerves not only encompass both sensory and motor components but also include sensory input from other pelvic floor organs [51].

A promising and translatable recording target are dorsal root ganglia (DRG). Antomically, DRG are nerve structures in the peripheral nervous system that contain sensory cell bodies whose axons originate from peripheral organs or limbs. DRG lay next to the lateral side of the spinal cord, existing as a part of the dorsal roots that merge with ventral roots at each spinal level into spinal nerves (Figure 4). At the sacral level, DRG contain sensory cell bodies whose axons extend through pudendal and pelvic nerves to innervate the lower urinary tract and other pelvic organs. Compared to peripheral nerves, DRG are a similar-diameter, if not larger, nerve structure that do not contain any motor neurons. Stimulating the DRG has also been shown to modulate bladder pressure with electrical current at low current amplitudes [52]. By using multi-channel microelectrode arrays in DRG, selectivity can be improved from using whole nerve ENG recording. Prior animal studies have successfully reconstructed bladder pressure from S1 and S2 cat DRG single unit activities and limb state from lumbar level cat DRG signals for closed-loop limb control with low error [53], [54]. However, with multi-channel data collected from DRG, an advanced algorithm is needed to accurately extract and process bladder state information for real-time closed-loop control.

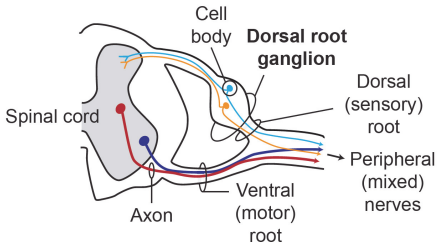

Figure 4. Connection between sacral level DRG, spinal cord, and the peripheral nerves, like at other DRG.

1.4 Signal Processing and Machine Learning for Bladder State decoding

High frequency multi-channel neural signals collected from nerve structures such as the DRG do not reflect pressure directly and need to be transformed to feedback signals for closed-loop bladder control using machine learning algorithms. Machine learning has many popular applications in neural engineering such as estimating motor intent, organ states, and inflamatory responses [55]–[57] from neural signals when direct measurment from the decoding target is inconvenient or unavailable. In machine learning applications, a classification (e.g. Naïve Bayes) or a regression (e.g. Linear, polynomial, logistic regression) model is established to estimate the target state through feature selection, training, validation, and testing steps. Possible features as algorithm input include firing rates from single unit activity (SUA), multi-unit activity (MUA), threshold crossings (TC), or frequency power spectrum from continuous recordings [58], [59]. Firing rates or frequency power of continuous recordings can be smoothed, normalized, or dimensionally reduced to obtain more refined input features.

For closed-loop bladder control, bladder sensory neuronal single unit activities can be recorded from the sacral level DRG, and based on their relationship with pressure they can be generally classified into three catergories: slow tonic, phasic, and derivative [60] activities, each containing a unique set of features or information that reflects the state of the bladder. Anatomically, bladder afferent signals of various types are densely packed in DRG with no known functional organization; therefore, to reach sufficint signal specificity, random sampling with multiple recording channels is required not only to collect sufficient bladder afferent activities, but also to separate other sensory input that may interfere with decoding. As the first step of feature extration in machine learning, channel selection is crucial in determining how much of the recorded signals effectively contribute to the bladder state estimation. Secondly, the

time window for firing rate calculation should be chosen based on the what best reflects the bladder pressure. A window too small might not be able to pick up any activity even when the pressure is high, while a window too large could smooth over important pressure changes. Other steps such as firing rate normalization and firing rate smoothing can potentially improve the robustness of the algorihtm and improve an estimate [61].

Generally speaking, mechanosensitive bladder neurons within the pelvic nerve are quiescent when the bladder is empty and gradually increase in firing as the bladder fills and pressure rises [62]. The relationship between bladder pressure and the firing rate of these neurons is nonlinear as there is hysteresis [63]. A static linear regression model that does not take into account this dynamic relationship between bladder pressure and neural activity can be susceptible to artifacts, and has yielded poor results previously [53]. A basic Kalman filter, though still a linear based model, can better handle noisy input signals by incorporating noise filtering and a dynamic transfer function [64]. A more complex model that takes into account the non-linear relationship between bladder pressure and firing rate may yield a better fit than linear methods. One approach is to use a non-linear auto-regressive moving average (NARMA) model identified through a recursive artificial neural network structure. Accurate closed-loop sensing depends on both appropriate algorithm choice and feature selection method to best characterize pressure feedback, which this dissertation work has sought to address.

1.5 Dissertation Organization

The overarching goal of this dissertation is to explore the feasibility of using DRG sensory feedback to improve current neuromodulation treatment for overactive bladder symptoms. This work is based on a pre-clinical cat model, with the potential to be translated to humans due to the high similarity in neural control of the bladder between cats and humans [65].

This dissertation begins with a careful examination of neural signal features from cat sacral level DRG with some of the machine learning algorithms that are common in brain computer interface applications. The optimized features and algorithms were then tested in real-time to validate the possibility for closed-loop application, followed by closed-loop pudendal nerve and sacral nerve stimulation with DRG feedback.

Chapter II explores feature selection methods (firing rate window, smoothing methods, firing rate normalization, etc.) and three machine learning algorithms (linear regression, Kalman filter, and a recurrent neural network) for bladder pressure decoding from anesthetized cat DRG signals. (My contribution is this work does not include setting up the neural network model.) More specifically, a broad spectrum of feature selection parameters was examined, including varied firing rate calculation interval, signal smoothing methods, channel selection criteria, and firing rate normalization. This study concluded that while the tested recurrent neural network was effective in minimizing decoding errors, a Kalman filter yielded the highest correlation coefficient, which more effectively reflects trends in bladder pressure changes.

In Chapter III, the optimized Kalman filter algorithm from Chapter II was implemented in real-time in anesthetized experiments, yielding satisfactory decoding performance for both normal healthy and simulated OAB conditions. Simulated OAB condition resulted in detrusor overactivity and reduced bladder capacity as two of the main OAB symptoms. The simulated OAB condition was also associated with an improved decoding performance, indicating a potential increase in afferent neuron sensitivity. More significantly, closed-loop stimulation with real-time decoding was demonstrated in pilot experimental trials and showed an increased bladder capacity compared to no stimulation.

In Chapter IV, the bladder state decoding algorithm as described in Chapter II and III was implemented as part of closed-loop SNM. In-vivo testing was performed in anesthetized cats. The study showed that closed-loop stimulation led to a significant increase in normalized bladder capacity compared to the control group (no stimulation), with an over half reduction in stimulation time as compared to continuous stimulation. Continuous stimulation led to a similar increase in bladder capacity while applying significantly more stimulation than closed-loop trials. This study demonstrated the potential for closed-loop stimulation to deliver at least the same level of therapy as compared to standard continuous SNM while applying stimulation for less than half of the time.

Chapter V serves as a steppingstone from anesthetized to awake and behaving experiments. In a total of four experiments, a protocol was established to record urodynamic parameters (e.g. bladder pressure, capacities, void volumes) and animal movements when the animals behaved freely in a contained area. In experiments 3 and 4, pudendal stimulation (5 or 33 Hz; 1.5 or 2 x motor threshold) was applied to explore how stimulation affected urodynamic parameters. 33 and 5 Hz were found to be effective in increasing voiding efficiency and bladder capacity, respectively. Animals were found to tolerate up to 2 x motor threshold amplitude when stimulation was ramped up gradually. In addition, the logistical challenges of implementing chronic implants and performing awake sessions were identified and addressed, including bladder irritation from suprapubic catheter implantation and low tolerance for some test conditions.

Across the chapters, this work demonstrates from a signal processing perspective that sacral DRG are a promising target for closed-loop neuromodulation of bladder function and suggests a possible direction to improve the current SNM therapy for OAB. It set a strong

foundation for future research that implements more advanced awake, behaving, and pathological models prior to clinical translation. Moving forward, the successful implementation of closed-loop SNM in these models relies on longitudinal use of more advanced and robust signal processing and machine learning techniques in addition to electrodes that will be optimized for interfacing with the DRG in a less invasive manner.

Chapter 2 Evaluation of Decoding Algorithms for Estimating Bladder Pressure from Dorsal Root Ganglia Neural Recordings

2.1 Abstract

A closed-loop device for bladder control may offer greater clinical benefit compared to current open-loop stimulation devices. Previous studies have demonstrated the feasibility of using single-unit recordings from sacral-level dorsal root ganglia (DRG) for decoding bladder pressure. Automatic online sorting, to differentiate single units, can be computationally heavy and unreliable, in contrast to simple multi-unit thresholded activity. In this study, the feasibility of using DRG multi-unit recordings to decode bladder pressure was examined. A broad range of feature selection methods and three algorithms (multivariate linear regression, basic Kalman filter, and a nonlinear autoregressive moving average model) were used to create training models and provide validation fits to bladder pressure for data collected in seven anesthetized feline experiments. A non-linear autoregressive moving average (NARMA) model with regularization provided the most accurate bladder pressure estimate, based on normalized root-mean-squared error, NRMSE, (17 ± 7%). A basic Kalman filter yielded the highest similarity to the bladder pressure with an average correlation coefficient, CC, of 0.81 ± 0.13. The best algorithm set (based on NRMSE) was further evaluated on data obtained from a chronic feline experiment. Testing results yielded a NRMSE and CC of 10.7% and 0.61, respectively from a model that was trained on data recorded 2 weeks prior. From offline analysis, implementation of NARMA in a closed-loop scheme for detecting bladder contractions would provide a robust control signal.

Ultimate integration of closed-loop algorithms in bladder neuroprostheses will require evaluations of parameter and signal stability over time.

2.2 Introduction

Loss of bladder control is a highly prevalent condition that can have severe impact on quality of life [66]. Typical nerve stimulation approaches to restore function do not utilize direct feedback on the bladder state. Conditional stimulation may provide an advantage over continuous stimulation by minimizing habituation of neural pathways [41], [42] and requiring less battery power. A system that can continuously monitor bladder state and deliver stimulation only as needed may be a tremendous benefit to patients.

A major challenge for developing a robust closed-loop system for bladder control is in determining an effective way to continuously monitor bladder state. Sensors directly implanted in the bladder muscle have been used to measure bladder pressure or bladder muscle activity, but there can be issues with device migration, tissue damage, and obtaining large reliable signals [67], [68]. A few studies have demonstrated feasibility of closed-loop control by detecting key pressure events, but their methods currently rely on directly measuring bladder pressure using external sensors and catheters [69], [70], which can cause urinary tract infections. Tapping into the body's natural sensors (mechanoreceptors in the bladder wall) via nerves that encode this information may provide increased accuracy and reliability over artificial sensors [45]. Researchers have used neural activity to estimate bladder pressure, bladder volume, or onset of bladder contractions [44], [51], [53], [71]–[73]. These approaches target the pelvic nerve [73], pudendal nerve [44], or spinal nerve [51], [71], where access can be challenging or may require a separate location to stimulate for bladder control. Our approach interfaces with the sacral dorsal root ganglia (DRG) which contain the cell bodies for afferent pelvic and pudendal fibers that

innervate the lower urinary tract entering the spinal cord. Here we can monitor information about the bladder state via pelvic nerve activity [74], [75] and also control bladder function by stimulating pudendal nerve inputs through reflex spinal pathways [52], [75].

Mechanosensitive bladder neurons within the pelvic nerve are quiescent when the bladder is empty and gradually increase in firing as the bladder fills and pressure rises [62]. The relationship between bladder pressure and the firing rate of these neurons is nonlinear as there is hysteresis [63]. A static linear regression model does not take into account this dynamic relationship between bladder pressure and neural activity, can be susceptible to artifacts, and has yielded poor results previously [53]. A basic Kalman filter, though still a linear-based model, can better handle noisy input signals by incorporating noise filtering and a dynamic transfer function [64]. A more complex model that considers the non-linear relationship between bladder pressure and firing rate may yield a better fit than linear methods. One approach is to use a non-linear auto-regressive moving average (NARMA) model identified through a recursive artificial neural network structure.

In addition to the specific algorithm itself, other input feature selection factors can influence the performance of a decoding model. One important factor is how the input neural signal channels are selected, whether by using all recorded signals or only those channels with specific correlations to bladder activity. Another factor is the approach used to sum the occurrence of neural activity. For microelectrode recordings that yield action potentials, the timing of these events are incorporated into a firing rate estimation, which smooths the time interval occurrence. The sampling period and smoothing duration can affect the firing rate calculation.

The goal of this study was to evaluate three different algorithms and their parameters to determine the tradeoffs between accuracy of fit and processing load for estimating bladder pressure from DRG signals in anesthetized cats. The models evaluated were simple linear regression, a Kalman filter, and NARMA. We hypothesized that the NARMA model would yield the best bladder pressure estimation and the Kalman filter would provide the second best fit. Our findings inform progress in development of an interface for closed-loop bladder control and provide insights for parameter selection in decoding applications for other physiological signals.

2.3 Materials and Methods

2.3.1 Animals

All procedures were approved by the University of Michigan Institutional Animal Care and Use Committee, in accordance with the National Institute of Health's guidelines for the care and use of laboratory animals. Eight spinal-intact adult male, domestic, short-hair cats (age: 0.9–1.4 years old, 4.2–6.3 kg, Liberty Research, Inc., Waverly, NY) were used in this study. Seven of the cats were acute, non-survival experiments and one cat was a chronic experiment. Cats were used due to their high relevance to human physiology and their long history of study in bladder neurophysiology [65]. Prior to use, animals were free-range housed with 0–3 other cats in a 38.4 m2 room with controlled temperature (19–21 C), relative humidity (35–60%), food and water available ad lib, and a 12 h light/dark cycle. Animals received enrichment via daily staff interaction and toys.

2.3.2 Surgical Procedure

As previously described [63],animals were anesthetized with a mixture of ketamine (6.6 mg/kg)–butorphanol (0.66 mg/kg)-dexmedetomidine (0.033 mg/ kg) administered intramuscularly (IM), intubated, and then maintained on isoflurane anesthesia (0.5–4%) during surgical procedures. Respiratory rate, heart rate, end-tidal CO_2, O_2 perfusion, temperature, and intra-arterial blood pressure were monitored continuously using a Surgivet vitals monitor (Smiths Medical, Dublin, OH). Fluids (1:1 ratio of lactated Ringers solution and 5% dextrose) were infused intravenously via the cephalic vein at a rate of 5–10 mL kg^{-1} h^{-1} (increased up to 30 mL kg^{-1} h^{-1} during surgery as needed). One or two catheters were inserted into the bladder at the bladder dome via a laparotomy and/or via the urethra for intravesical fluid infusion and pressure monitoring. If the urethra catheter was used during data collection, its size (3.5 Fr) did not prevent urine leakage at a full bladder.

A midline dorsal incision was made to expose the L7 to S3 vertebrae and a laminectomy was performed to access the S1 and S2 sacral DRG [63], [74]. Penetrating iridium oxide microelectrode arrays (Figure 5a) with shank length of 0.5 or 1.0 mm and inter-shank spacing of 0.4 mm (Blackrock Microsystems, Salt Lake City, UT) were implanted into DRG (Figure 5b) using a pneumatic inserter (Blackrock Microsystems). Arrays of various configurations (3 x 8 up to 5 x 10) were inserted unilaterally or bilaterally, as detailed in Table 1. Array reference wires were placed near the spinal cord and ground wires were attached to a stainless-steel needle inserted in the skin (lateral and caudal to the laminectomy incision site). At the conclusion of surgical procedures, prior to experimental testing, animals were transitioned to intravenous alpha-chloralose (C0128, Sigma Aldrich; 70 mg/kg induction; 20 mg/kg maintenance). Analgesia was augmented with 0.01 mg/ kg buprenorphine every 8–12 h intravenously.

2.3.3 Experimental Setup and Data Collection

DRG neural data was sampled at 30 kHz and lowpass filtered (7.5 kHz cutoff frequency) using a Grapevine neural interface processer and Trellis recording system (Ripple, Salt Lake City, UT). Bladder pressure was monitored with a pressure transducer (DPT-100, Utah Medical Products, Midvale, UT) and transducer amplifier (TBM4M, World Precision Instruments, Sarasota, FL). The bladder pressure signal was sampled by the Grapevine system at 1 kHz and all data was stored on a desktop computer. During testing saline was infused into the bladder with a syringe pump (NE-1000, New Era Pump Systems, Inc., Farmingdale, NY or AS50 Infusion Pump, Baxter International, Deerfield, IL). Figure 5c shows the experimental set-up.

Bladder pressure and neural recordings were collected during two bladder infusions at 2 mL/min. The bladder was verified as empty by withdrawing from a catheter prior to each infusion. Fluid infusion was stopped when leakage occurred. After the first infusion, the bladder was emptied and a rest period of at least 30 min occurred before a second bladder infusion. In analyses described below, the first infusion was used to train a given algorithm and the second infusion was used to validate that algorithm. We considered a microelectrode pair on the same side (LS1, LS2 or RS1, RS2) to constitute a set. In total, 12 data pairs of training and validation sets were collected from 12 unique S1, S2 DRG location pairs from 7 non-survival cat experiments. If an experiment had bilateral implant sets then each side was separately analyzed as a distinct data set with unique neural signals. In Experiments 2 and 4, the microelectrode array pairs were removed and physically re-inserted in the same DRGs before two new bladder infusions were performed. We considered this an opportunity to collect a new, unique data set from the new electrode implant locations with a different set of neural recordings (Table 1).

After completion of all testing, animals were euthanized with a 2–3 mL intravenous or intracardiac dose of sodium pentobarbital (390 mg/mL) while under deep isoflurane anesthesia.

2.3.4 Algorithm Development and Analysis

Figure 6 shows the overall algorithm flowchart with the different feature selection methods used. Individual components are described in further detail below. All data processing, model development, and analyses (unless otherwise specified) were performed using MATLAB (Mathworks, Natick, MA). Acute experiment trials were used to train and validate algorithms and system parameters, while the chronic experiment trials were used to train and test the algorithm and model parameters.

2.3.5 Multi-Unit Thresholding

A consistent threshold for identifying neural activity was used across experiments. For each neural channel, the signal was filtered using a 250 Hz high-pass digital filter. Automatic dual thresholds were set at ± 4.5 x the standard deviation of the estimated noise [76]. Noise was considered any signal within ± 2.7 x the full signal standard deviation. The thresholding was recalculated periodically to accommodate change of noise level over time. This filtering and thresholding was done offline. In this study, we did not isolate single unit activity, but instead used the unsorted threshold crossings (i.e., multiunit activity) as inputs to our bladder state decode models. As has been demonstrated in brain-computer interface applications [58] and DRG recordings for closed-loop control of electrical stimulation to control limb state [54], sorting threshold crossings into individual units can provide a marginal improvement in accuracy, for low channel counts, but requires additional computational load.

2.3.6 Neural Signal Firing Rate

The bladder pressure and thresholded multi-unit activity from each bladder fill sequence were then further processed offline and used to evaluate the performance of different models. Bladder pressure was low-pass filtered at 4 Hz and down-sampled to align with the time intervals used to calculate the firing rate (see below). Three approaches were used to calculate the firing rate for each microelectrode channel, at intervals of 0.1, 0.5, 1, and 2 s, using causal methods. In SmoothBin the number of spikes were counted in interval bin widths and the counts were smoothed over prior time points [54]. In TriangleC the instantaneous firing rates were convolved with a triangle kernel of width twice the firing rate interval [77]. In Boxcar all spikes within an interval were counted and divided by the bin width to obtain the firing rate. We also considered the use of a firing rate normalization (Eq. 1), to decrease the variance in contributions across channels and to potentially increase the robustness of each algorithm [78]. When applied, normalization takes the current firing rate (f) and divides by the sum of the firing rate range in the first 30 s of the trial (r) and a scalar term (v) of 20 spikes/s.

$$z = \frac{f}{r + v} \quad (1)$$

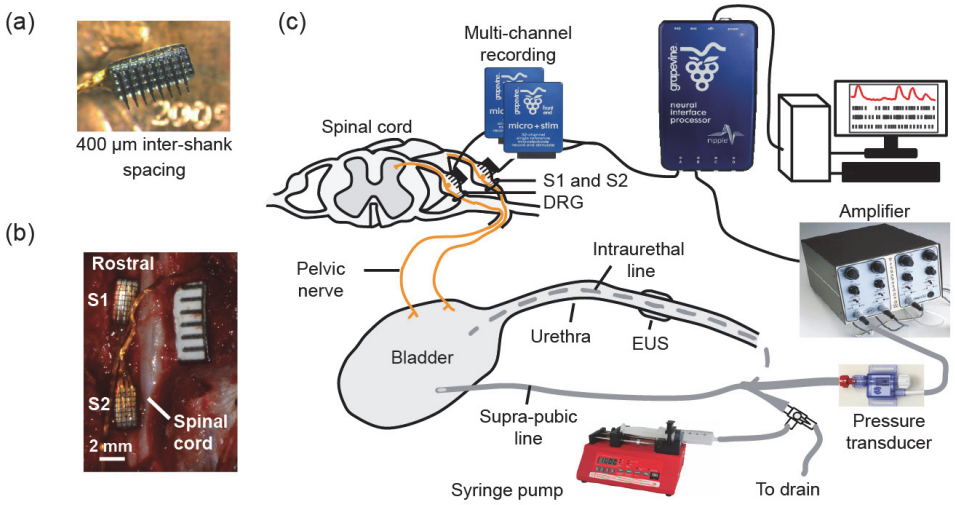

Figure 5. Experimental setup. (a) Blackrock iridium-oxide microelectrode arrays with parylene-C insulation. Shank lengths were either 0.5 mm or 1.0 mm with 0.4 mm inter-shank spacing. (b) Arrays implanted in left S1 and S2 sacral DRG in Experiment 8 (chronic). (c) Illustration of the testing setup (modified from [52]*). Neural recordings were acquired with a Ripple Grapevine system and Trellis software via arrays implanted in S1 and S2 DRG. Trials consisted of recording neural data and bladder pressure (monitored with a pressure transducer and amplifier) during saline infusions at a controlled rate either via a supra-pubic or an intraurethral bladder catheter. Pressure data was also recorded with the Grapevine system after amplification.*

Table 1. Microelectrode array configurations for each experiment and data set.

		Electrode layout		
Experiment	Data Set	1st DRG	2nd DRG	Shank Length
1	a1	LS1: 5x10	LS2: 4x10	1.0 mm
2	a2	LS1: 5x10	LS2: 4x10	1.0 mm
2	a3	RS1: 5x10	RS2: 4x10	0.5 mm
2	a4	RS1: 5x10	RS2: 4x10	0.5 mm
3	a5	LS1: 5x10	LS2: 4x10	1.0 mm
3	a6	RS1: 5x10	RS2: 4x10	0.5 mm
4	a7	LS1: 5x10	LS2: 4x10	0.5 mm
4	a8	LS1: 5x10	LS2: 4x10	0.5 mm
5	a9	LS1: 5x10	LS2: 3x8	0.5 mm
5	a10	RS1: 4x10	RS2: 3x8	0.5 mm
6	a11	RS1: 5x10	RS2: 4x10	0.5 mm
7	a12	RS1: 4x8	RS2: 4x8	1.0 mm
8 (chronic)	c1	LS1: 4x8	LS2: 4x8	1.0 mm

2.3.7 Input Channel Selection

DRG channels used in an algorithm were selected based on three general approaches. First, channels were selected based on the correlation coefficient between their firing rate and the bladder pressure in the training trial. Channel sets were identified for correlations exceeding each of 0.2, 0.3, 0.4, 0.5, 0.6, and 0.7. The second approach involved using the least absolute

shrinkage and selection operator (or LASSO) method [72], which is a linear regression method that minimizes the mean-squared error (MSE) similar to the least-squares method but with an upper bound on the sum of the absolute coefficients (Eq. 2). MSE is minimized for a selected regularization term, λ. This results in some coefficients set to zero and shrinks others towards zero, effectively choosing a model that uses a subset of the input observations. f_k is the training firing rate of length N_2 (number of channels) at time bin k, and p_k is the training bladder pressure. β_0, β; and β_{k2} are the coefficients. A two-fold cross validation was performed to determine k and coefficients that minimized MSE. These values were selected to be used in validation (acute) and testing (chronic) sessions. Thus only a subset of DRG channels were used in LASSO selection. The third channel selection method used is all channels.

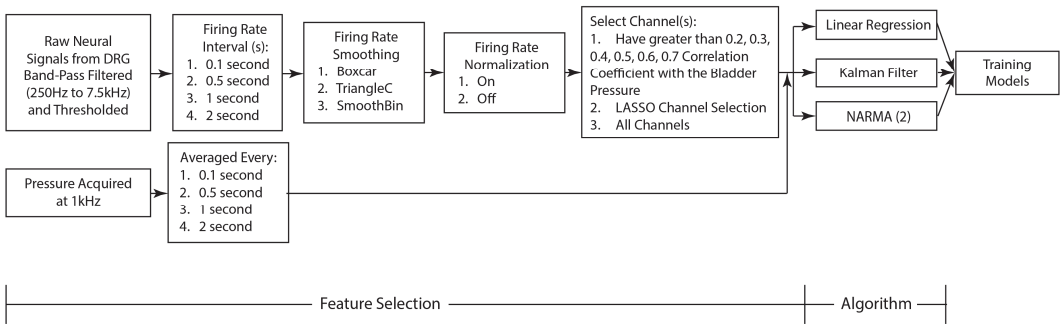

Figure 6. Flowchart of bladder pressure decoding algorithms and feature selection methods used.

$$MSE = \frac{1}{2N}\sum_{k=1}^{N}(p_k - \beta_0 - \beta f_k)^2 + \lambda \sum_{k2=1}^{N2} |\beta_{k2}| \qquad (2)$$

2.3.8 Linear Regression Algorithm

First, a simple static linear regression (LinReg) was used to determine whether a linear relationship was adequate for modeling the relationship between DRG neural signals and the

bladder pressure. During training, a linear filter $\hat{B}$ was obtained (Eq. 3) using the bladder pressure P_{train} and firing rates Ftrain of the selected channels in the training trial. During validation (acute) or testing (chronic), $\hat{B}$ was applied to the new firing rates $F_{val,test}$ of the same channels to estimate the bladder pressure $\hat{P}$ (Eq. 4).

$$\hat{B} = P_{train}F_{train}^{T}(P_{train}^{T}F_{train})^{-1} \quad (3)$$

$$\hat{P} = \hat{B}F_{val,test} \quad (4)$$

2.3.9 Kalman Filter Algorithm

In order to reduce the effect of noise from the neural inputs, a basic Kalman filter (Kalman) was evaluated. The Kalman filter is a recursive algorithm that combines a physical trajectory model and a neural signal-based observational model using a weighted average method to nominally achieve a better estimation. Below we provide the details regarding development of this model. To create a Kalman filter model, the data from the training infusion trial was used to calculate the linear filter and noise term (A and W) for the trajectory model and observational model (C and Q). Linear filter A was obtained by regressing the previous bladder state matrix P_{k-1} against the current bladder state matrix P_k (Eq. 5). Each state matrix includes bladder pressure, bladder pressure rate (dP/dk) and a constant term 1 for a series of time points (k = 0, 1, 2,…, N, N = last time interval bin number). This matrix was initialized at [0, 0, 1] at the beginning of each trial. The corresponding noise term (W) was then calculated (Eq. 6).

$$A = P_{train|k}\,P_{train|k-1}^{T}/(P_{train|k-1}P_{train|k-1}^{T}) \quad (5)$$

$$W = \frac{(P_{train|k} - AP_{train|k-1})(P_{train|k} - AP_{train|k-1})^T}{N\ time\ pts - 1} \quad (6)$$

Next, the linear filter C for the observational model was determined by regressing the pressure state matrix against the firing rate (Eq. 7). The corresponding noise term for the observational model was also calculated (Eq. 8).

$$C = F_{train}\, P_{train}^T / (P_{train} P_{train}^T) \quad (7)$$

$$Q = \frac{(F_{train} - CP_{train})(F_{train} - CP_{train})^T}{N\ time\ pts} \quad (8)$$

During testing, after firing rates were calculated, a trajectory model estimation $\hat{p}_{k|k-1}$ was made (Eq. 9). The error covariance matrix $E_{k|k-1}$ (Eq. 10) was calculated to determine how accurate this estimation was. This matrix was used to calculate the Kalman gain K_k (Eq. 11), which was used to obtain a new weighted average estimation $\hat{p}_k$ that incorporates the firing rate input (Eq. 12). Then a new error covariance matrix E_k was calculated for the new estimation (Eq. 13) for the next time interval period.

$$\hat{p}_{k|k-1} = A\hat{p}_{k-1} \quad (9)$$

$$E_{k|k-1} = AE_{k-1}A^T + W \quad (10)$$

$$K_k = E_{k|k-1}\, C^T / (CE_{k|k-1}C^T + Q) \quad (11)$$

$$\hat{p}_k = \hat{p}_{k|k-1} + K_k(f_{val,test|k} - C\hat{p}_{k|k-1}) \quad (12)$$

$$E_k = (I - K_k C)E_{k|k-1} \quad (13)$$

2.3.10 NARMA Algorithm

A more complex NARMA artificial neural network model that took into consideration the nonlinear dynamics between bladder pressure and DRG neural activity was also evaluated. Inputs to the model were firing rates from selected channels and the previous estimated bladder pressure. Two artificial neurons in a hidden layer applied a nonlinear gain (hyperbolic tangent sigmoid function) and a bias to each of the inputs, with outputs summed together to yield a single intermediate output. This intermediate output was then processed through a linear function to give an estimate output (Figure 7). A general form of the model is given in Eq. 14.

$$\hat{p}_k = \alpha_1 \hat{p}_{k-1} + \beta_0 f_k + \beta_1 f_{k-1} \qquad (14)$$

In Eq. 14, $\hat{p}_k$ is the output estimated pressure, f is the input firing rate, and k and k-1 indicate values at the current and prior time points. The model coefficients (α_1, β_0, β_1) were identified through training in the NARMA network. The neural network toolbox in MATLAB was used to create, identify, and validate the models. Each model utilized a Bayesian regularization method to improve generalization and minimize overfitting. Training was stopped when one of two following criteria were met: the algorithm's performance reached a performance goal of NRMSE < 20% of the recorded bladder pressure or the errors on the validation subset increased consecutively for several epochs.

2.3.11 Performance Measures

The normalized root-mean square error (NRMSE, Eq. 15) and Pearson correlation coefficient (CC, Eq. 16) were calculated to determine how well each model fit the training, validation

(acute) and testing (chronic) data sets. We considered an NRMSE under 20% and a CC above 0.8 as our target performance metrics.

$$NRMSE = \frac{1}{p_{max} - p_{min}} \sqrt{\frac{\sum_{k=1}^{N} (\hat{p}_k - p_k)^2}{N}} \quad (15)$$

$$CC = \frac{E[P, \hat{P}] - E[P]E[\hat{P}]}{\sqrt{E[P^2] - [E[P]]^2} \sqrt{E[\hat{P}^2] - [E[\hat{P}]]^2}} \quad (16)$$

For (15), $\hat{p}_k$ and p_k are the estimated and measured bladder pressure, $(p_{max} - p_{min})$, is the difference between maximum and minimum measured pressure for a trial, and N is the total number of time bins. For (16), $\hat{P}$ and P are the estimated and measured pressure stored in vectors, and E is the expected value. Both performance measures are used here as prior decoding studies for bladder and non-bladder applications have relied on either CC [53], [58], [71] or RMSE [54], [73] to evaluate their results.

2.3.12 Statistical Analysis

In total, three algorithms with 192 possible feature selection method combinations for each algorithm were evaluated in this study (4 firing rate intervals, 3 firing rate smoothing methods, 8 channel selection methods, and on or off of the firing rate normalization). This resulted in 576 total possible combinations. First, we used a mean-value approach to identify the best parameter combinations that yielded the lowest NRMSE and highest CC for each of the three algorithms. Through this approach, parameter sets were identified that had the best mean performance metric across the twelve acute testing data sets, for each of the six total combinations of three algorithms and two performance measures. In a separate analysis, we plotted data residuals on a

normal probability plot, which indicated that the data distribution is not normal. Thus, a rank-based non-parametric Kruskal– Wallis test was used to identify parameters that contribute significantly to the estimation accuracy. Any significant parameter was then tested with a post hoc multiple comparison Kruskal Dunn Test, with a Bonferroni correction on the p-values. All statistical analyses were performed in R with the Pairwise Multiple Comparison of Mean Ranks (PMCMR) package. A significance level of 0.05 was used. In the PMCMR package, the Bonferroni correction is performed by multiplying p-values by the appropriate number of comparisons being performed in a given test. These adjusted p-values are reported in the Results below, allowing for a direct comparison to the significance level.

In this manuscript, we present the impact of single variables on each algorithm-performance metric combination. Higher level interactions among variable combinations were also examined, with the outcomes reported in our data repository on the Open Science Framework (https://doi.org/10.17605/OSF.IO/ZFYCH.).

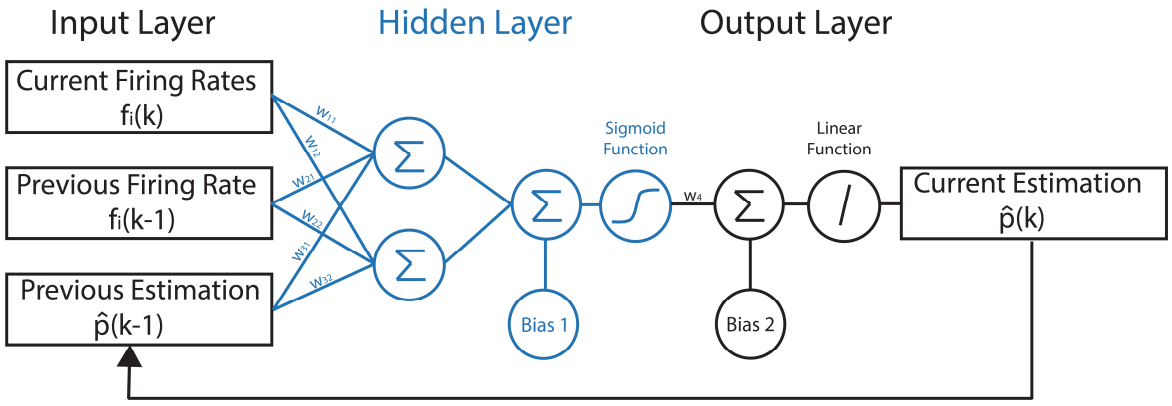

Figure 7. Structure of the NARMA model. The firing rates, f(k), at the current time point, k, and the previous time point, k-1, from DRG channels are inputs into the model. The previous estimated bladder pressure, $\hat{p}$(k-1), is also an input to the model. The model outputs the current estimated pressure, $\hat{p}_{k|k-1}$.

2.3.13 Chronic Experiment

The primary analyses of this study were performed using data collected in acute, non-survival experiments as detailed above. The optimal algorithm and parameters were selected through training and validation sets from these experiments (NARMA for best NRMSE). To assess the potential utility of this approach, we implemented the best algorithm from acute experiments on data collected from one animal with long term, chronic DRG implants (two 4 x 8 Blackrock arrays in left S1 and S2 DRG). Surgical implantation and data collection were as described previously [75]. Neural recordings and bladder pressure from a bladder fill under dexmedetomidine sedation (0.03 mg/kg IM) were used to create a pressure estimate algorithm that was tested on data collected under similar circumstances 14 days later. Performance measures were calculated as described above.

2.4 Results

2.4.1 Bladder Neural Signals

Twelve data sets (a1–a12) were collected from seven acute experiments (Table 1). Raw and analyzed data and MATLAB scripts used in data analysis can be found online (https://doi.org/10.17605/OSF.IO/ZFYCH.). There were 4–12 bladder-correlated channels with a correlation coefficient greater than 0.2 in each data set. There was some variability in the number of bladder-correlated channels depending on the firing rate calculation parameters used (Table 2). Most channels identified in the training trials (correlation coefficient > 0.2) were still correlated with bladder pressure in the validation trial (53–68%, depending on feature selection method). However, in some cases there were changes in the number and location of some identified channels (Figure 8).

Table 2. The selected number of bladder channels depends on the firing rate interval and smoothing method. Values represent mean (± standard deviation) number of channels per data set (within a1-a12) with CC > 0.20

Firing Rate Smoothing	Firing Rate Interval (s)			
	0.1	0.5	1	2
Boxcar	4 ± 3	7 ± 5	7 ± 5	8 ± 5
TriangleC	5 ± 3	7 ± 5	8 ± 5	9 ± 6
SmoothBin	6 ± 4	7 ± 5	6 ± 5	12 ± 10

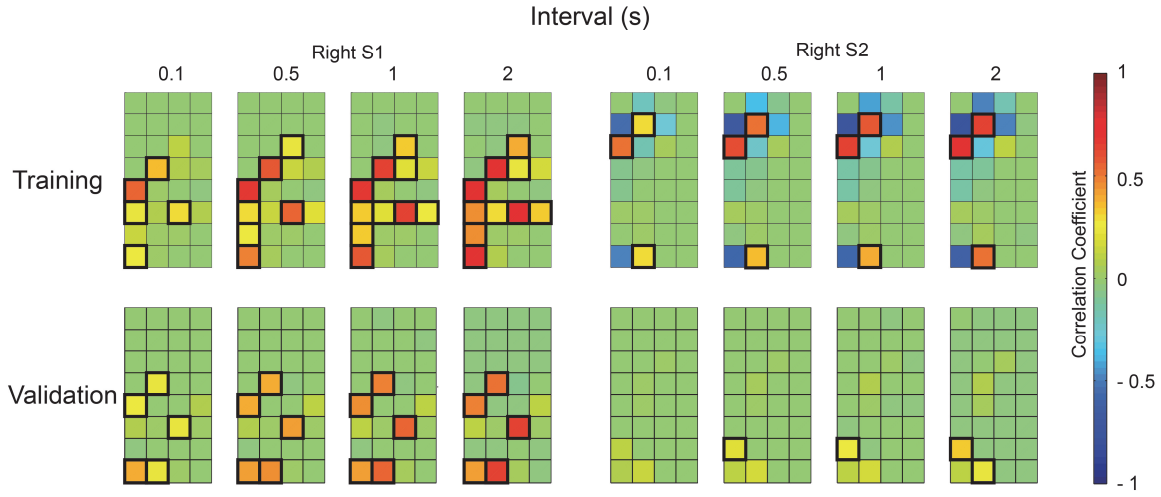

Figure 8. Correlation coefficient maps between the measured bladder pressure and firing rate of thresholded DRG neural activity for each electrode channel in S1 and S2 in data set a12 for training (top) and validation (bottom). The firing rates were calculated with Boxcar smoothing at the specified intervals. In this example, the firing rate interval and the time between trials (training to validation) can affect the number of channels with correlation coefficients of interest. Channels with correlation coefficients above 0.2 are indicated by a black square.

2.4.2 Channel Selection

Our results showed that as the correlation coefficient threshold for channel selection increased, the fit increased (Figure 9). However, the number of trials that have at least one channel with a correlation coefficient greater than or equal to the CC threshold decreases (Table 3). This suggests that a constant threshold for all trials may be impractical, since not all trials have highly correlated channels. Although simply choosing the lowest correlation coefficient threshold would consistently provide the most usable number of channels, a higher correlation coefficient

threshold yielded better pressure estimates (Figure 9). Thus, we utilized a variable channel-selection threshold across data sets, selecting the highest threshold (among 0.2–0.7) that yielded a non-zero number of bladder channels.

The LASSO channel selection method always yielded channels for model use (27 ± 13, mean ± standard deviation) and on average selected at least 3 times more channels than the correlation coefficient channel selection method. This is most likely due to the differences in approach. With LASSO, different combinations of coefficients are evaluated with the set of coefficients that gives the lowest MSE selected. This in turn determines what channels to include in the decoding algorithms. Using the LASSO approach, the selected channels had a wide range of correlation coefficients compared to the approach of selecting channels that are above a certain correlation coefficient threshold.

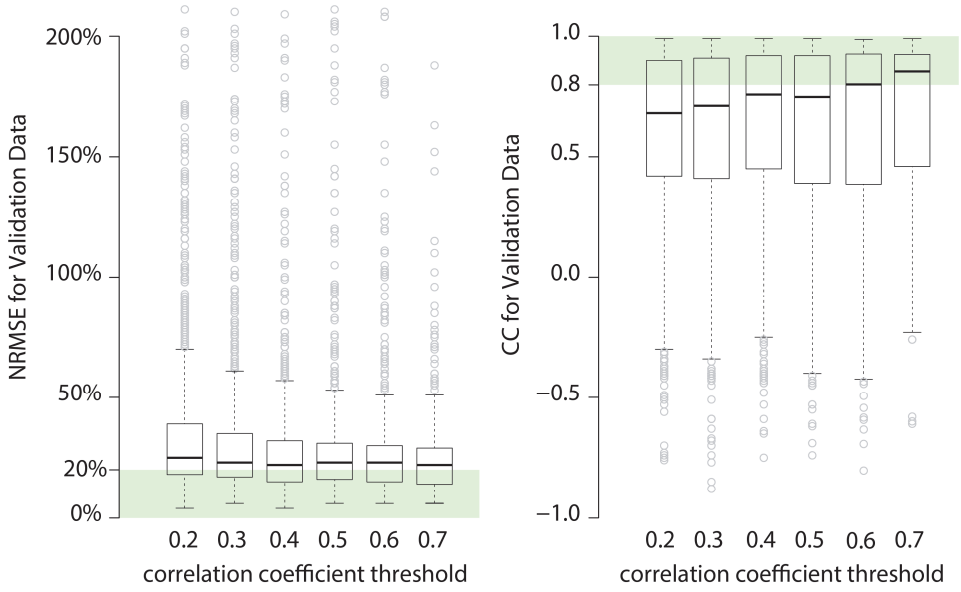

Figure 9. Boxplots of CC and NRMSE testing data sets performance measures for different channel selection thresholds used for model training. Shaded regions in each figure represent our target performance levels.

Table 3. As the correlation coefficient threshold for channel selection increases, the number of data sets that have at least one channel that meets this criteria decreases ("# Sets").

Channel CC Threshold	Firing Rate Interval (s)							
	0.1		0.5		1		2	
	# Chs.	# Sets	# Chs.	# Sets	# Chs.	# Sets	# Chs.	# Sets
0.2	4 ± 3	12	7 ± 5	12	7 ± 5	12	8 ± 5	12
0.3	2 ± 2	10	5 ± 4	12	6 ± 4	12	7 ± 6	12
0.4	2 ± 2	9	3 ± 3	10	4 ± 3	12	5 ± 4	12
0.5	1 ± 1	6	3 ± 2	10	3 ± 3	10	4 ± 4	11
0.6	0 ± 1	3	2 ± 2	10	3 ± 2	10	3 ± 3	10
0.7	0 ± 0	1	1 ± 1	4	1 ± 2	7	2 ± 2	10

For each CC threshold and firing rate interval, the mean (± standard deviation) number of channels that meet the criteria across all twelve sets is also given ("# Chs."). Boxcar smoothing method used.

2.4.3 Algorithm Optimization

A mean-value based approach was used to select the best parameter combinations for each of the three algorithms (Table 4). Across the 12 acute data sets with the best parameter combinations, NARMA provided the lowest mean NRMSE and a Kalman Filter provided the highest mean CC with smallest CC standard deviation (Table 4; Figure 10). For these parameter combinations, the computational time to make the next bladder pressure estimation during validation are also given in Table 4. Training of each algorithm took no longer than a few seconds (LinReg) to a few minutes (NARMA). Bladder pressure estimations for one dataset using the three algorithms with their NRMSE-best model parameters (selected from Table 4) are shown in Figure 11.

Table 4. Optimal feature combinations for each algorithm that provide the best NRMSE (top) or CC (bottom).

Algorithm	Interval (s)	FR Method	FR Norm	NRMSE	CC	Channel Selection
NARMA	0.5	Boxcar	1	17 ± 7%	0.69 ± 0.35	Highcc
LinReg	0.5	Boxcar	1	22 ± 6%	0.51 ± 0.30	Highcc
Kalman	2	Boxcar	1	25 ± 15%	0.67 ± 0.40	Highcc

Algorithm	Interval (s)	FR Method	FR Norm	NRMSE	CC	Channel Selection
NARMA	1	SmoothBin	0	21 ± 8%	0.72 ± 0.33	Highcc
LinReg	2	SmoothBin	1	32 ± 34%	0.70 ± 0.29	Highcc
Kalman	0.1	rTriangleC	0	27 ± 15%	0.81 ± 0.13	Lasso

Results are given as mean ± standard deviation.

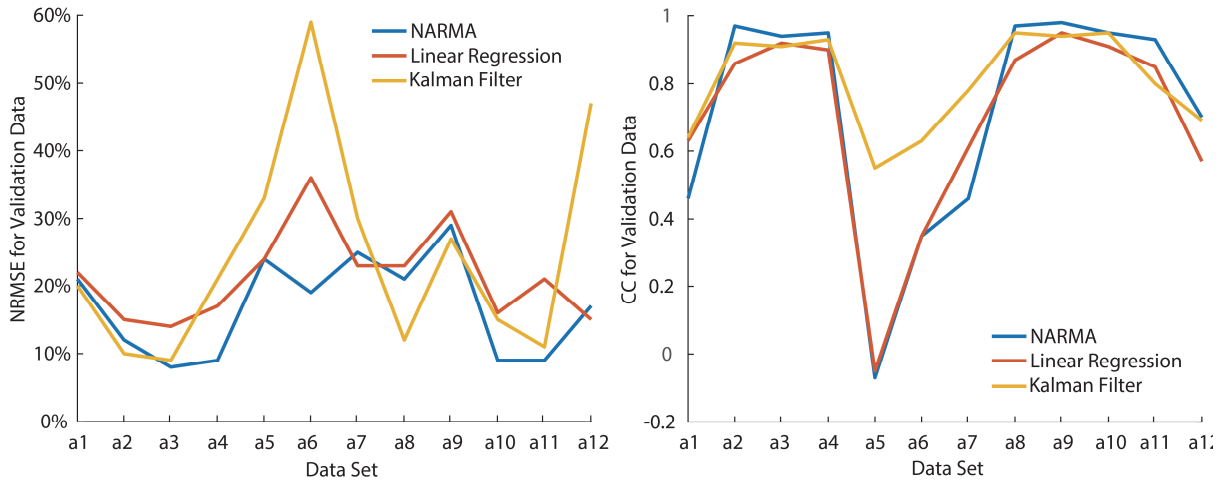

Figure 10. Comparison of performance measures across data sets. Plots show the resulting NRMSE for the NRMSE-selected features of Table 4-upper (left panel) and the resulting CC for the CC selected features of Table 4-lower (right panel) for each acute data set.

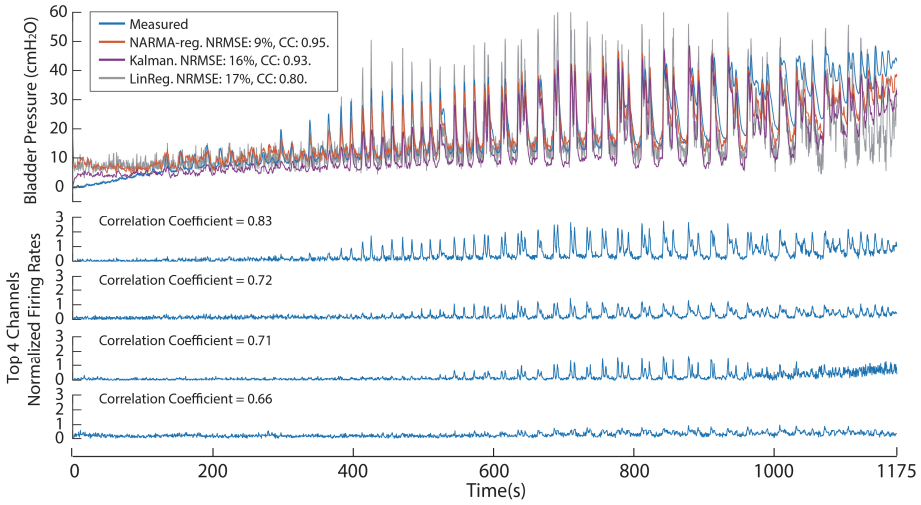

Figure 11. Use of best model parameters (for NRMSE, in Table 4-upper) for decoding bladder pressure in dataset a4. The top plot shows the measured bladder pressure and the estimated bladder pressure using each algorithim. The NRMSE and CC for each fit is also given.

Within NARMA algorithm results, we found that using a correlation coefficient-based channel selection method provided a significant decrease in NRMSE compared to using LASSO ($p<0.0001$) or simply including all channels ($p<0.0001$). It also yielded a significantly higher CC compared to using LASSO ($p<0.0001$) and all channels ($p<0.0001$). The firing rate interval was not significant in reducing NRMSE and was marginally significant in increasing CC ($p = 0.033$), with a 1-s interval slightly superior than a 0.1-s interval ($p = 0.049$).

Within Kalman filter results, we found that the firing rate interval had a significant role in reducing NRMSE ($p = 0.005$), with a 0.1-s interval better than 2-s ($p = 0.01$) and 1-s ($p = 0.02$) intervals, though the interval was not a significant factor for CC. A correlation coefficient-based channel selection method yielded a significantly lower NRMSE compared to using LASSO ($p<0.0001$) or all channels ($p<0.0001$). It also provided a significantly greater CC compared to using all channels ($p<0.0001$).

Finally, within linear regression results, we have found that firing rate interval did not play a significant role in affecting NRMSE, but was significant in improving CC ($p = 0.0001$), with a 2-s interval ($p<0.0001$) and a 1-s interval ($p = 0.019$) better than a 0.1-s interval. Similar to NARMA, a correlation coefficient based channel selection method provided a decreased NRMSE compared to using LASSO ($p<0.0001$) or all channels ($p<0.0001$). It also provided an increased CC compared to using all channels (p value<0.0001). Overall, we also found that firing rate smoothing methods alone did not provide any statistical significance in reducing NRMSE or improving CC in any of the three algorithms. The firing rate normalization provided a significant decrease in NRMSE for all three algorithms (NARMA $p = 0.0004$, Kalman $p = 0.013$, and Linear $p = 0.045$), but there was no statistical improvement in CC.

2.4.4 Chronic Data Set

In the chronic experiment, bladder pressure and DRG neural signals were recorded at 34 and 48 days after microelectrode implantation. Use of the best algorithm parameter set for NRMSE (NARMA, Table 4) yielded overall excellent fits on the training and subsequent testing data sets, with NRMSE and CC for testing being 10.7% and 0.61, respectively (Figure 12). All channels

that were highly correlated with bladder pressure on the training date were still identified at the testing date.

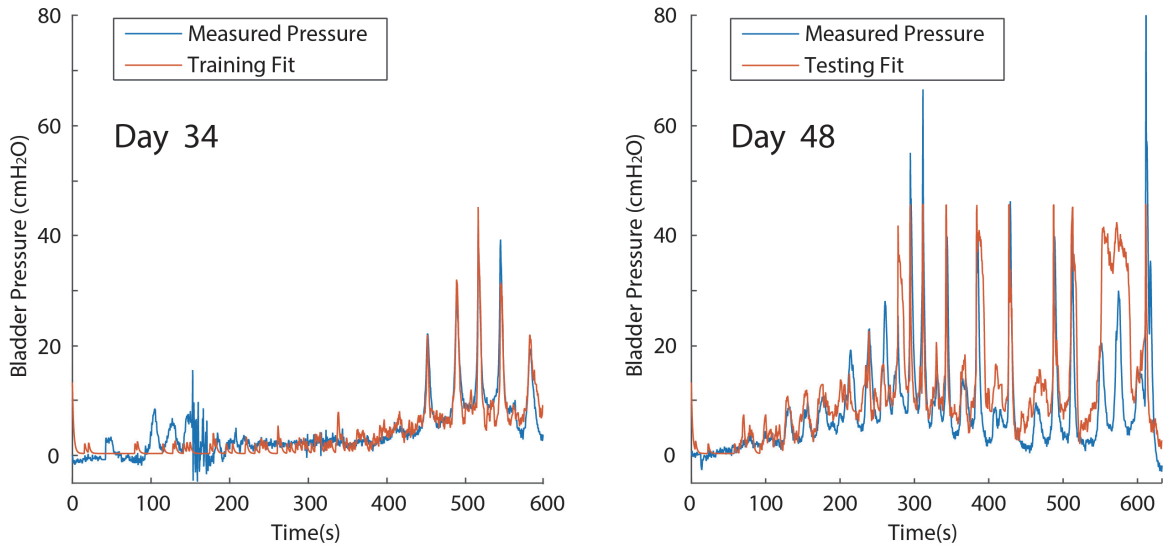

Figure 12. Evaluation of best acute-experiment algorithm (NARMA for best NRMSE in Table 4-upper) on data obtained in a chronic experiment. The NRMSE and CC for the training data set (day 34 after implant) were 6.2% and 0.89, respectively. The NRMSE and CC for the training data set (day 34 after implant) were 6.2% and 0.89, respectively. The NRMSE and CC for the testing data set (day 48) were 10.7% and 0.61, respectively. In the training data set (at 170 s) a catheter was bumped which caused a high frequency artifact. This artifact was not removed during the training model fit and did not affect the testing performance significantly.

2.5 Discussion

In this study, we demonstrated the feasibility of using thresholded multi-unit DRG activity to decode bladder pressure (Figures 11 and 12). We evaluated a broad range of feature selection methods and three algorithms (multivariate linear regression, basic Kalman filter, and nonlinear autoregressive moving average model or NARMA) to evaluate which combinations yielded the best fits for two performance measures—NRMSE and CC (Table 4). Across our twelve acute data sets, NARMA provided the best fit in NRMSE, and channel selection methods had a significant impact on the resulting estimate of bladder pressure (Figures 8 and 9; Tables 2 and 3).

Towards our ultimate goal of closed-loop neuroprostheses, NRMSE is the more critical of our two performance measures as it minimizes overall error better than CC. Considering this, our findings supported our hypothesis that a NARMA model provides the most accurate estimation of the bladder pressure, with a low NRMSE (Table 4; Figures 10 and 11). The NARMA model captured important nonlinear dynamics between bladder neuron activity, seen here as thresholded DRG signals, and bladder pressure [62], [63]. For our secondary performance criteria of CC, a Kalman filter yielded the highest similarity to the results (Table 4). A closed-loop system that does not directly apply absolute pressure value might take advantage of the Kalman filter algorithm (e.g., frequency of non-voiding contractions, relative amplitude of non-voiding contractions, etc.). The multivariate linear regression algorithm was not outstanding in terms of either performance measure.

NARMA models resulted in the best NRMSE fit and a first-order NARMA network with one hidden layer and two artificial neurons was sufficient in capturing dynamics of interest. Further analyses can be done to determine if increasing the order of the model, the number of layers, and/or the number of artificial neurons can improve bladder decoding performance. For example, a prior study utilized two hidden layers in a neural network with 15 neurons per layer to estimate bladder pressure from pudendal nerve electroneurogram (ENG), obtaining greater accuracy than with a linear model [79]. However, increasing the complexity of the model can increase overfitting and computational time and may not yield a great improvement compared to current models.

While isolated single units provide more specificity for underlying signals, using threshold-crossing events is more reliable and computationally feasible for online use. In our firing rate calculation for each microelectrode channel, we did not differentiate between any

observed large-amplitude single units and small-amplitude threshold crossings. These small-amplitude snippets may be recognized as noise in sorting of single-units, but might still provide useful information. This conclusion is also consistent with previous cortical interfacing studies [58], [80], in which there was a consistent conclusion that threshold-crossing events provided a comparable decoding accuracy as single unit activity.

Only including DRG channels that correlated highly with bladder pressure improved decoding performance. However, as Table 3 shows, there is a tradeoff as the number of channels included in the model decreases. It may not be advantageous to use a constant correlation coefficient threshold for input channel selection. Instead, our data suggests that it is more beneficial to go with the highest correlation threshold that yields a non-zero number of input channels. This approach of using a subset of neural recording channels is comparable to other decoding studies which range from using a single input, such as pudendal nerve ENG [79], to using signals from multiple electrode channels in DRG [53], the spinal cord [81], or the motor cortex [82], and selecting channels based on a combination of the correlation coefficient and subjective judgement.

Statistically, a correlation coefficient-based channel selection method provided the lowest NRMSE in all three algorithms. This result is partially due to this method's ability to maximize the bladder signal-to-noise ratio compared to using all channels or the LASSO method, by selecting only a few channels that contain a high concentration of relevant sensory information. The LASSO and all channel methods usually selected more channels than the correlation coefficient-based method, thus incorporating more variability in the input channels and decreasing the estimation accuracy. This statistical result is consistent with Table 4.

The firing rate smoothing methods alone did not provide any statistical significance in reducing NRMSE or improving CC in any of the three algorithms, which is consistent with a prior study [61]. This effect is in part because both NARMA and Kalman filter algorithms have a recursive mechanism, which has a similar working mechanism as the firing rate smoothing method. Additionally, the thresholded multi-unit activities and relatively large time intervals (> 100 ms) together provide a smoother firing rate compared to what would be obtained for firing rates calculated from single unit activity with smaller time intervals. This statistical outcome is consistent with the varying methods identified across algorithms in Table 4.

Firing rate normalization contributed significantly to reducing the NRMSE in all three algorithms largely due to its ability to reduce the contribution variance among selected channels. As a result, the channels with high firing rates have a more balanced impact on the magnitude of the estimation result compared to channels with low firing rates. However, CC was not expected to be significantly affected because the firing rate only went through a linear transformation. This is consistent with our statistical results, as well as Table 4.

The firing rate interval determines how smooth the firing rate trace is, and how many data points can be used to train from a trial. Larger intervals yield smoother firing rates and potentially improve estimations, especially CC, by providing more channels with correlated firing rates (Tables 2 and 3; Figure 8). This explains why larger intervals improved CC in Linear Regression. In NARMA and Kalman filter, their recursive mechanisms smoothed out the firing rates, which provides an explanation why larger intervals in this case did not improve estimation further. On the other hand, smaller intervals provide a larger number of data points that can be used for training, which resulted in a reduced NRMSE with the Kalman filter. This tradeoff can be reflected as the inconsistent optimal firing rate interval across different algorithms and

performance measures. A drawback of small firing rate intervals is that smaller intervals result in weaker correlations between the firing rate and the bladder pressure (Tables 2 and 3; Figure 8). In one data set, there were no channels with a correlation greater than 0.2 when using the lowest firing rate interval (Table 3).

Compared to prior studies that used sorted single unit activity to estimate limb states [54], [77] or bladder pressure [58], our method has a lower computational load due to the simple thresholding method. The accuracy is comparable to prior relevant bladder studies [53], [79] due to NARMA's ability to capture the underlying structure of the data sets. Compared to limb state decoding applications, where an artificial neural network might be computationally heavy, bladder decoding is a more suitable application for neural networks because the need for frequent updates is low (every ~ 0.5 s). The step time for new pressure estimates for all models are well below any of the firing rate intervals used here and easily applicable for online decoding (Table 4).

To our knowledge, this work also provides the first proof of concept for decoding bladder pressure from neural recordings using an algorithm based on data collected at an earlier date in a chronic implant (Figure 12). The feature selection method and algorithm used on the chronic data was based on the best acute study analysis, as discussed above. Although this data set only had 2 weeks between training and testing trials, our prior chronic DRG studies indicated that bladder sensory neurons can be tracked at least 6 weeks after implant using current technology [75]. Finally, this preliminary work shows it is possible to translate results from acute studies to chronic studies of bladder pressure.

Our results were obtained from spinally intact felines. Since our goal is to develop a closed-loop neuroprosthesis for bladder control in patients suffering from SCI and other

neurogenic bladder dysfunctions, our decoding algorithms need to be assessed in these models. After spinal cord injury, voluntary bladder control is lost and the bladder initially becomes areflexic, later becoming hyperreflexive with re-emergence and remodeling of spinal reflex pathways [83], [84].These changes are thought to be partly due to changes in bladder afferent activity. Unmyelinated chemosensitive C-fibers become mechanosensitive and overactive leading to non-micturition contractions at low bladder volumes [85], [86]. After SCI, there will still be activity from myelinated pelvic afferent fibers that correlate with bladder pressure, but we anticipate increased bladder afferent activity occurring at lower bladder volumes due to C-fibers. We expect that bladder-decoding models will still be effective after chronic SCI, however a model may have low efficacy shortly after injury before neuroplasticity has stabilized. Additional studies are needed to evaluate the consistency of our decoding algorithms at different times after SCI.

Further studies should be performed to test the performance of these algorithms online in real-time and in closed-loop bladder control experiments. In addition, for each of the trials presented here, we trained on only one infusion trial and tested on a later individual trial. Multiple training sets may provide a more robust performance than single-set training, particularly for chronic studies where neural signals may shift over time [75].

Chapter 3 Real-time Bladder Pressure Estimation for Closed-loop Control in a Detrusor Overactivity Model

3.1 Abstract

Overactive bladder (OAB) patients suffer from a frequent urge to urinate, which can lead to a poor quality of life. Current neurostimulation therapy uses open-loop electrical stimulation to alleviate symptoms. Continuous stimulation facilitates habituation of neural pathways and consumes battery power. Sensory feedback-based closed-loop stimulation may offer greater clinical benefit by driving bladder relaxation only when bladder contractions are detected, leading to increased bladder capacity. Effective delivery of such sensory feedback, particularly in real-time, is necessary to accomplish this goal. We implemented a Kalman filter-based model to estimate bladder pressure in real-time using unsorted neural recordings from sacral-level dorsal root ganglia, achieving a 0.88 ± 0.16 correlation coefficient fit across thirty-six normal and simulated OAB bladder fills in five experiments. We also demonstrated closed-loop neuromodulation using the estimated pressure to trigger pudendal nerve stimulation, which increased bladder capacity by 40% in two trials. An offline analysis indicated that unsorted neural signals had a similar stability over time as compared to sorted single units, which would require a higher computational load. We believe this study demonstrates the utility of decoding bladder pressure from neural activity for closed-loop control; however, real-time validation during behavioral studies is necessary prior to clinical translation.

3.2 Introduction

Overactive bladder (OAB) is defined as urinary urgency, with or without incontinence, typically accompanied by frequency and nocturia [87]. The cause of overactive bladder can be neurogenic (e.g. spinal cord injury, traumatic brain injury, multiple sclerosis, stroke), non-neurogenic (e.g. aging, multiple pregnancies) or nonspecific. OAB affects millions of people worldwide, leading to a variety of side effects such as poor sleep, anxiety, and depression [88].

Sacral neuromodulation (SNM), in which a stimulation lead is placed near the S3 sacral root, is a standard clinical treatment after conservative approaches fail [14]. SNM is applied constantly to reduce the effects of OAB. However, continuous stimulation can facilitate habituation of neural pathways [41] and consume battery power [44]. Sensory feedback-based, or closed-loop stimulation may offer greater clinical benefit by driving bladder function only when necessary, leading to increased bladder capacity and voiding efficiency [44], [47].

Several studies have demonstrated the possibility of detecting bladder pressure changes, or bladder volume increases by recording at different nerve sites with offline analyses of recorded data [53], [79], [89]–[91]. These offline validation studies applied various parameters combinations to a detecting or decoding algorithm and selected parameters that generated the lowest error. However, final parameters were not tested in new sets of data in real-time to rule out overfitting. A few studies have applied optimized parameters to nerve recordings [44], [73] to detect bladder volume or contractions in real-time, though pressure was not explored in this manner. For OAB, we hypothesize that pressure feedback will be more valuable because it may directly reflect the level of urgency [12]. In this study, we specifically examine real-time estimation of bladder pressure towards closed-loop neuromodulation.

Bladder-related neural signals can be observed at potential neuromodulation sites such as the pudendal nerve [44], pelvic nerve [92] and sacral dorsal root ganglia (DRG) [74], [91], making closed-loop control possible without an additional surgical procedure to implant a bladder pressure sensor. Among these recording sites, sacral-level DRG uniquely contain afferent-only signals from the detrusor muscle and urethra, via proximal pelvic and pudendal nerve fibers, while also containing pudendal sensory pathways that can drive spinal circuits modulating bladder function [52], [93]. Our long-term goal is to take advantage of this sensory nerve convergence at sacral DRG and develop a single-site neural interface for both monitoring and controlling the bladder state.

In this study, we used sacral-level DRG as a recording site to estimate bladder pressure and the onset of bladder contractions in real-time for both normal and simulated OAB conditions, through the infusion of acetic acid irritant. Although acetic acid-induced bladder overactivity does not fully imitate the urgency component of clinical OAB, it is commonly used in preclinical studies to simulate an increase in spontaneous contractions and a decrease in bladder capacity [94]. In two experiments, we used the estimated pressure to initiate pudendal nerve stimulation upon detection of bladder contractions, as a demonstration of closed-loop relaxation of the bladder. This is the first study to test a bladder pressure decoding algorithm from neural signals in real-time, as well as apply it to a demonstration of closed-loop bladder control.

3.3 Methods

3.3.1 Animals

All procedures were approved by the University of Michigan Institutional Animal Care and Use

Committee, in accordance with the National Institute of Health's guidelines for the care and use of laboratory animals. Five spinal-intact adult, domestic, short-hair cats (0.97 ± 0.20 years old, 4.48 ± 0.83kg, 2 female, 3 male, Liberty Research, Inc., Waverly, NY) were used in this study (designated as experiments 1–5). Cats were used due to their high relevance to human physiology and their long history of study in bladder neurophysiology [65]. Prior to use, animals were free-range housed with up to 3 other cats in a 413 ft^2 room with controlled temperature (19-21 °C) and relative humidity (35-60%), food and water available ad lib, and a 12-hour light/dark cycle. Animals received enrichment via staff interaction and toys.

3.3.2 Surgical Procedure

As in prior studies [63], animals were induced for anesthesia with a mixture of ketamine (6.6 mg/kg), butorphanol (0.66 mg/kg), and dexmedetomidine (0.02-0.03 mg/kg) administered intramuscularly. Animals were intubated and subsequently maintained on isoflurane anesthesia (0.5-4%) during surgical procedures. Respiratory rate, heart rate, end-tidal CO_2, O_2 perfusion, temperature, and intra-arterial blood pressure were monitored continuously using a Surgivet vitals monitor (Smiths Medical, Dublin, OH). Fluids (1:1 ratio of lactated Ringers solution and 5% dextrose) were infused intravenously via the cephalic vein at a rate of 5–10 mL/kg/hr (increased up to 30 mL/kg/hr during surgery as needed). Catheters were inserted into the bladder at the bladder dome via a laparotomy (experiment 1-2, both female) or via the urethra (experiment 3-5, all male, catheter diameter 3.5-5 Fr) for intravesical fluid infusion and pressure monitoring. The urethra was not ligated.

A midline dorsal incision was made to expose the L7 to S3 vertebrae and a partial laminectomy was performed to access sacral DRG. Iridium oxide microelectrode arrays with shank

length of 1.0 mm and inter-shank spacing of 0.4 mm (4x8 configuration; Blackrock Microsystems, Salt Lake City, UT) were implanted bilaterally into S1 DRG using a pneumatic inserter (Blackrock Microsystems). Although S2 DRG contain more bladder neurons than S1 DRG in cats [95], the larger size of S1 DRG aligned better with the microelectrode array footprint and our prior work obtained sufficient bladder signals for decoding from S1 DRG [63]. Array reference wires were placed near the spinal cord and ground wires were attached to a stainless steel needle inserted below the skin (lateral and caudal to the laminectomy incision site). At the conclusion of surgical procedures (8.3±0.7 hr surgery length, plus 0.1-0.5 hr for array insertion), prior to experimental testing, animals were transitioned to intravenous alpha-chloralose (C0128, Sigma Aldrich; 70 mg/kg induction; 20 mg/kg maintenance). As this transition was at least six hours after induction, we expect that there were no residual effects on bladder function due to the induction dosing of ketamine, butorphanol, or dexmedetomidine. Analgesia was augmented with 0.01 mg/kg buprenorphine every 8–12 hours subcutaneously.

3.3.3 Experimental Set-up and Data Collection

Neural data was sampled at 30 kHz and band-passed filtered (250 Hz to 7.5 kHz) using a Grapevine Neural Interface Processer and Trellis recording system (Ripple, Salt Lake City, UT). Threshold crossings were detected by setting a dual threshold at 3–5.5 times the root-mean-squared value of the signal. Bladder pressure was monitored with a pressure transducer (DPT-100, Utah Medical Products, Midvale, UT) and transducer amplifier (TBM4M, World Precision Instruments, Sarasota, FL). The bladder pressure signal was sampled by the Grapevine system at 1 kHz, and all data was streamed to an online decoder developed in MATLAB Graphic User Interface (Mathworks, Natick, MA) through a Trellis MATLAB software interface. During each

bladder infusion trial, 0.9% saline or 0.5% acetic acid (R13032, Fisher Scientific, Hampton, NH) in saline was infused into the bladder with a syringe pump (AS50 Infusion Pump, Baxter International, Deerfield, IL and Model NE-1000, New Era Pump Systems, Inc., Farmingdale, NY). Acetic acid is an irritant that increases bladder overactivity and was infused to simulate an OAB condition [94], [96].

Each experiment had two or more bladder fill sequences, in which bladder pressure and neural recordings were collected during infusion at 2 mL/min. Prior to an infusion, the bladder was emptied by withdrawing from the catheter. Fluid infusion was stopped after the bladder was full (leakage observed or a sustained bladder contraction was observed for over 10 seconds). In experiment 3, some trials were stopped early because the heart rate increased at least 40 bpm above baseline. Because of this, summary statistics on the bladder capacity was not included below for experiment 3. The bladder capacity was estimated as the volume withdrawn from the bladder at the end of the trial. The first infusion in each sequence was used to train a decoding model, and the second fill was used to test the model in real-time. Depending on experimental progress, that second fill may have then been used to train a new model as the first fill of a new sequence. At least 3 saline-only fills were conducted prior to acetic acid trials. In general, training and testing fills used the same condition (saline-normal or acetic acid-simulated OAB) but in a few cases saline fills were used to train a model that was tested for a simulated OAB fill.

3.3.4 Real-time Decoding Algorithm

The real-time closed-loop control system was developed as a MATLAB graphic user interface (GUI). A previously described Kalman filter modeling algorithm [91] was trained offline then tested in real-time, using the following parameters. For offline training, after a full bladder fill

cycle was completed, the firing rates of threshold crossings on all channels were calculated at a 2-second interval using a boxcar smoothing method, as a balance between computational load and estimation accuracy [91]. The firing rates were then normalized by dividing each by the firing rate range of the first 30 seconds of each trial. The bladder pressure was also averaged every 2 seconds. The correlation coefficient (CC) between each channel firing rate and the bladder pressure was calculated. While 64 total microelectrodes were implanted for each experiment, only channels highly correlated with bladder pressure (CC > 0.7) during a training fill sequence were used. If no channel met this criterion, the threshold was iteratively lowered by 0.1 until sufficient channels were available to make a robust estimate. Following channel selection, the Kalman algorithm was used to model bladder pressure as a weighted average of the previous bladder pressure and firing rates of the input channels. During testing, the threshold crossing times were streamed to the GUI in real-time (1.1 ± 1.4 ms calculation time). Firing rates were calculated every 2 seconds and fed into the model to obtain an estimate of the bladder pressure for comparison to the measured pressure. Figure 13 shows the experimental workflow.

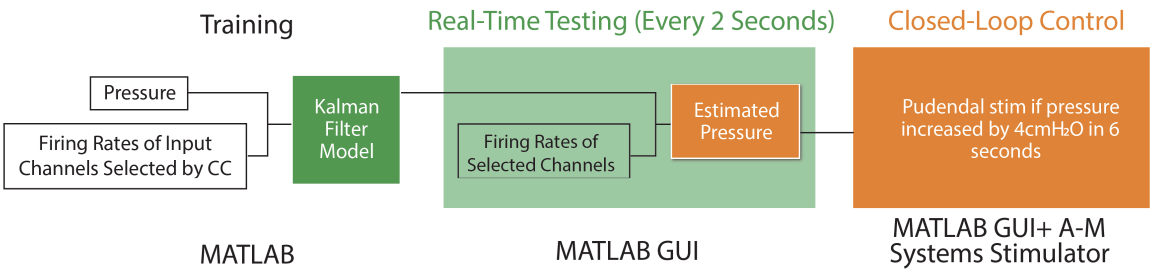

Figure 13. Flow diagram of real-time decode training and testing and closed-loop control.

3.3.5 Real-time Closed-loop Control

In experiments 3 and 4, a bipolar nerve cuff (2.0 mm inner diameter Silastic 508-009 tubing; 0.4 mm stainless steel Cooner wire contacts) was placed on the left pudendal nerve after a postero-lateral gluteal incision and access. During one testing trial in experiment 3, electrical stimulation

(Model 2100 Isolated Pulse Stimulator, A-M Systems, Sequim, WA) was manually turned on for 23.7 ± 3.6 seconds after the onset of each of five contractions, visually identified from the real-time estimated pressure. In experiment 4, this process was automated in MATLAB to trigger stimulation when the estimated pressure monotonically increased at least 4 cm H_2O in 6 seconds. The six-second interval was selected as three consecutive pressure estimates, based on the 2-second real-time pressure updates. In each stimulation interval, 10 Hz stimulation (balanced biphasic, 200 μs pulse width) was used to drive bladder relaxation, based on a previous study that reported its efficacy over other frequencies in a similar experimental set-up [97]. Neither the closed-loop timing nor stimulation paradigm were optimized for this study but were selected to demonstrate the potential utility in this application. A cross-channel invalidation and blanking method was used to reduce stimulation artifacts in DRG recordings. In the artifact blanking method, a 2 ms sliding time window was applied in real-time to the input spike times. If a spike was present in the same 2 ms window for over 50% of the channels, then that spike and any occurring in the next 40 ms were removed. This method was empirically determined from offline analysis to remove the effect of stimulation artifacts on decoding performance.

3.3.6 Euthanasia

After completion of all testing, animals were euthanized with 2-3 mL of intravenous or intracardiac sodium pentobarbital (390 mg/mL) while under deep isoflurane anesthesia.

3.3.7 Statistical Analyses

Two primary metrics were used to evaluate the accuracy of bladder decoding. The correlation coefficient (R, equation 1) and normalized root-mean-squared error (NRMSE, equation 2) between

the measured (P) and estimated pressure ($\hat{P}$) were calculated for each real-time testing trial. The correlation plays an important role because it reflects the level of similarity in shape between the estimated pressure and the measured pressure. A high correlation coefficient indicates that the basic features (reflex contraction, sustained contraction, relaxation etc.) in the cystometry curve were captured, and that it is possible to extract events with machine learning algorithms. Although R and CC use the same underlying correlation coefficient calculation, we use different variables to distinguish the different types of data sets being compared (R compares estimated to actual bladder pressure, and CC compares neural firing rates to the actual bladder pressure).

$$R = \frac{E[P,\hat{P}]-E[P]E[\hat{P}]}{\sqrt{E[P^2]-[E[P]]^2}\sqrt{E[\hat{P}^2]-[E[\hat{P}]]^2}} \qquad (1)$$

$$NRMSE = \frac{1}{(P_{max}-P_{min})}\sqrt{\frac{\sum_{t=0}^{t=N}(\hat{P}_t-P_t)^2}{N}} \qquad (2)$$

To verify that acetic acid was producing a simulated OAB state, an unpaired t-test was used to determine if bladder capacity was reduced significantly from saline-only fills to acetic-acid fills. An unpaired t-test was also used to determine if acetic acid caused significantly earlier onset of non-voiding contractions. To analyze the stability of threshold crossings within each experiment, a paired t-test was used to quantify any changes between firing rates and bladder pressure from training to testing trials and from saline to acetic acid trials. For all tests, a significance level of 0.05 was used. When appropriate, values are given as mean ± standard deviation.

3.4 Results

Real-time decoding was performed in all 5 experiments, with 20 saline and 15 acetic acid testing trials in total. We demonstrated closed-loop control in experiments 3 and 4.

3.4.1 Normal Bladder and Simulated OAB Models

The simulated OAB model produced significantly lower bladder capacities (23.4 ± 12.1 mL, n = 13, $p < 0.0001$; Figure 14) than normal saline bladder capacities (44.5 ± 10.1 mL, n = 21). In experiments 1 and 4, an earlier onset of non-voiding contractions during acetic acid infusion was observed, though this finding was not significant. The infused volumes until the first non-voiding contraction were 12.1 ± 2.7 mL (saline, n = 7) and 7.8 ± 1.1 mL (acetic acid, n = 2) for experiment 1 (example in Figure 14), and 17.2 ± 2.7 mL (saline, n = 5) and 13.7 ± 1.8 mL (acetic acid, n = 4) for experiment 4. No other experiments had consistently identifiable non-voiding contractions across all trials. Experiments with urethra catheters had significantly larger bladder contractions ($p < 0.001$; 55.6 ± 6.7 cm H_2O, n = 9 for Experiment 4; 54.8 ± 8.3 cm H_2O, n = 8 for Experiment 5; not measured in Experiment 3) than those with supra-pubic catheters (20.7 ± 3.1 cm H_2O, n = 9; 20.1 ± 5.0 cm H_2O, n = 8 for Experiments 1 and 2), likely due to the catheter partially occluding the urethra. These later experiments also used larger males (5.7, 5.1 kg) than the females in supra-pubic experiments (3.4, 4.0 kg), which may have been a factor in the larger pressures. Bladder volumes for either saline or acetic acid infusion trials were not different between supra-pubic and urethra catheter experiments (Figure 14).

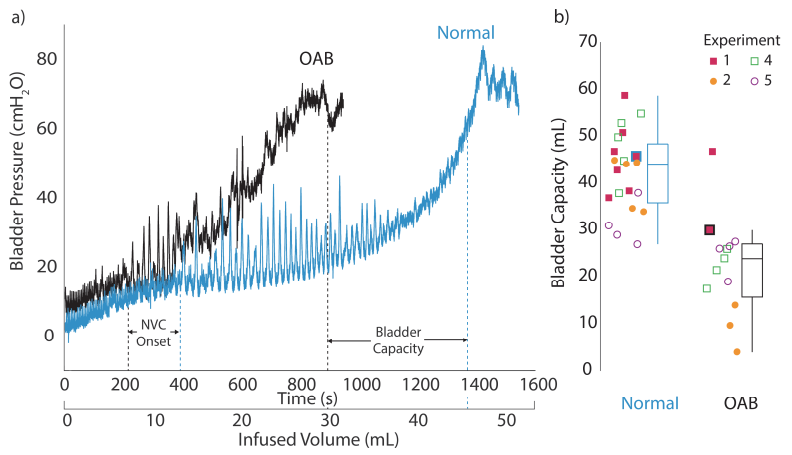

Figure 14. a) Example bladder fills sequences for saline (in blue) and acetic acid (in black) infusions from experiment 1. b) Summary of bladder capacities in experiment 1, 2, 4 and 5 in box plots. Simulated OAB capacities (n = 13) were significantly lower than normal bladder capacities (n = 21; p < 0.0001). Icons for fills in (a) indicated with thick outline in blue or black.

3.4.2 Real-time Decoding

Thirty-five real-time decoding testing trials were performed, with a minimum of six testing trials per cat (Table 5). The first bladder fill for an experiment and bladder condition was used to train a model and a following bladder fill was used for real-time decode testing of that model (for both stimulation and non-stimulation trials). That second bladder fill then became a training data set for a new model, in an alternating manner up to the total number of testing bladder fills per experiment and condition given in Table 5. On average, 5.6 ± 3.7 DRG channels were used in each testing trial (range 1-14). Table 5 lists the mean channel counts used in each experiment. Twenty-two of 35 trials (62.9%) used the maximum 0.7 CC threshold for channel selection, with an average CC threshold of 0.58 ± 0.18 (range: 0.2–0.7) used across all trials. Table 6 summarizes the NRMSE and R metrics for the real-time algorithm performance. On average, simulated OAB trials had a significantly higher correlation ($p = 0.026$) and non-significantly lower NRMSE ($p = 0.445$) than normal saline trials. Figure 15 shows an example real-time decoding trial. Figure 16 shows the individual R values for all training and testing trials. There was no trend in R or NRMSE across testing trials within each individual experiment. Four

simulated OAB testing trials across the experiments used models created from normal saline training fills. The performance metrics for these four trials (R: 0.94 ± 0.04; NRMSE: 0.30 ± 0.26) were not different from the simulated OAB testing trials trained on acetic acid fills (n = 11; R: 0.95 ± 0.04; NRMSE: 0.20 ± 0.14).

Table 5. Trial Summary

Experiment	Saline	Acetic Acid	Closed-Loop	Channels per Model
1	5	1	0	5.8 ± 2.1
2	4	3	0	2.1 ± 0.4
3	4	4	1 (manual)	6.8 ± 3.1
4	4	3	2	4.4 ± 3.9
5	3	4	0	8.6 ± 4.6
Total	20	15	3	5.6 ± 3.7

Table 6. Real-time Decode Summary Statistics

	R	NRMSE
Normal (saline) (n =20)	0.84 ± 0.19	0.28 ± 0.13
OAB (acetic acid) (n = 15)	0.95 ± 0.04	0.23 ± 0.18
Normal & OAB (n = 35)	0.88 ± 0.16	0.26 ± 0.21
Automated Closed-loop (n=2)	0.79 ± 0.05	0.19 ± 0.02

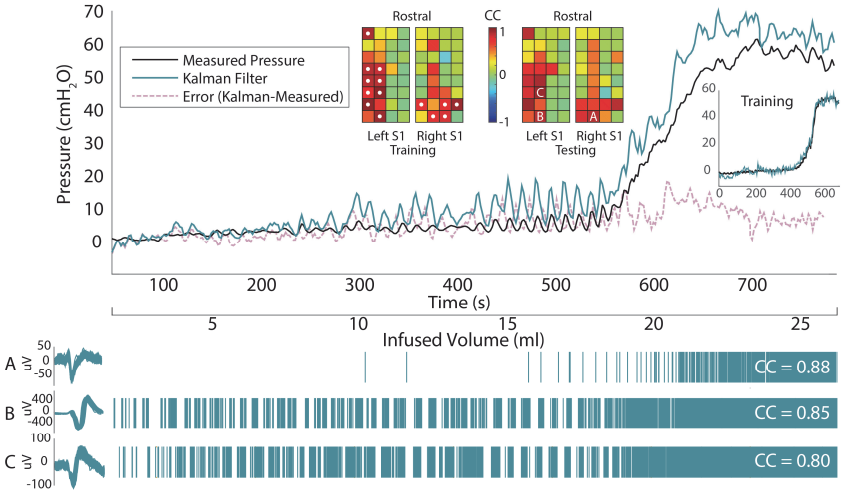

Figure 15. Example real-time OAB decoding trial from Experiment 5. NRMSE = 0.098, R = 0.9895. Fourteen channels were used for decoding. At middle top, the correlation coefficient mapping of threshold crossings and bladder pressure are shown for all microelectrode with channels used for decoding indicated by a white dot. At bottom are raster plots for units from three example channels.

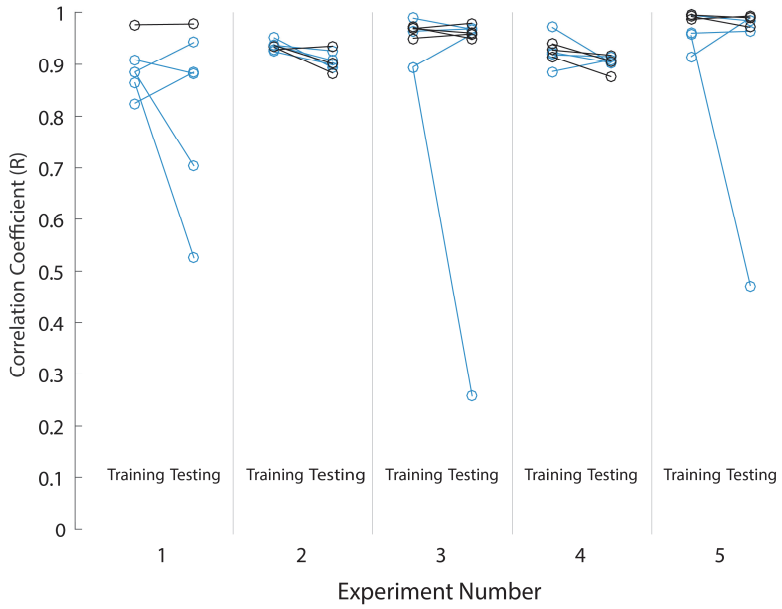

Figure 16. Performance summary of correlation coefficients (R) for all trials. Saline trials are denoted by blue icons; acetic acid OAB trials by black icons. Transitional trials (training with saline and testing with acetic acid) are denoted by black dashed lines Table 6 contains summary statistics across all trials.

We performed three post-hoc analyses to understand the sources of prediction error and to inform improvements to the algorithm. First we tested the stability of unsorted neural activity between paired training and testing trials. In two experiments, there was a significant change in the correlation coefficients (CC) according to a paired t-test (Table 7). We also modeled the relationship between pressure and single-channel threshold crossing firing rates with a linear regression model and tested whether the slopes and intercepts changed between training and testing trials. In two experiments, there was a statistically significant change in slope, and in four experiments, there was a significant change in intercept (Table 7). Each experiment had a significant change in at least one parameter but only one experiment had a significant change in all three. Table 7 also gives the mean ratio between each parameter in the testing data set to the training data set value.

Next, we investigated if changes in channel firing-rate correlation coefficients resulted from changes in single-unit activity. An expert spike sorter manually sorted single units (Offline

Sorter, Plexon, Dallas, TX) that responded to bladder filling in each trial. Thirty-six sortable bladder single units were identified across the five experiments (range: 1-15 per experiment), fourteen of which occurred in all trials for their respective experiment (no sorted units were persistent in experiment 2). Figure 17 shows CC across trials for twelve of these persistent units. Figure 18 also shows the variation in CC for unsorted channels that have the highest average CC in the same experiment. The averages of the standard deviation in CC for these single units and the unsorted threshold crossings were not different (0.16 and 0.17, respectively; $p = 0.65$), suggesting that variations in channel firing rate coefficients were related to changes in underlying single unit activity.

Because acetic acid trials had both lower NRMSE and higher R (Table 6, Figure 16), our final post-hoc analysis investigated the effect of the simulated OAB model on single-unit firing rate to bladder pressure correlation. We quantified the behavior of single-unit neurons and threshold crossings from saline to acetic acid trials. Out of twelve single-unit neurons that we analyzed, ten neurons had an increased sensitivity to bladder pressure during acetic acid trials (average change in CC: $+0.10 \pm 0.25$; range: $-0.51 – +0.58$), though the overall mean CC was not different between the saline and acetic acid trials (saline: 0.48 ± 0.22; acetic acid: 0.59 ± 0.20; $p = 0.25$). Out of twelve unsorted channel multi-units, eleven had an increased sensitivity to bladder pressure during acetic acid trials (average change in CC change per channel: $+0.19 \pm 0.14$; range: $-0.17 – +0.30$), and the overall mean CC was significantly higher (saline: 0.48 ± 0.13; acetic acid: 0.67 ± 0.19; $p = 0.009$).

Table 7. Mean Test: Train Ratio and (p-value) Summary for Tests of Unsorted Neural Activity between Training and Testing Trials.

Exp.	CC	Slope	Intercept
1	0.97 (0.76)	0.63 **(0.01)**	1.06 (0.73)
2	0.90 (0.15)	1.03 (0.81)	2.55 **(<0.001)**
3	0.92 **(0.01)**	1.00 (0.96)	2.43 **(<0.001)**
4	0.51 **(<0.001)**	*0.33(0.02)*	3.13 **(0.006)**
5	0.93 (0.18)	0.99 (0.86)	1.23 **(<0.001)**

(p < 0.05 highlighted with bold text)

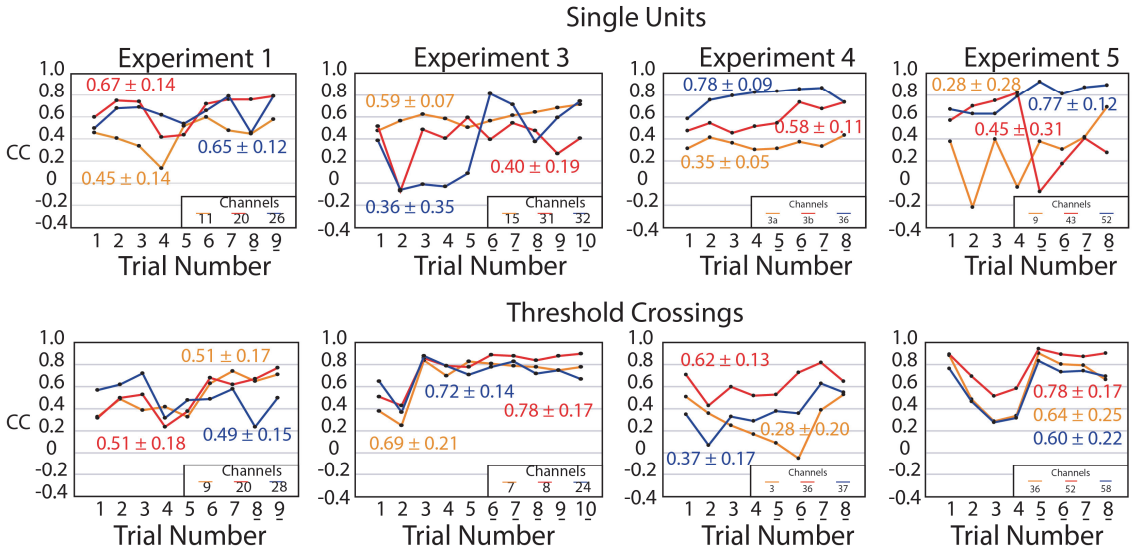

Figure 17. Sorted single units (top) and highly-correlated unsorted channels (bottom) had similar variability across each experiment. Mean (± standard deviation) CC is given next to each trace. An underlined trial number indicates acetic acid infusion trials.

3.4.3 Closed-loop Control

One decoding trial in experiment 3 and two trials in experiment 4 were combined with manual or automated closed-loop pudendal stimulation (Table 5). In experiment3, manual-driven closed-loop stimulation successfully suppressed bladder contractions during an acetic acid trial. However, stimulation produced artifacts in DRG recordings, which led to large decoding errors during stimulation. In experiment 4, the real-time algorithm was updated to reject stimulation artifacts. For two closed-loop trials, the NRMSE (0.17, 0.21) and R (0.84, 0.74) were similar to non-closed-loop trials. We also successfully demonstrated that bladder contractions can be

automatically inhibited (Figure 18). The maximum bladder volume increased from 22.3 ± 3.2 mL (n = 4; range: 17-26 mL) without stimulation to 31.3± 1.3 mL (n=2; range 30-32.5 mL) with closed-loop stimulation, a 40.4% increase in bladder capacity. Across the two automated closed-loop trials, 33 stimulation epochs preceded a drop in actual pressure with an average delay of 0.64±0.70 s while 11 epochs followed a decrease in actual pressure by an average of 1.17 ± 0.34 s. After stimulation was terminated, the bladder pressure resumed non-voiding contractions until eventually leakage occurred (Figure 18). In these closed-loop trials, stimulation was turned on 114.1 ± 14.1 ms after the rising-pressure condition was met. Closed-loop trials were not performed in experiment 5 due to a lack of an inhibitory response to pudendal nerve stimulation at 5 Hz and 10 Hz.

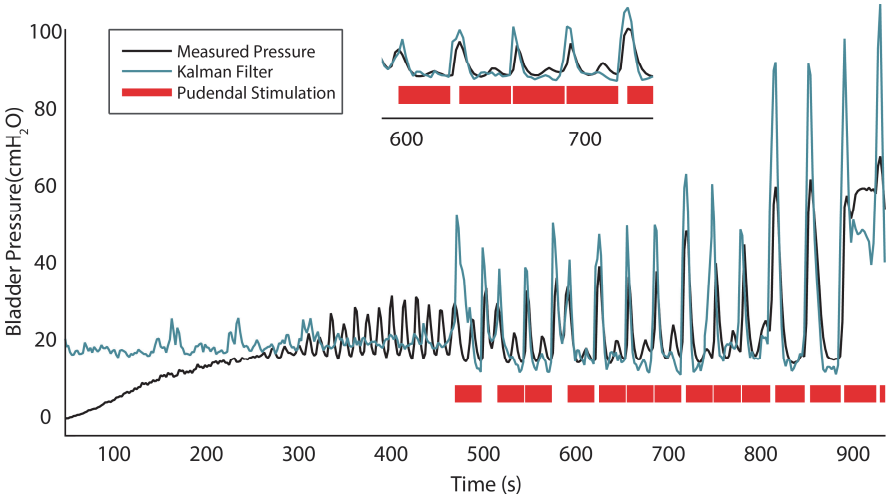

Figure 18. Real-time closed-loop control of bladder relaxation with pudendal nerve stimulation (R = 0.74). A zoomed-in view of part of the trial is shown at top. Pudendal stimulation was applied for 30 seconds when there was an increase in decoded pressure of 4 cm H_2O in 6 seconds. The stimulation effect was most obvious for large non-voiding contractions.

3.5 Discussion

To our knowledge, this is the first study to decode bladder pressure from neural signals in real-time. This development is necessary towards the implementation of an effective closed-loop

neuromodulation algorithm. In prior studies decoding bladder pressure from neural signals [53], [89]–[91], only offline validation was performed. In this study, we built upon a previously developed model [91], and showed that it can be applied during active recording from electrodes. Additionally, we demonstrated that the level of accuracy in these new data sets is sufficient to provide closed-loop feedback.

We demonstrated the feasibility of decoding bladder pressure from DRG recordings in both healthy and simulated OAB conditions with high performance (Figure 15, 16; Table 6). As we have shown previously, there is a hysteretic relationship between bladder neuron firing rates and bladder pressure during contraction and relaxation cycles [63]. The real-time Kalman filter successfully modelled this relationship by combining previous estimated bladder states with current firing rate inputs using a weighted average method. During post hoc analyses, we quantified the stability of sensory neurons during the experiments, observing variability across neural signals (Table 7) that was similar between unsorted channels and sorted single units (Figure 17). We also demonstrated how this method can be incorporated into real-time closed-loop control of bladder relaxation (Figure 18).

The average correlation coefficients for saline trials and acetic acid trials for real-time estimation (Table 6) are higher than two previous offline studies where correlation coefficients were reported (0.81 in Ross et al. and ~0.82 in Im et al.) [90], [91]. The higher bladder decoding correlations in our study suggest that our Kalman model provides an improved approach over prior studies, particularly in tracking relative changes in bladder pressure. Other offline decoding studies reported NRMSE (or RMSE, which can be translated to NRMSE) ranging from 0.06 to 0.17 [53], [79], [89], [91]. Our study had a higher NRMSE, but unlike offline studies there was no room for parameter tuning, which can yield more accurate results. Lumbar-level DRG have

been used to decode limb state with similar performance offline (NRMSE of 0.04-0.22, R of 0.12-0.88) [56]. For an ultimate closed-loop application, the high correlation coefficients are a more critical parameter than NRMSE as they demonstrate our ability to detect relative changes in bladder pressure that can be used to trigger stimulation upon the start of a contraction. Also, our results suggest that an irritant like acetic acid is correlated with a general increase in the sensitivity of both threshold crossings and single units, leading to an improved decode. This increased sensitivity could be due to greater activation of bladder neurons by the irritant or a secondary effect of a faster rise in the bladder pressure due to an effectively smaller bladder. Simulated OAB trials were able to use a saline-fill training model successfully, suggesting there was consistency in neural activity across at least those four bladder fill pairs.

For the conditions used in our study, our results support the use of unsorted channel activity to create robust bladder decoding models. The offline analyses of our data indicated that channel threshold crossings are as stable as single units, in terms of correlation coefficient with bladder pressure (Figure 17). Also, systems that use threshold crossings consume less computational power than those that use single units, which can be challenging to extract with high accuracy [58]. However, this study was performed under anesthesia and only bladder sensory neurons were actively driven during bladder filling, thereby limiting non-relevant signals within the unsorted channel recordings. In an ultimate clinical use, other sensory pathways will also be active and may generate confounding signals. Studies using extraneural cuff or wire electrodes to detect bladder activity [44], [79], [89], [92] may have challenges ignoring non-bladder signals [98]. As we observed in this study, previous work has shown that bladder activity can be differentiated from non-bladder activity with intraneural microelectrodes at DRG [74], [75], [99], which we expect will increase decoding tolerance to non-bladder signals. It may be

necessary to sort neural activity to obtain a robust algorithm for differentiating bladder and non-bladder activity.

Among the five experiments, the shift in baseline firing rates was the most common cause of an error in absolute pressure estimation. This is represented by the significant change in the intercept of a linear pressure-firing rate relationship from training to testing trials in four of the five experiments (Table 7), some of which had a large increase in the ratio between testing and training intercepts. One example of this effect can be seen in the decoded pressure offset at the start of Figure 18. In the majority of experiments, the correlation coefficient and slope between threshold crossing firing rates and bladder pressure remained stable (note ratios near 1.0 in Table 7), which made it possible to decode relative pressure increases and decreases. The instability could be a result of the trauma from array insertion or a slight settling in of the array during the experiment. With durable recording electrodes, these sensory neuron recordings are expected to stabilize over time during chronic implant experiments [75]. The estimated bladder pressure, even with an initial offset in some cases, still allowed us to reliably detect the onset of bladder contractions. In three closed-loop trials, we successfully suppressed bladder contractions when they were detected and increased the bladder capacity compared to fills without stimulation. Seventy-five percent of the stimulation epochs preceded a decrease in bladder pressure, which generally occurred within a second of stimulation onset. The remaining epochs were initiated about one second after the pressure had already started to decrease, suggesting that shorter time intervals between bladder pressure updates may have led to a quicker initiation of stimulation or no triggering of stimulation for a smaller estimated pressure change. As the closed-loop algorithm was not optimized for this study, we expect that the total duration of applied stimulation can be significantly shortened.

The methods developed in this study are translatable to clinical use. Implementation of closed-loop control such that continuous neuromodulation like SNM is only applied when needed could lead to a larger bladder capacity [44] and longer battery life for implanted pulse generators. For clinical use, the closed-loop algorithm will need to be optimized to have high specificity for bladder contraction onsets and/or an increase in baseline tone, depending on a patient's symptoms. In order to mimic a potential clinical calibration method, in the last three experiments we transitioned from supra-pubic bladder catheters to less-invasive urethral catheters. Decoding trials had similar accuracy using either catheter approach (Figure 16), even with larger bladder contractions. While DRG were accessed with a laminectomy in this study, DRG can also be accessed percutaneously at the lumbosacral level [100]. In that approach, a non-penetrating electrode may be more feasible than penetrating arrays, which may need more vertical space for insertion. Recent research has demonstrated that DRG cell bodies are more likely to be located near the surface of the DRG [101], and that a thin-film surface electrode can record bladder pressure single units [99]. New electrodes with a lower profile and minimal immune response may be more feasible to implement clinically and may yield a higher count of bladder-relevant signals.

This study had several limitations. We observed a normal low level of overfitting, which can be alleviated through adding regularization components to the algorithm. Infusion of acetic acid into the bladder can cause damage to the tissue for a prolonged exposure [96]. An increased heart rate and the presence of blood in urine were occasionally observed. An elevated heart rate may also be a result of the anesthetic depth changing over time. Elevated heart rates resulted in some trials being ended prematurely. Although additional resting time between trials was given in order to return the stability of vitals, an alternate simulated OAB model such as the use of

Prostaglandin E2 (PGE2) might have better clinical relevance [102]. We made an effort to keep the number of saline and acetic acid trials consistent across different experiments, however we were limited by experimental and anesthetic factors in some cases. This arrangement still allowed us to achieve statistically significant results in key parameters. Prediction errors were often due to shifts in channel and underlying single-unit correlations to bladder pressure. This may have been the effect of electrodes settling during an acute procedure. We anticipate that a stable chronic interface will alleviate this variation. Finally, our anesthetized animal model limited sensory inputs. Testing with varied bladder and non-bladder signals, such as with behavioral studies, are necessary to determine whether unsorted microelectrode recordings provide sufficient specificity.

Further development of real-time estimation and closed-loop control opens the possibility of a more practical bladder neuroprosthetic device. In future studies, we plan to compare on-demand closed-loop stimulation with other paradigms such as a fixed 50% duty cycle. We also plan to optimize bladder pressure estimation, including evaluating algorithm robustness during activation of non-bladder pathways and across repeated test sessions for chronic-implanted animals, and incorporate adaptive stimulation to maximize the efficacy of bladder neuromodulation in both normal and simulated OAB models. As microelectrode development continues, future studies interfacing with bladder-neuron dominant S2 DRG may also yield improvements in algorithm efficiency. Future work will also include pilot clinical trials with electrodes and stimulation parameters that are more suitable for human use.

3.6 Data Availability

All data and MATLAB code are available online (https://osf. io/h6835/).

Chapter 4 Closed-loop sacral neuromodulation for bladder function using dorsal root ganglia sensory feedback in an acute feline model

4.1 Abstract

Overactive bladder patients suffer from a frequent and uncontrollable urge to urinate, which can lead to a poor quality of life. Current sacral neuromodulation therapy uses open-loop electrical stimulation to alleviate symptoms, which limits battery life and can lead to neural habituation. In this study, we aim to improve therapy by developing a conditional stimulation paradigm using neural recordings from dorsal root ganglia (DRG) as sensory feedback. Experiments were performed in 5 non-survival, anesthetized felines, in which the sacral-level DRG and spinal roots were exposed bilaterally. A bipolar cuff electrode was placed on a S1 root distal to the DRG for stimulation. Microelectrode arrays were implanted in the same or opposite S1 and/or S2 DRG. We implemented a Kalman filter-based algorithm to estimate the bladder pressure in real-time using DRG neural recordings. The Medtronic Summit Research Development Kit was used to control sacral root stimulation when the algorithm detected an increase in bladder pressure. Closed-loop neuromodulation was performed during continuous cystometry and compared to bladder fills with continuous and no stimulation. Overall, closed-loop stimulation with DRG sensory feedback increased bladder capacity by 13.8% over no stimulation ($p < 0.001$). While there was no statistical difference in bladder capacity between closed-loop and continuous stimulation ($p = 0.80$), closed-loop stimulation reduced stimulation time by 57.7%. High-confidence bladder single units had a reduced sensitivity during stimulation, with lower linear

trendline fits and higher pressure thresholds for firing observed during stimulation trials. This study demonstrates the utility of decoding bladder pressure from neural activity for closed-loop control of sacral neuromodulation. An underlying mechanism for sacral neuromodulation may be a reduction in bladder sensory neuron activity during stimulation. Real-time validation during behavioral studies is necessary prior to clinical translation of closed-loop sacral neuromodulation.

4.2 Introduction

Overactive bladder (OAB) is a dysfunction that affects millions of people worldwide. Patients suffer from frequent urinary urgency, with or without incontinence [87], leading to a variety of side effects such as poor sleep, declined mental health, and a low quality of life [88]. Conservative therapies such as anticholinergic drugs and intravesicular Botox injections are both associated with undesirable side effects, leading to low patient compliance [11], and anticholinergics are also associated with an increased risk of dementia [8]. Currently there is no pharmaceutical therapy that permanently reduces or eliminates the symptoms without serious side effects [8], [10].

Sacral neuromodulation (SNM) is a standard clinical treatment for OAB after conservative approaches such as behavioral modification and pharmaceuticals fail [39]. One study reported that 82% of patients discontinued OAB medication after SNM treatment for at least 22 months [33]. In SNM, a stimulation lead is placed near the S3 or S4 sacral nerve in a minimally invasive surgery. SNM is applied constantly at 14 Hz to reduce the symptoms of OAB [103]. SNM often has higher success rates, defined as the percentage of patients with at least a 50% improvement in symptoms, at improving urinary incontinence and voiding frequencyand

less severe side effects than Botox for refractory OAB [104] . However, it has been reported that SNM patients can experience relapse of symptoms after 24 months [38] or longer [39]. Continuous stimulation can facilitate habituation of neural pathways over time [41], which may contribute to the relapse of symptoms. Pre-clinical and clinical pilot studies have demonstrated that sensory feedback-based, or closed-loop, stimulation of relevant nerves may offer greater clinical benefit by driving bladder function only when necessary, leading to increased bladder capacity [17], [43]. However, these methods either require patient activation multiple times a day or need a separate procedure for implanting a direct pressure monitoring device.

Bladder sensory signals can be observed at sacral dorsal root ganglia (DRG) [74]. In addition to physical proximity to the sacral neuromodulation site, sacral-level DRG contain afferent-only signals from the detrusor muscle and urethra, via proximal pelvic and pudendal nerve fibers [52], [93]. In this study, we used sacral-level DRG as a recording site to estimate bladder pressure and the onset of bladder contractions in real-time [105] to automatically trigger closed-loop neuromodulation in acute, healthy cats. This is the first study to examine closed-loop SNM on bladder capacity using neural signals as feedback. While from a pre-clinical research perspective, bladder capacity is usually considered as the most important performance metric, in this study we also evaluate non-voiding bladder contraction behavior. Sensory neurons activated during bladder pressure increases and voiding contractions are also usually activated during non-voiding contractions [105]. These non-voiding contractions may contribute sensations of urgency in OAB, and are therefore undesirable. We hypothesize that closed-loop stimulation increases bladder capacity over no-stimulation trials and reduces the frequency of non-voiding contractions (NVCs) to the same extent as continuous stimulation while applying significantly less stimulation.

4.3 Methods

4.3.1 Animals

All procedures were approved by the University of Michigan Institutional Animal Care and Use Committee (IACUC), in accordance with the National Institute of Health's guidelines for the care and use of laboratory animals. Five adult, domestic, short-hair male cats (0.99 ± 0.27 years old, 4.70 ± 0.57 kg, Marshall BioResources, North Rose, NY) were used in this study (designated as experiments 1–5). Cats were used due to their high relevance to human physiology and their long history of study in bladder neurophysiology [65]. Prior to use, animals were free-range housed with up to 3 other cats in a 413 ft^2 room with controlled temperature (19-21 °C) and relative humidity (35-60%), food and water available ad lib, and a 12-hour light/dark cycle. Animals received enrichment via staff interaction and toys.

4.3.2 Surgical Procedure

As in prior studies [91], [105], animals were anesthetized with a mixture of ketamine (6.6 mg/kg), butorphanol (0.66 mg/kg), and dexmedetomidine (0.011 mg/kg) administered intramuscularly. Animals were intubated and subsequently maintained on isoflurane anesthesia (0.5-4%) during surgical procedures. Respiratory rate, heart rate, end-tidal CO_2, O_2 perfusion, temperature, and intra-arterial blood pressure were monitored continuously using a SurgiVet vitals monitor (Smiths Medical, Dublin, OH). Fluids (1:1 ratio of lactated Ringers solution and 5% dextrose) were infused intravenously via the cephalic vein at a rate of 10 mL/hr during surgery as needed. A 3.5 Fr dual-lumen catheter was inserted to the bladder through the urethra for fluid infusion and pressure monitoring. The urethra was not ligated. A midline dorsal incision was made to expose the L7 to S3 vertebrae and a partial laminectomy was performed to access

sacral DRG. A lab-fabricated bipolar stimulation cuff (1.5 or 2 mm inner diameter) was placed on the left or right S1 root encompassing both the sensory and motor branches.

Two iridium oxide microelectrode arrays for neural recordings (4x8 configuration; 1.0 mm shank length; 0.4 mm shank pitch; Blackrock Microsystems, Salt Lake City, UT) were implanted into (1) left and right S1 DRG or (2) S1 and S2 DRG on the same side using a pneumatic inserter (Blackrock Microsystems). Array reference wires were placed near the spinal cord and ground wires were attached to a stainless steel needle inserted below the skin (lateral and caudal to the laminectomy incision site). At the conclusion of surgical procedures, prior to experimental testing, animals were transitioned to intravenous alpha-chloralose (C0128, Sigma Aldrich; 70 mg/kg induction; 20 mg/kg maintenance). This transition was at least six hours after induction, and we expect that there were no residual effects on bladder function due to the induction dosing of ketamine, butorphanol, or dexmedetomidine. Analgesia was augmented with 0.01 mg/kg buprenorphine every 8–12 hours subcutaneously.

4.3.3 Closed-loop SNM System

Prior to the main cystometry experiments, stimulation parameter optimization was performed. In isovolumetric trials, 5 Hz (200 μs pulse width) stimulation on the S1 root was more effective at inhibiting bladder non-voiding and voiding contractions at 2 times the motor threshold (MT) for scrotum, anus or tail twitching, compared to 2, 7, 10, 15, and 33 Hz. 5Hz was selected for all experiments in this study. The stimulation amplitude used for cystometry trials was varied across experiments, within 1-4 x MT (0.10 mA-0.72 mA), depending both on how effective bladder contractions were suppressed and the extent of movement artifacts that were caused by

stimulation. Experiments 1 and 5 used 1-1.5 x MT, experiments 2 and 3 used 4 x MT, and experiment 4 used 2 x MT.

Sacral nerve stimulation and microelectrode array recordings were integrated through the Medtronic Summit Research Development Kit (RDK) to deliver closed-loop stimulation. The RDK is comprised of an Olympus RC+S (B35300R) Implantable Neural Stimulator (INS) connected to a four-electrode stimulation lead (Medtronic Model 3889), the Summit Application Programming Interface (API), and other supporting hardware components including a Research Lab Programmer (RLP, a tablet mainly for setting stimulation parameters and safety limits), Clinician Telemetry Modules (CTMs) that enable wireless connection between the INS and the research host computer (for delivering closed-loop stimulation) or the RLP, a Patient Therapy Manager (PTM, for charging the INS and parameter setting), and a Recharge Therapy Manager (RTM) that enables inductive charging of the INS through the PTM. This full system was not specifically necessary to perform closed-loop stimulation during these anesthetized experiments, as we have demonstrated in a previous pilot experiment [105]. One of our goals for this study was to demonstrate feasibility with a wireless human use system [106] as a steppingstone for behaving preclinical experiments with a fully implantable system towards clinical translation.

The two stimulation cuff lead wires were attached to two of the four electrodes on the INS lead with modelling clay, which served both as an adhesive and an insulator for the connection. A setup diagram is shown in Figure 1. The Summit RDK software package allows programmatic control of the INS through a MATLAB interface, in which a previously developed Kalman filter algorithm [91], [105] was implemented to decode bladder pressure (as a control signal) from the neural recordings (collected at 30 kHz per channel through the Ripple Grapevine system and Trellis software). The neural recordings were processed into threshold crossings with

a positive and negative dual threshold at ±3.5-5.5 × root-mean square of the raw signal. A spike only needed to cross one of the thresholds to be captured. The algorithm extracted unsorted threshold crossing firing rates using a non-sliding 1-second interval window from recording channels and combined them with a state-dependent model to estimate the bladder pressure using a weighted average method. DRG microelectrode channels with a firing rate to bladder pressure correlation of greater than 0.7 were included in the model. If no more than one channel had a correlation greater than 0.7, then this cutoff was reduced in 0.1 increments until there was at least two channels used by the model. A cross-channel invalidation method was applied before the firing rates were calculated to remove threshold crossings that simultaneously appeared on over 90% of the channels, to minimize the effect of stimulation artifacts.

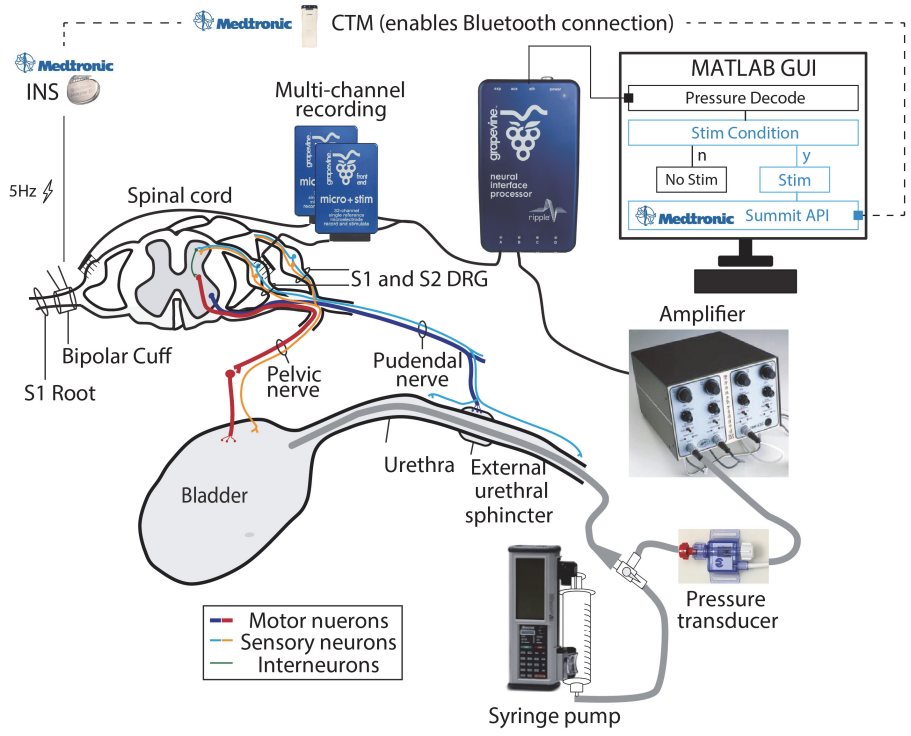

Figure 19. Illustration of the testing setup. DRG neural recordings were acquired with a Ripple Grapevine system and accompanying Ripple Trellis software via microelectrode arrays implanted in S1 and S2 DRG. Trials consisted of recording neural data and bladder pressure (monitored with a pressure transducer and amplifier) during saline infusions at a controlled rate via an intraurethral bladder catheter. Pressure data was recorded with the Grapevine system after amplification. Real-time decoding was performed in a MATLAB GUI that contains the Summit Application Programming Interface (API) that enables Bluetooth control of the Implantable Neural Stimulator (INS) through a Clinician Telemetry Module (CTM).

4.3.4 Experimental Trials

Cystometry trials were performed in which the bladder was infused with 0.9% saline (warmed to 41 °C) through a 3.5 Fr urethra catheter at 2 ml/min from an empty volume to when the first leak around the urethra catheter was observed. In each trial, one of three stimulation paradigms was used: continuous ("continuous SNM"), closed-loop stimulation, or no stimulation (except in experiment 5, in which only no-stimulation and closed-loop stimulation were performed due to unanticipated experimental circumstances that limited the testing time). In closed-loop trials, stimulation was initiated based on a bladder contraction detection algorithm, indicating when the DRG decoding algorithm showed an increase in bladder pressure within a certain time window. The first two experiments were exploratory, in which the contraction detection algorithm was varied and closed-loop sacral nerve stimulation was conditionally turned on for a fixed duration of 15-60 s when an estimated bladder pressure increase of 3-10 cmH_2O was observed from the start of a 3-6 s window. Observations from cystometry trials and additional isovolumetric trials in these two experiments and a third, separate experiment without cystometry trials were used to select the final contraction detection algorithm. In the last three experiments, the contraction detection algorithm was fixed, and closed-loop stimulation was turned on for 15s after a 6 cmH_2O increase in estimated pressure was observed from the start of a 4-second moving window. The primary goal of this study was to demonstrate closed-loop stimulation, we prioritized running as many closed-loop and no-stimulation trials as possible within a limited experimental time; therefore, the order of the trials was not completely random.

After each trial ended, the bladder capacity was measured as the amount of fluid in the bladder when the first leak was observed. This was done by adding the fluid volume manually emptied from the bladder (through a urethral catheter) and any leak volume collected by a weigh boat. The bladder was allowed to rest for at least 15 minutes before initiating the next cystometry trial.

4.3.5 Euthanasia

After completion of all testing, animals were euthanized with a dose of intravenous sodium pentobarbital while under deep isoflurane anesthesia, and death was ensured with a secondary method of euthanasia as approved by the IACUC.

4.3.6 Data Analysis

Bladder capacity was measured in each trial and normalized to the control (no-stimulation) group average in each experiment (animal). A rank-based non-parametric Kruskal-Wallis test was used to evaluate statistical significance in bladder capacity among no-stimulation, closed-loop stimulation, and continuous stimulation across all trials. A significance level of 0.05 was used. Post hoc pair-wise comparisons were performed with a Kruskal-Dunn test, with Bonferroni correction on p-values.

We defined bladder contractions (NVCs or voiding contractions) as bladder pressure increases of at least 6 cmH_2O in a 4-second interval (independent from the contraction detection algorithm). The number of bladder contractions were counted for each trial and normalized to the average of the no-stimulation trials for each experiment. The timing of each bladder contraction was matched with the stimulation initiation timing, and the true positive rate was calculated by

dividing the number of true positives (a bladder contraction successfully identified by the algorithm) by the total number of true bladder contractions. The average interval between bladder contractions for each trial was normalized to the no-stimulation group average for each experiment (animal). Similarly, the peak pressure (maximum pressure during voiding) for each trial was also normalized to the no-stimulation group average for each experiment (animal). The bladder pressure decoding performance was determined using the normalized root mean squared error (NRMSE) and the correlation coefficient (R) between the measured pressure and estimated pressure [91], [105].

While reviewing data after completion of experiments, we observed that stimulation may have had an effect on neural signalling. Thus we performed an additional post hoc analysis in which we identified bladder single units that appeared in at least one no stimulation trial and one continuous SNM trial. The units were isolated in Offline Sorter (Plexon, Dallas, TX) with automated clustering via principal component analysis followed by manual review of snippet waveform shapes by an experienced spike sorter. Only high-confidence single units that had a clearly identifiable waveform shape were included in this analysis. For SNM trials, 5 Hz stimulation artifacts were isolated from neural activity based on clearly differentiable waveforms appearing at a fixed frequency. We confirmed that stimulation artifacts did not obscure any of the bladder unit snippets. To quantify the relationship between identified bladder units and pressure, the correlation coefficient, linear regression slope, and minimum pressure at which a unit started firing (pressure threshold) were determined for each unit. We determined that a unit had started to fire when a single spike was detected. The average change in these parameters from no stimulation trials to SNM trials was calculated. A limited statistical analysis was performed due to a small sample size, as described below.

4.4. Results

Overall, we performed 30 no-stimulation, 23 closed-loop stimulation, and 9 continuous SNM trials across five experiments. Bladder pressure decoding was performed in all closed-loop trials, and some of the no-stimulation and continuous SNM trials. Example testing trials in one experiment for all three conditions are shown in Figure 20.

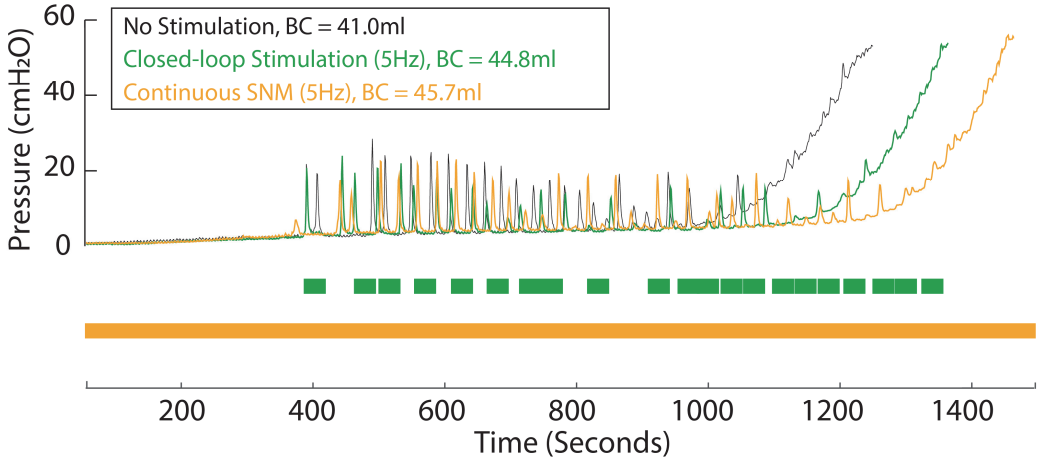

Figure 20. Cystometry curves for example no-stimulation, closed-loop stimulation, and continuous SNM in Experiment 2. Closed-loop stimulation and continuous SNM increased bladder capacity (BC) compared to no-stimulation trials in these examples.

4.4.1 Normalized Bladder Capacity

To assess the effectiveness of each SNM paradigm, we calculated the ratio between the bladder capacity for each trial and the average no-stimulation capacity in an experiment across experiments and all trials for each stimulation type. We observed a 12.8 ± 4.6% mean per-experiment increase in normalized bladder capacity in the closed-loop stimulation group across all 5 experiments, and a 12.9 ± 6.5% per-experiment increase in normalized bladder capacity in the continuous SNM group in 4 experiments (no continuous SNM in experiment 5). Across all individual trials performed, the increase in normalized capacity was 13.8% ($p < 0.001$, range: -12 to 34%) for closed-loop stimulation (n = 23 trials) and 9.1% ($p = 0.26$, range: -27% to 42%) for

continuous SNM (n = 9, Figure 3a) compared to the control trials (n = 30). Closed-loop stimulation resulted in a similar bladder capacity as compared to continuous SNM (p = 0.80). Due to time limitations in each acute experiment, different counts of stimulation trial types were performed in each experiment, with an emphasis placed on performing as many closed-loop and no-stimulation (for control and buffering between stimulation trials) trials as possible. Across experiments, stimulation amplitude and the animal itself did not affect bladder capacity.

We observed a positive correlation (R2 = 0.13) between normalized bladder capacity and stimulation percentage (total time when stimulation was on divided by total trial time, Figure 3b). While this indicates that more stimulation was associated with a stronger bladder inhibition effect, there was no difference between partial (closed-loop) stimulation and continuous SNM in terms of bladder capacity (p = 0.80).

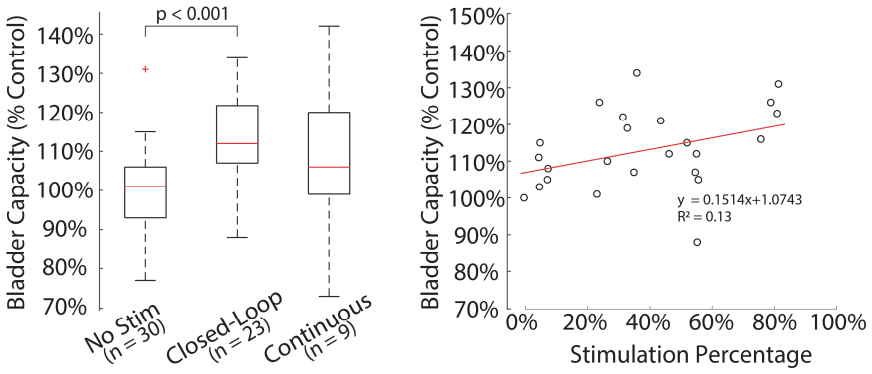

Figure 21. (a) Bladder capacity for each stimulation type for all trials. (b) Bladder capacity against stimulation percentage for each trial.

4.4.2 Closed-loop Algorithm Performance

To determine bladder contraction detection accuracy, we evaluated the ratio between correctly identified contractions and total number of contractions for each trial and across each experiment. On average, 39.5 ± 12.5% (across n = 5 experiments) of the non-voiding contractions were correctly identified by the decoding algorithm, triggering stimulation. The true

positive rate was 35.9% (11.4% and 48.4% for the first and second halves of the cystometry trials, averaged across n = 5 experiments). Of the stimulation bouts triggered in all trials, 51% of the stimulation occurred in the first 75% of the cystometry, while 49% of the stimulation occurred in the last 25% of the cystometry (n = 5 experiments). Figure 4 shows the distribution of stimulation by time-normalized quartiles across all 23 closed-loop trials.

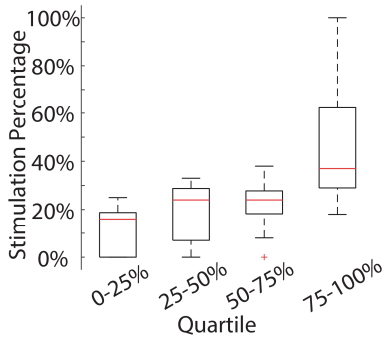

Figure 22. Box plots showing the quartile distribution of stimulation for closed-loop stimulation trials.

To examine the effect of stimulation on non-voiding contractions, we calculated two ratios across the experiments: between the average inter-contraction intervals in each trial and the average intervals in no stimulation trials in an experiment, and between contraction counts in each trial and the average contraction counts in no stimulation trials. Overall, closed-loop stimulation led to a 112.4% increase in the normalized non-voiding contraction interval (n = 5 experiments), while resulting in a small 3.2% decrease in the normalized number of contractions (n = 5 experiments) per trial. We observed that in some cases the start of stimulation corresponded with an NVC occurrence. This effect was not quantified but may have contributed to a minimal change in NVC count in the closed-loop stimulation group. While continuous SNM increased the non-voiding contraction interval by only 26.8%, it decreased the number of non-voiding contractions per void by 51.2%. The peak bladder pressure was slightly increased by closed-loop and continuous stimulation (1.5% and 3.9%).

4.4.3 Decoding Performance

To evaluate the decoding performance of the algorithm during stimulation, we calculated the NRMSE and R between the estimated bladder pressure and measured bladder pressure for each trial. Bladder pressure decoding was performed in real-time in each type of trial (Table 1). On average, decoding was performed with 5 DRG microelectrode channels (range: 2-11) in each experiment. As predicted, closed-loop stimulation trials had an increase in NRMSE and a decrease in R for bladder pressure estimation, as additional channel threshold crossings were detected during stimulation. While a cross-channel invalidation method was applied to remove threshold crossings that appeared on over 90% of the channels at the same time, we still observed an overestimation of the bladder pressure during stimulation. This was mostly due to stimulation-driven units and stimulation artifacts that appeared on fewer than 90% of the channels. In addition, we observed a positive correlation between normalized bladder capacity and the decoded pressure correlation coefficient R but not NRMSE (Figure 5).

Table 8. Decoding performance by NRMSE and R across stimulation trials

	NRMSE			**R**		
	No Stim	CLS	Continuous SNM	No Stim	CLS	Continuous SNM
Mean	0.19	0.29	0.18	0.83	0.62	0.78
St. Dev.	0.07	0.17	0.04	0.18	0.22	0.01
n	9	23	3	9	23	3
% Increase		55.27%	-4.57%		-25.91%	-7.07%

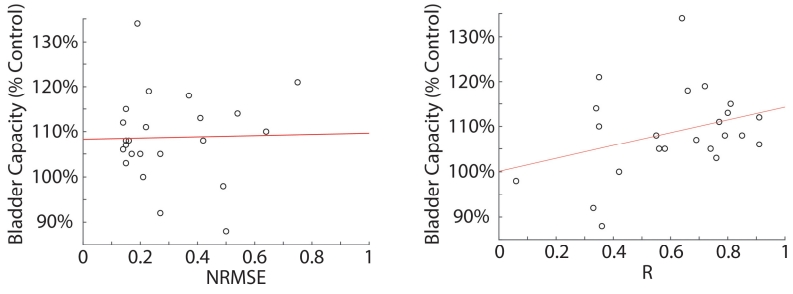

Figure 23. (a) Normalized bladder capacity vs. NRMSE (R^2 = 0.02, p = 0.52) (b) Normalized bladder capacity vs. R. (R2 = 0.08, p = 0.18).

4.4.4 Single Unit Analysis

To investigate a potential interaction between SNM and bladder sensory neurons, we examined the relationship between their neural signals and bladder pressure during stimulation and no-stimulation conditions. In experiments 1-4, eight bladder units that appeared in at least one no-stimulation and one continuous SNM trial were identified with manual spike sorting. While overall we observed a much larger number of DRG microelectrode channels with bladder activity, only single units that were clearly distinguishable from stimulation artifacts were included in this analysis. On average, the correlation coefficient between the firing rate of these units and the bladder pressure during SNM trials was 9.1 ± 57.2% lower than during no-stimulation bladder fills. The slope of linear regression trendlines between the single unit firing rate and bladder pressure in SNM trials was 35.5 ± 47.1% lower than no-stimulation trials. The minimum pressure at which bladder units first fired in SNM trials was 4.7 ± 5.5 times higher than in no-stimulation trials. For all bladder unit trials pooled together by stimulation type, continuous stimulation trials had a significantly higher pressure threshold (3.9 ± 3.7 cmH_2O, range 0.8-10.2 cmH_2O, median 2.3 cmH_2O, $p = 0.024$) than no-stimulation trials (1.8 ± 2.4 cmH_2O, range 0.1-8.7 cmH_2O, median 0.9 cmH_2O) according to a Mann Whitney U test. Two of these bladder units are shown in Figure 6, with a representative 3-second interval showing differentiation of bladder units and SNM artifacts in Figure 6c. The parameters for each bladder unit are presented in Table 2.

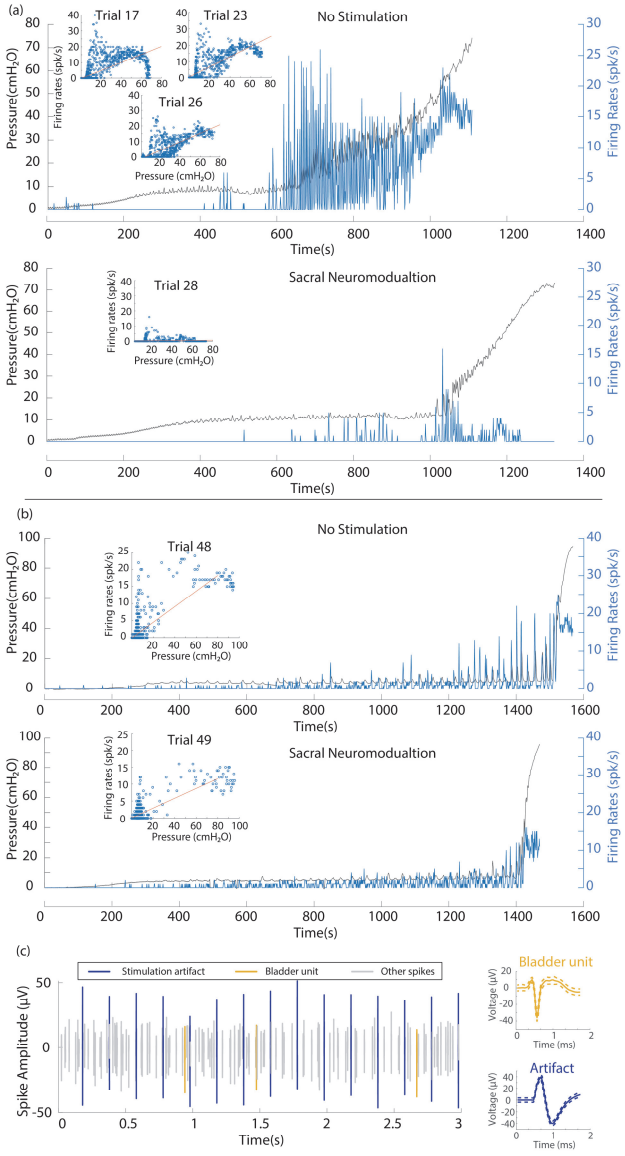

Figure 24. Two examples of sorted bladder single units, from experiments 1 (a) [unit 1] and 4 (b), which demonstrate a reduction in sensitivity to bladder pressure changes during continuous SNM. Inset figures plot firing rate against pressure at each calculation interval, with linear regression trend lines overlaid in red. For (a), the no-stimulation Trial 26 is plotted against time. (c) Left: Raster plot of sorted threshold crossings showing a bladder unit, stimulation artifacts, and other crossings during an example SNM trial [exp. 1, unit 2], demonstrating differentiation of signals. Right: averaged bladder unit waveform (yellow) and stimulation artifact waveform (blue).

Table 9. Bladder unit change in correlation coefficient, linear regression slope, and pressure threshold change with stimulation.

Exp	Unit #	R Change	Slope Change	Pressure Threshold Change	No-Stim Trials	SNM Trials	Stimulation & recording electrode relative spinal nerve locations
1	1	-83.8%	-97.6%	389.2%	3	1	Opposite
1	2	3.4%	-43.8%	37.7%	3	1	Opposite
1	3	-1.2%	-16.8%	85.0%	3	1	Opposite
1	4	4.1%	-1.3%	65.2%	2	1	Opposite
1	5	101.8%	46.9%	-80.0%	3	1	Opposite
2	1	-74.5%	-92.6%	1337.0%	3	1	Opposite
3	1	-23.6%	-42.0%	1136.4%	4	3	Opposite
4	1	1.1%	-37.1%	764.6%	1	1	Same
	Mean	-9.1%	-35.5%	466.9%			
	St. Dev.	57.2%	47.1%	546.5%			

4.5 Discussion

In this study, we explored the short-term efficacy of closed-loop sacral nerve stimulation for increasing bladder capacity in an anesthetized animal model. If translatable, our results suggest that closed-loop SNM could have a potential clinical impact by providing automated, individualized therapy that is linked to objective, physiological signals, a reduction in battery drain due to stimulation, and a reduction in unwanted or unpleasant stimulation sensations, which are a common adverse event [39]. While a reduction in battery use is primarily advantageous for primary cell devices, in the context of rechargeable devices that remain implanted in the patient for longer periods of time [107], closed-loop SNM may increase the recharge interval and improve chronic maintenance of therapy. Our study demonstrates that closed-loop stimulation may allow for this by providing the same or improved performance while applying stimulation at a fraction of the time. A reduction in total stimulation time may reduce nerve habituation over time and preserve the responsiveness of the stimulation target. However, the control system necessary to record neural signals and implement closed-loop control will require battery power. Systems for low-power neural recording and closed-loop

control are being developed for other applications [108], [109], and could be implemented for bladder control as the technology matures. Decoding can also be turned off for a period of time after voiding events are detected to save battery power. Additionally, our results suggest that SNM desensitizes bladder sensory neurons to changes in bladder pressure. This potential mechanism of SNM may be an important contributor to its therapeutic benefit and warrants further exploration.

We successfully achieved closed-loop SNM by integrating real-time bladder pressure decoding from DRG with the Medtronic Summit RC+S stimulation system, which has been used in clinical research [106]. We demonstrated this full integration with in-vivo experiments and showed that closed-loop stimulation had at least the same level of effectiveness as continuous SNM in increasing bladder capacity (Figure 3a), however stimulation was only applied 42.3% of the time. The average normalized increase in bladder capacity across all closed-loop trials (13.8%, $p < 0.001$ compared to no stimulation) was not significantly different than continuous SNM (9.1%) in this study and similar to a previous study (13.4%) that also performed sacral root stimulation with a chloralose-anesthetized feline model [97]. Zhang et al found that stimulating the dorsal side of the subdural sacral root increased bladder capacity in cats by 64% but used a different stimulation frequency (10Hz) [110]. Their experimental model also had a more invasive procedure than ours, in which one ureter was cut and tied, while the other was used for draining. Jezernik et al. observed that stimulating the dorsal root eliminated reflex bladder contractions [51]. Stimulating only the dorsal side is challenging in humans considering its proximity to the spinal cord and tight space in the spinal column. It may be possible to target the dorsal root or DRG for stimulation, instead of the whole spinal root as for SNM, using the percutaneous lead insertion method developed for DRG stimulation for pain [111]. However, the standard SNM

surgical procedure, in which the lead is inserted directly through the S3 foramen to target the spinal nerve, is a simpler and less invasive procedure.

Many closed-loop studies have shown that stimulation on peripheral nerves during voiding, non-voiding contractions, or later parts of a bladder fill cycle can increase bladder capacity significantly, sometimes to the same level as continuous stimulation [17], [43], [44]. Potts et al. found in rats that SNM only in the second half of the bladder fill cycle increased bladder capacity significantly, while stimulating the first half did not [43]. Wenzel et al. found that pudendal nerve stimulation at the beginning of bladder contractions increased bladder capacity twice as much as continuous stimulation [44]. Similarly, in our study, closed-loop stimulation was dependent upon bladder contractions, and there was more stimulation in the second half of the bladder fill as bladder contractions became more frequent (Figure 4) and this was fundamentally different than an intermittent stimulation paradigm (i.e. stimulation applied in a 10 s on/off schedule) that does not utilize any sensory feedback. Clinical studies of dorsal genital nerve stimulation also suggest that stimulation only after the urge to void, for as short as 30s in duration, can lead to mean subjective improvements of 73% in the incontinence score [17]. Compared to these closed-loop strategies, our method does not require patient intervention and uses a sensor implanted near the stimulation site.

An increased NVC frequency or a decreased NVC interval are often associated with overactive bladder in pre-clinical models [96]. While it is unclear whether NVCs occur more often in human patients with OAB, NVCs activate the same bladder sensory neurons as voiding contractions and can therefore elicit an unnecessary urge for voiding that needs to be suppressed [105]. In this study, we demonstrated that both closed-loop stimulation and continuous SNM led to a lower number of non-voiding contractions per filling cycle, indicating that contractions were

inhibited. Also, closed-loop stimulation increased the interval between contractions compared to the no-stimulation group while slightly decreasing the number of NVCs per trial, which suggests a redistribution of NVC temporal patterns. It is unclear if this has clinical relevance. We did not expect the peak pressure to increase as a result of stimulation, and our study results were consistent with this expectation. We hypothesize that this outcome is because SNM relaxed the detrusor muscle, rather than tightened the sphincter muscle, which will lead to higher peak pressure. As a result, the overall bladder volume increased while peak pressure stayed consistent across trials.

Five Hz stimulation was chosen for SNM based on frequency optimization trials that were performed in one pilot experiment. The selection of this frequency is consistent with a prior study demonstrating that 5 Hz dorsal root stimulation was optimal for increasing bladder capacity when compared to other frequencies [110] and similar results from another study that concluded 7.5Hz or 10Hz are optimal in minimizing iso-volumetric contractions [97]. This frequency seems to consistently inhibit bladder contractions within felines, as we confirmed a reduced isovolumetric contraction amplitude in all experiments in this study [97]. This use of a stimulation amplitude above motor threshold is common in anesthetized experiments (e.g. [97] achieved similar outcome measures as here; many others use twice motor threshold or higher in animal studies), as it helps mitigate against the suppressive effects of anesthesia. A previous behaving pudendal nerve stimulation study of ours had greater bladder outcomes at a stimulation amplitude that was twice motor threshold, which was well tolerated by the animals when the amplitude was ramped up [112]. Similarly, ramping up and down of SNM stimulation amplitudes has been described as mitigating uncomfortable sensations of stimulation initiation and cessation in clinical subjects [113]. Brink et al. [114] reported that supra-motor threshold

SNM stimulation that increased bladder capacity was successfully used and tolerated in fully conscious large animals. Additionally, this study used normal animals, which may have contributed to the need for higher stimulation amplitudes as compared to an OAB or simulated OAB model.

The NRMSE and R decoding performance (Table 1) for no-stimulation trials was an improvement upon (NRMSE) or consistent with (R) our previously published bladder pressure decoding results (0.28 ± 0.13 and 0.84 ± 0.19, respectively) [105]. As anticipated, closed-loop stimulation increased the NRMSE (0.29, similar to [105]) and decreased the R for bladder pressure estimation, as additional threshold crossings were detected during stimulation (due to possible stimulation artifacts and/or stimulation driven units). Refinement of our cross-channel invalidation may be necessary. Additionally, stimulation itself may have led to a reduction in bladder sensory neuron sensitivity (Figure 6), which would have decreased decoding efficacy during SNM trials. However, it is unclear if sensory feedback is critically necessary during stimulation itself and may not have significantly altered the decision-making process of the closed-loop algorithm.

We did not observe a strong correlation between bladder capacity and the NRMSE for pressure estimation (Figure 5a). Stimulation was only triggered by the closed-loop algorithm based on a relative increase in the bladder pressure, therefore the system could tolerate a small prediction error as well as any amount of baseline offset due to a shift in the noise floor. A large absolute error (or a large NRMSE) might not lead to a high error rate in our closed-loop system, but a low correlation coefficient may indicate a possible loss of channels and lead to inaccurate sensory feedback, less efficient stimulation, and ultimately, lower bladder capacity. The weak but positive correlation between R and normalized bladder capacity suggests that an increase in

bladder capacity may be associated with accurate sensory feedback and the timing of stimulation being applied in closed-loop neuromodulation. The accuracy of identifying bladder contractions was higher in the second half of trials, when stimulation was triggered more often (Figure 4) as the NVC rate increased.

A potential hypothesis for the mechanism of action of SNM is that SNM stimulates sensory pathways, bringing down the level of urgency by inhibiting sensory neural firing [110], [115]. A study in cats showed that stimulating sacral-level dorsal roots inhibits isovolumetric bladder contractions, while stimulating the ventral root did not [110], which is consistent with this hypothesis. In our study, we analyzed the effect of SNM on some bladder sensory neurons (Figure 6, Table 2). For these neurons, we found that the pressure threshold increased and the firing rate as a function of pressure decreased during SNM. This could be a result of a direct effect of the stimulation on the bladder sensory neurons (e.g., collision block) or an indirect effect. We think an indirect effect is more likely given that in 6 /7 of the neurons that responded the stimulation lead was on the opposite side of the recording array. There are several possible mechanisms including inhibition of interneuronal transmission and inhibition of the preganglionic efferent neurons of the micturition reflex [115]. This was a small sample size and one neuron did not follow the trend of the other 7 units, however we believe this warrants additional follow up and may yield important insights into the mechanism of SNM.

Both pre-clinical and clinical neurostimulation evidence suggests that continuous stimulation may not be necessary to deliver optimal improvement in bladder capacity and incontinence [17], [43], [44]. Therefore, it is important to minimize the overall amount of stimulation delivered, as long-term chronic stimulation can facilitate neural habituation [42], reduce the effectiveness of SNM, and result in unwanted and unpleasant sensations [39]. The

methods developed in this study are translatable to clinical use. In this study, DRG were accessed with an invasive laminectomy that is unlikely to be performed clinically. DRG can also be accessed percutaneously at the lumbosacral level, as is done clinically for dorsal root stimulation for pain [100]. A similar approach may allow for less-invasive delivery of a non-penetrating or minimally-penetrating microelectrode within the limited vertebral space around a target DRG. Recent research has demonstrated that DRG cell bodies are more likely to be located near the surface of feline and human DRG [101], [116], and that a thin-film DRG-surface electrode can record neural activity from the bladder in felines [99]. New electrodes with a lower profile and minimal immune response would be more feasible to implement clinically than those used in this study.

An aim of this study was to increase bladder capacity, as low bladder capacity is one of the primary symptoms in overactive bladder. The anesthetized non-OAB animal model described in this paper has several limitations, including preventing a full evaluation of clinical OAB parameters such as urinary frequency, urinary urgency, incontinence episodes, and other symptoms. The non-dysfunctional bladder state of these animals may have limited the improvements that were possible for the bladder measures. It is also possible that anesthesia had a suppressive effect, or the relatively short intervals between bladder fills with different stimulation types had a carry-over effect. Awake testing with a dysfunctional bladder model across multi-week intervals may eliminate these potential confounds and would enable longitudinal comparisons between continuous stimulation and closed-loop stimulation. Our previous pudendal nerve stimulation study [112] demonstrated the feasibility of performing bladder neuromodulation with stimulation at or above motor threshold while recording urodynamic parameters (e.g. cystometry curve, bladder capacity, and voiding efficiency) in a

freely behaving feline model, and in a separate study we have observed bladder units in chronic feline experiments across multiple weeks [117]. Moving forward, experiments using awake, behaving animals may be most useful for evaluating both the acute and chronic effects of closed-loop SNM without the influence of anesthesia, and would allow for assessment of stimulation amplitudes at and below motor threshold.

4.6 Conclusion

We have demonstrated that closed-loop SNM using DRG signals as sensory feedback can lead to a significant increase in bladder capacity in an anesthetized feline model. Our closed-loop approach matched the effectiveness of continuous SNM while using significantly less stimulation time. Additionally, our neural recordings from bladder sensory afferents suggested that SNM may cause a direct or indirect shift in the relationship between bladder sensory neuron firing rates and bladder pressure, which is consistent with a hypothesis that SNM works by reducing bladder afferent activity. Long-term studies with behavioral animal models will mitigate the effects of anesthesia and repeated bladder fills in a short time frame, and will be critical as a bridging translational step prior to clinical studies.

4.7 Data Availability

Raw data and analysis software code are available at https://osf.io/jq5hn/.

Chapter 5 Behavioral Monitoring and Neuromodulation of Feline Voiding Function

5.1 Abstract

Neuromodulation is a standard treatment for bladder dysfunction. Although preclinical studies continue to develop new approaches, these experiments are often performed under anesthesia that can affect normal bladder system activity. The goal of this study was to evaluate the use of typical neuromodulation parameters in an awake, behaving large-animal model. During an aseptic surgery, catheters were inserted into the bladder of two male felines and a cuff electrode was placed around the left pudendal nerve. Catheters and electrode leads were housed in an enclosure mounted on the lower back. After recovery, test sessions in an open enclosure were performed approximately weekly. In each session, body-temperature saline was infused while the bladder pressure was monitored until the animal voided one or more times. During some bladder fills, electrical stimulation of the pudendal nerve was applied (5 or 33 Hz; 1.5 or 2 x motor threshold - MT) to determine whether stimulation parameters affected the interval between voiding events or the voiding efficiency. Animals tolerated supra-threshold stimulation as long as the current was slowly increased to a target level. Five Hz stimulation increased the voiding interval over 33 Hz and no stimulation trials while 33 Hz stimulation at 2 MT led to a greater voiding efficiency. These results follow trends observed in non-behavioral studies, and support the use of this animal model in further translational bladder neuromodulation research.

5.2 Introduction

Neuromodulation is a standard treatment for bladder dysfunction after conservative approaches have failed. Most preclinical bladder neuromodulation studies are performed using anesthetized animal models [97], [118]–[120]. Anesthesia not only suppresses voluntary control but also alters the autonomic control of the bladder [121]–[123]. Many anesthetized studies use high stimulation amplitudes well above thresholds for activating motor fibers [97], [118]–[120]. It is not well reported whether these amplitudes are tolerated by awake, behaving animals. For clinical implementation of preclinical developments, it is critical that necessary stimulation levels are fully tolerable. Only a few studies have used non-anesthetized bladder neuromodulation models, such as an immobile spinal cord injury feline model [124], [125], a diabetic rat model [126], and a stationary sheep model [114], in part due to the challenges of instrumenting and performing experiments with behaving animals. To our knowledge, there are no studies reporting the effect of neuromodulation on bladder function in a fully mobile large animal. This is a valuable preclinical model that has utility for a variety of bladder dysfunction types [127]. In this pilot study with awake, behaving felines, we demonstrated that supra-threshold stimulation is tolerable and that bladder function can be modulated depending on the stimulation parameters.

5.3 Methods

5.3.1 Surgical Procedures

All experimental procedures were approved by the University of Michigan Institutional Animal Care and Use Committee. Aseptic techniques were used for all surgical procedures, which were performed in a total of 4 animals. The first two animals did not have a pudendal nerve cuff

implanted, as detailed below, and had behavioral bladder monitoring sessions without nerve stimulation for an external collaboration. These animals are not discussed further here. The third and fourth animals underwent all procedures described in this chapter.. These primary animals (Experiments 1 & 2) were two male, domestic, short-hair felines (age: 1.0 years each; weight 6.4 and 5.1 kg; Liberty Research, Inc.). Prior to surgery, they were anesthetized with a mixture of ketamine (6.6 mg/kg)- butorphanol (0.66 mg/kg)-dexmedetomidine (0.033 mg/kg) administered intramuscularly, intubated, and then maintained on isoflurane anesthesia (0.5-4%) during surgical procedures. Respiratory rate, heart rate, end-tidal CO_2, O_2 perfusion, and temperature were monitored continuously using a vitals monitor (Surgivet, Smiths Medical). Fluids (1:1 ratio of lactated Ringers solution and 5% dextrose) were infused intravenously via the cephalic vein at a rate of 5-10 ml/kg/hr. After a laparotomy, two catheters (1 mm inner diameter, Silastic 508-005, Dow Corning) with injection ports mounted on the end were inserted into the bladder dome and secured in place with purse-string sutures. The catheter ends in the bladder were modified to have an arrow-like profile, with side wings that provided anchors inside the bladder. The catheters were tunneled subcutaneously to a dorsal midline incision just rostral to the tail. A custom-made bipolar electrode cuff (2 mm inner diameter) was placed around the left pudendal nerve via a postero-lateral incision. Catheter ports and electrode connections were housed within a 3-D printed photopolymer resin backpack (Formlabs) mounted rostral to the tail [117]. To mount the backpack, a stainless-steel base plate was secured under the skin to the iliac crests, with stainless steel wire wrapped around bone screws embedded in the bone. The housing of the backpack was screwed into four transcutaneous posts of the baseplate after all incisions were closed. Figure 25 shows a radiograph for one animal two weeks after surgery. After surgery completion, felines were weaned off anesthesia and ventilation and allowed to wake up on their

own. Each feline was monitored for at least 5 days after surgery before testing sessions were started. A feline was considered recovered from surgery when it was walking, eating, and behaving normally. Analgesics were administered for 3 days during the post-surgery period. Animals were free-range housed with 2–4 fellow felines in a 413 ft^2 room with controlled temperature (19–21 °C) and relative humidity (35– 60%), food and water available ad lib, and a 12 hr light/dark cycle. Enrichment was provided by toys and daily staff interaction.

5.3.2 Awake Testing Sessions

Test sessions were conducted approximately weekly in an enclosure consisting of two adjoined animal playpens (each with eight linked 0.61-m width by 1.22-m height panels) containing a litter box, non-absorbable litter, wet and dry food, and enrichments to encourage movement of the animal. Animals were either directly put in the cage or sedated first by an intramuscular injection of dexmedetomidine (0.019– 0.039 mg/kg, Dexdomitor, MWI Veterinary Supply). Pressure lines were connected to the catheter ports prior to testing and were hung from the ceiling to reduce tangling and provide strain relief (Figure 26). Bladder pressure was recorded by connection of fluid-filled tubing to the catheters, with one catheter also used as an infusion line. All pressure lines were flushed prior to experimentation to verify catheter patency. Pressure lines were connected to transducers (DPT-100, Utah Medical Products) and recorded with a PowerLab 8/35 (ADInstruments) or Grapevine Neural

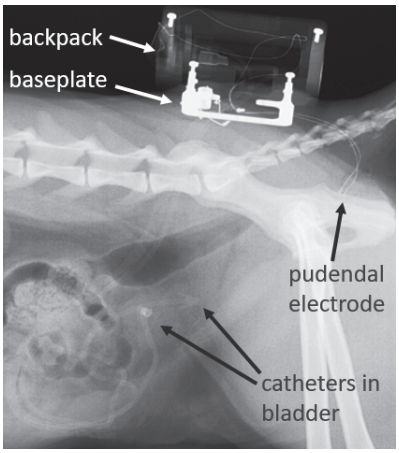

Figure 25. Radiograph of Experiment 1 feline showing implanted materials.

Interface Processor (Ripple) at 1 kHz. An isolated Pulse Stimulator (Model 2100, A-M Systems) was connected to the wires of the pudendal cuff electrodes with alligator clips for delivering electrical stimulation. A push-button input to the recording system was used to track stimulus initiation and termination. The motor threshold (MT) was evaluated in each test session by identifying the minimum stimulation amplitude that elicited visible external anal sphincter contractions. If sedated, animals were injected intramuscularly with Antiseden (0.19–0.38 mg/kg, MWI Veterinary Supply) to reverse the effects of dexmedetomidine to begin the test session. Data recording began upon full awakening of the animal. Each test session consisted of one trial, where each trial consisted of multiple voiding events as a result of continuous infusion. In all test sessions, 41 °C sterile saline was infused at 0.5 ml/min into the bladder using a syringe pump (AS50 Infusion Pump, Baxter International). Bladder pressure was measured continuously. Electrical stimulation was only delivered in a subset of bladder fills, applied continuously from the end of a previous void to the end of the current void. The stimulation amplitude was constant within a test session, set at 1.5 or 2.0 of the MT. The frequency during stimulation was either 5 Hz or 33 Hz with 200 μs pulse width. Stimulation frequency and amplitude combinations were randomized across trials. The stimulation amplitude was increased slowly, to limit pain or behavioral effects for the animal. In later sessions, nonabsorbable litter (Kit4Cat) was used to allow for manual collection of urine and more accurate measurement of voided volumes. Test sessions were recorded with video (C920 webcam, Logitech) for identifying voiding events and analyzing behavior. Animals were also continuously monitored with video in their housing room for overall health and behavior after implant procedures.

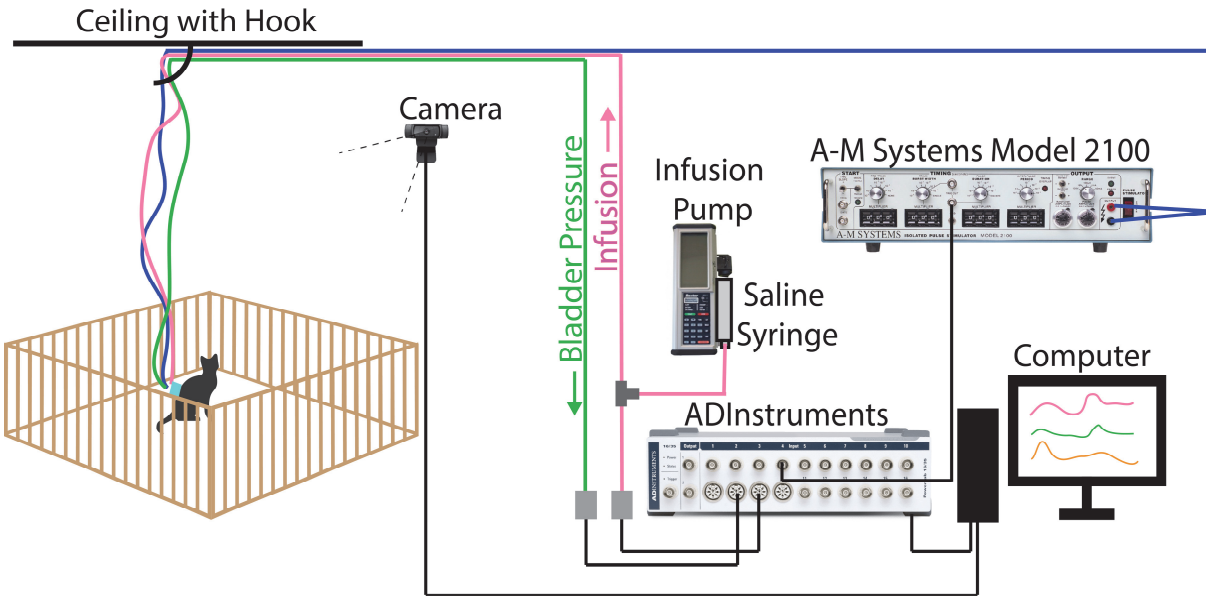

Figure 26. Experimental test setup. Bladder infusion and pressure

5.3.3 Data Analysis

Voiding intervals were calculated by determining the onset of each void based on reviewing the session video and bladder pressure data. Voiding efficiencies were calculated by dividing the voided volume by the infused volume plus an estimate of urine generated (1.1 ml/kg/hr [128]). Efficiencies were normalized within animals, to account for the assumed constant urine generation rate yielding efficiencies over 100% for a few voids. A two-way ANOVA with pair-wise comparisons was performed to evaluate the effect of frequency and amplitude on voiding interval and efficiency. Statistical significance was determined for $\alpha = 0.05$.

5.4 Results and Discussion

In total, four animals received implants and underwent test sessions. The first two animals were used to develop behavioral bladder monitoring procedures and an external collaboration, and

data from these experiments are not reported here. For the two primary animals, ten sessions (9.2 ± 4.8 d interval) were recorded for the first animal (Experiment 1) and five (7.0 ± 1.6 d interval) for the second animal (Experiment 2), yielding 94 voids. Voiding efficiencies were obtained for 77 of these trials (82%). All data can be found at https://osf.io/v96kg/.

5.4.1 Awake Behavior and Motor Thresholds

Across test sessions, no signs of pain were observed as a result of stimulation. When no stimulation was applied, the animals walked around, rested, ate food, or played. At low stimulation amplitudes, there was no noticeable change in behavior. As the stimulation amplitude was slowly ramped to ~0.25 MT, the animal typically paused their current activity then resumed or walked around, suggesting perception. In some cases, the animal groomed their pelvic region. As the stimulation was increased to above MT, scrotum twitching became visually noticeable for 5 Hz stimulation. In a few trials, voluntary or involuntary left leg extension was observed while the animal was sitting or eating. However, no signs of pain were observed, such as vocalization, withdrawal, or shivering. Animals tolerated being in the enclosure for up to 2.3 hr. The MT had a decreasing trend over time in both animals (Figure 27). The average MT were 285.0 ± 56.4 μA and 494 ± 107.8 μA, for Experiments 1 and 2 respectively. These levels are comparable to those reported for anesthetized studies with a similar setup [118]. The presence of the implant system itself modified overall animal behavior. During a multi-day observation period, the Experiment 1 feline visited a litter box every 2.1 hr on average, with 18.9% of voids occurring within 10 min of waking from sleep. The Experiment 2 feline had a shorter mean inter-void interval of 0.6 hr, with 18.2% of voids occurring within 10 min after waking. This contrasts with prior to surgery, as voiding intervals of 5.2 ± 3.7 hr and 3.3 ± 3.8 hr were observed for the two felines across a

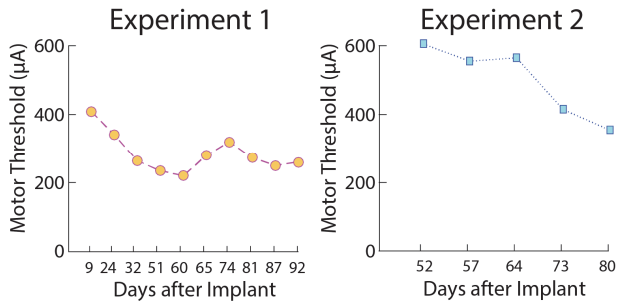

Figure 27. Motor thresholds per testing date for each experiment.

24-hour period, with no voids within ten minutes of waking. We expect that a combination of the catheter within the bladders causing some irritation and general scarring around the implants led to a reduction in functional bladder volume.

5.4.2 Behavioral Bladder Pressure Monitoring

Awake bladder pressure traces were obtained for each session. Signal artifacts due to movement were not significant, particularly compared to pressure changes during a bladder contraction for voiding. Figure 28 shows an example test session with multiple voids during periods of no stimulation and neuromodulation. The general characteristics of non-voiding contractions and voiding contractions were similar to those reported in anesthetized felines [91], [96]. However, we observed that the contraction amplitudes were generally higher (40–100 cmH_2O) than reported levels for anesthetized voids, and the onset of voiding contractions was often more rapid (data not reported). These observations support that anesthesia has a general suppressive effect on bladder activity. Our setup did not allow the pressure transducer to move with animals. Thus, changes in posture could affect the relative pressure reading against the fixed-location transducers. During initial testing, we used a modified backpack that allowed for on-animal mounting of pressure transducers however, this was cumbersome for the animal and created stress.

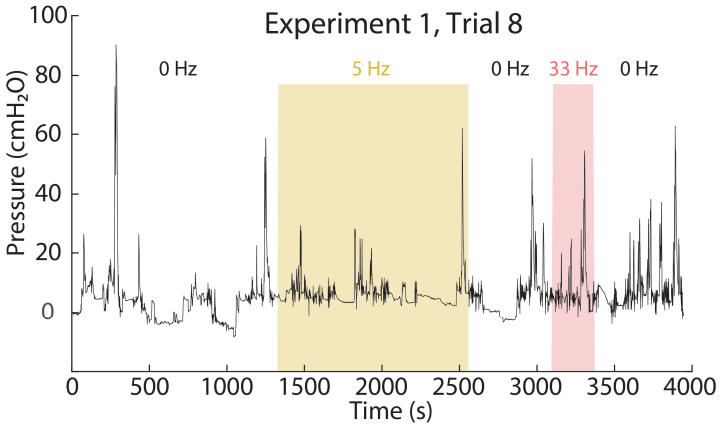

Figure 28. Example session with multiple voids across no-stimulation

5.4.3 Stimulation Effect on Voiding

We observed that the voiding interval can be modulated by stimulation frequency and amplitude. Stimulation at 5 Hz increased the median voiding interval for both 1.5 MT and 2 MT compared to no-stimulation and 33 Hz stimulation voids, with 2 MT yielding a stronger effect (Figure 29). This observation aligns with previous anesthetized studies showing that increasing the stimulation amplitude leads to greater inhibition of bladder activity [120], [124], and that 5 Hz is effective at increasing the voiding interval or bladder capacity [97], [120]. We also found that the voiding efficiency can be modulated, with the stimulation amplitude having a greater effect than the frequency (Figure 30, Table 10). At 1.5 MT, the median voiding efficiency showed a slight decrease for both 5 Hz and 33 Hz voids compared to no stimulation. At 2 MT, the voiding efficiency was significantly greater than at 1.5 MT ($p = 0.017$, Table 11). Only 33 Hz at 2 MT increased the median voiding efficiency as compared to no stimulation periods, though the difference was not significant. The use of 33 Hz for increasing voiding efficiency aligns with prior studies with anesthetized animals [118], [119]. Regardless of stimulation amplitude, 5 Hz stimulation consistently resulted in longer voiding intervals and lower voiding efficiencies compared to 33 Hz. Regardless of stimulation frequency, 2 MT consistently resulted in both higher voiding intervals and higher voiding efficiencies. This suggests that higher-amplitude stimulation can potentially deliver better overall clinical results if

given at a tolerable level. In contrast, there may not be a single stimulation frequency that most effectively modulates all urodynamic parameters, as different stimulation frequencies may be necessary to maximize clinical utility for both continence and micturition

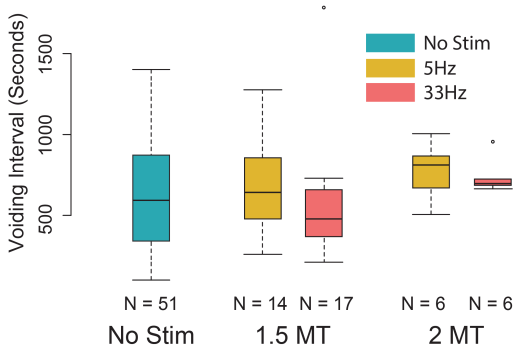

Figure 29. Effect of stimulation amplitude and frequency on interval between voids. Box plots indicate median values (middle line), 25th and 75th percentiles (lower and upper edges of boxes = interquartile range IQR), and minimum and maximum values (lower and upper error bars), with outliers that are 3 x IQR outside the 25th or 75% percentile indicated by individual dots.

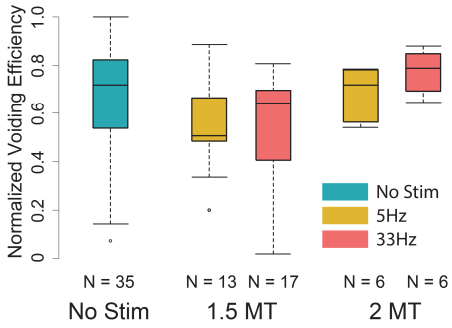

Figure 30. Effect of stimulation amplitude and frequency on normalized voiding efficiency. Data within box plots as in Figure 29.

Table 10. ANOVA Results(p-values) for Effect of Neuromodulation on Voiding Parameters

Factor	Voiding Interval	Voiding Efficiency
Frequency (no stim, 5 Hz, 33 Hz)	0.366	0.304
Amplitude (no stim, 1.5 MT, 2 MT)	0.208	0.034
Frequency x Amplitude	0.605	0.299

Table 11. Stimulus Amplitude Pair-wise Comparison Results (p-values) for Effect of Amplitude Alone on Voiding

Factor Level Combination	Voiding Efficiency
No Stimulation – 1.5 MT	0.514
No Stimulation – 2 MT	0.107
1.5 MT – 2 MT	0.017

5.5 Conclusion

This is the first study to investigate the effect of neuromodulation on bladder function in a healthy, behaving large-animal model. We found that in an awake animal, stimulating the pudendal nerve as high as 2 MT is well tolerated and can result in improved voiding efficiency and longer voiding intervals. While 5 Hz was preferential for continence-like effects such as increasing the voiding interval, 33 Hz was preferential for enhancing micturition, as has been reported previously. Further study, with a larger sample size will allow for increased quantification of urodynamic parameters, a wider exploration of the stimulation parameter space, and evaluating conditional rather than continuous stimulation.

Chapter 6 Discussion and Future Directions

6.1 Summary of Main Findings and Discussion

This dissertation work closely examined the feasibility of using DRG neural recordings as sensory feedback for closed-loop neuromodulation of bladder function. Built upon prior knowledge of bladder afferent neurons, this work further explored their potential for use as sensory feedback in closed-loop control through algorithm development and evaluation, real-time decoding implementation, proof-of-concept demonstration, and ended with method development for awake and behaving animal experiments as a steppingstone towards more advanced animal models and clinical translation.

The first study (Chapter II) found that both algorithm and feature selection methods were significant in affecting bladder pressure decoding accuracy. State dependent, non-linear models performed better in both absolute pressure estimation and correlation coefficient (CC) compared to a non-state-dependent linear model. This result aligned with the original hypothesis because state dependent models addressed the hysteresis relationship between bladder afferent signals and pressure and smoothed out firing rate fluctuations of the noise floor by weighing in the previous state estimation. More specifically, a recursive Kalman filter yielded a higher average correlation coefficient (CC) to the measured pressure compared to both linear regression and a one-hidden-layer neural network model, and was successfully implemented in the closed-loop system that used relative pressure increase in later experiments (Chapter III).

While a Kalman filter has been widely used for brain computer interfacing and peripheral nerve motor intent decoding in the past [64], [129], this is the first time such an algorithm was optimized and implemented to estimate the state of an autonomic organ and shown to be superior to a linear model. It is important to note that other non-linear algorithms have been tuned offline for bladder pressure or volume decoding [79], [89], [90], [130] (around the same time this study was published), using intraneural dorsal horn or less selective extraneural pudendal and pelvic nerve activities, but these sensory targets do not guarantee sensory-only information and have low translational value, as they have infrequently been successfully accessed for clinical therapy delivery. While it is exciting to see methods being developed to decode bladder pressure from various other targets with similar results to this study, intraneural DRG signals remains a highly possible sensory feedback site for use in clinical translation of closed-loop neuromodulation.

Another promising finding was that single unit neural signals, even with their high specificity and lack of noise, provided a comparable decoding performance as threshold crossings activity [53], a conclusion that is consistent with previous cortical interfacing studies [58], [80]. With similar signal qualities, threshold crossings are a more appealing algorithm choice because they are computationally cheaper to process and potentially more stable in the long-term. Due to the slow rhythm of the bladder, larger firing rate calculating intervals (1-2 seconds) yielded smoother firing rates and improved estimations, especially CC, by providing more channels with correlated firing rates. This work also provides the first proof-of-concept for decoding bladder pressure from neural recordings using an algorithm based on data collected at an earlier date in a chronic implant. Overall, this study (Chapter II) selected the optimal algorithm and corresponding parameters to calculate bladder pressure from DRG signals; the

pressure estimate can potentially be implemented for closed-loop application, leading to the next study with a focus on real-time algorithm testing.

The second study (Chapter III) showed a successful implementation of the optimized decoding method from the prior study (Chapter II) in real-time under both healthy and simulated OAB conditions. The simulated OAB model presented a significant reduction in bladder capacity and an earlier onset of non-voiding contractions (NVCs) compared to the healthy model. It is beneficial to use such a model in anesthetized experiments, as anesthesia normally increases bladder capacity and potentially suppresses bladder afferent activities, but bladder irritants can have an opposing effect based on empirical observations from the study. This is the first study to use neural signals for bladder state decoding in real-time (or online). As the primary result, online decoding yielded a comparable correlation coefficient and absolute pressure estimation compared to prior offline bladder pressure decoding literature [53], [79], [89]–[91], [130]. A post-hoc analysis was performed to understand the source of errors that contributed to the gap between the estimation and measurement, and the results showed the shift in baseline firing rates from training to testing trials was the most common cause of an error in absolute pressure estimation. As an unexpected finding, this study suggests that an irritant like acetic acid is correlated with a general increase in the sensitivity of both threshold crossings and single units, leading to an improved decode. This increased sensitivity could be due to greater activation of bladder neurons by the irritant or a secondary effect of a faster rise in the bladder pressure due to an effectively smaller bladder. This observation is supported by a prior study comparing pelvic nerve activity between acetic acid and saline fills in a rat model [94]. However, a study using a different irritant (Prostaglandin E2, or PGE2) showed that decoding using a saline fill model in a PGE2 trial resulted in underestimation of pressure, which was corrected by incorporating PGE2

in the training model [89]. At the end, two pilot closed-loop trials showed potential of this approach by demonstrating a 40% bladder capacity increase (n=2) compared to the baseline. Real-time decoding from lumbar-level DRG has been done in the past for closed-loop limb control in a controlled, anesthetized setting [54]. Although also under a very controlled environment, this study is the first time that DRG signals have been used to demonstrate effectiveness in closed-loop control of bladder capacity. While pudendal nerve stimulation, as seen in this study, has been used to manage OAB symptoms, the sacral root is a much more prevalent and established clinical target.

The third study (Chapter IV) demonstrated the short-term efficacy of DRG signal-based closed-loop SNM for increasing bladder capacity. The study showed that closed-loop SNM significantly increased bladder capacity compared to no stimulation. This increase was comparable to continuous stimulation while reducing over half of the stimulation time. In closed-loop trials, the total stimulation delivered in the last 25% of the bladder fill was almost the same amount as the total stimulation delivered in the first 75% of the fill, when the bladder was mostly quiescent. While previous closed-loop studies using direct pressure measurements have pointed to similar conclusions [131], [132], this is the first time that recordings from DRG have been used as sensory feedback for closed-loop bladder control. If translatable, our results suggest that closed-loop SNM could have a potential clinical impact by providing automated, individualized therapy that is linked to objective, physiological signals, a potential extension in device longevity due to less battery drain during stimulation, though the power needed to control the algorithm is yet to be studied. Additionally, our results suggest that SNM may desensitize bladder sensory neurons to changes in bladder pressure. This potential mechanism of SNM may be an important contributor to its therapeutic benefit and warrants further exploration.

Moving from algorithm development [91] to real-time bladder pressure decoding [105], and eventually closed-loop SNM [133], this dissertation systematically demonstrates that DRG signals are a promising source of sensory feedback to improve SNM therapy for OAB symptoms. Prior closed-loop work with similar neurosensory feedback goals used whole nerve cuff recordings from the pudendal [44] or sacral nerves [51], which contain motor components and low sensory signal selectivity. While these studies provided moderate-quality feedback that delayed voiding events [44] and suppressed isovolumetric contractions [51] acutely in controlled, anesthetized animal models, whole nerve recordings are unlikely to yield high fidelity signals during long-term survival experiments. Other closed-loop neuromodulation work used non-neural feedback, such as external anal sphincter muscle EMG (in SCI patients) [47], bladder volume [43], and patient on-demand feedback [17], [134], some of which has advanced to clinical evaluations and yielded positive results [17], [47], [134], [135]. These are promising sensory feedback options; however, EMG does not directly reflect bladder sensory information; bladder volume is difficult to measure accurately especially when the volume is low under OAB conditions and does not necessarily reflect urgency; and patient on-demand control ultimately leads to more patient burden as compared to a fully automated closed-loop system. In comparison, multi-channel recordings from DRG signals offer the potential for direct bladder state monitoring while minimizing patient involvement.

The first three chapters of this dissertation advanced the field as they improved neurosensory feedback for bladder control by integrating bladder sensory information from multi-channel intraneural signals, obtaining high robustness in bladder state estimation and potential usability in behaving models. While advanced bladder state decoding and algorithm optimization has been performed in prior studies using various neurosensory targets, such as the

lumbosacral dorsal horn [90], [130] and pudendal nerve trunk [79], and yielded similar decoding accuracy compared to DRG decoding, these studies did not advance to real-time or even closed-loop demonstration.

The final study (Chapter V) developed an awake testing protocol for ambulatory monitoring of urodynamic parameters during neuromodulation in felines. Bladder pressure and voiding events were successfully measured in four animals while the animals were moving and behaving with minimal restriction. Voiding efficiency and bladder capacity were calculated for two animals that voided with or without pudendal nerve stimulation, which were focused on in this dissertation. The neuromodulation effect of 5 Hz on bladder capacity and 33 Hz on voiding efficiency and bladder excitation in awake felines was consistent with conclusions drawn from anesthetized studies [97], [118]–[120]. Not only did this pilot study yield comparable results as prior anesthetized studies but it also provided a steppingstone towards closed-loop studies in awake and behaving animal models. This is the first study to investigate the effect of neuromodulation on bladder function in a healthy, behaving large-animal model. This is a step forward from previous neuromodulation studies, which were either performed under sedation or anesthesia [97], [118]–[120], or an awake setting but the animals were immobilized [114], [125]. Achieving this milestone has opened up the possibility of testing advanced closed-loop neuromodulation paradigms in more clinically relevant animal models.

6.2 Future Directions

Moving forward, further tuning of the closed-loop control is crucial in more advanced models. Towards that, we are evaluating closed-loop SNM in awake, behaving felines. This new study has a secondary goal of improving the understanding of DRG signal composition and the effect

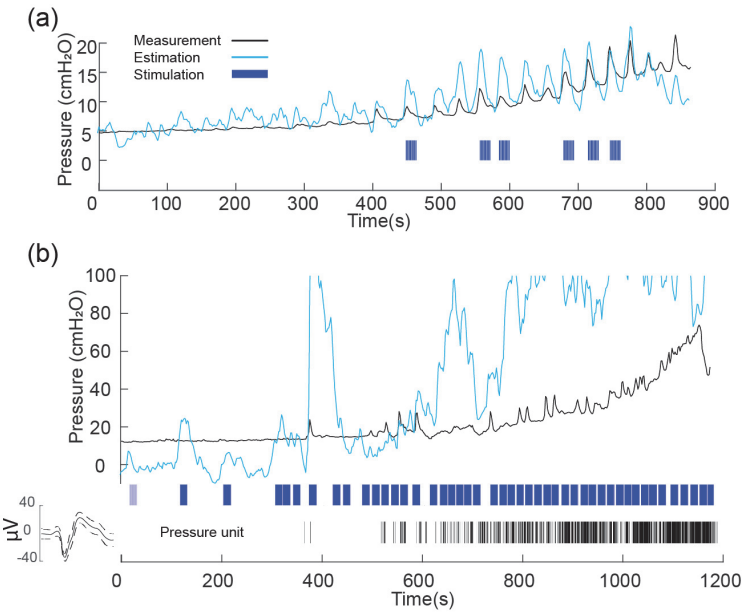

Figure 31. (a) Closed-loop pudendal nerve stimulation under alfaxalone anesthesia. The correlation coefficient (R) for the pressure estimation was 0.82. (b) Behavioral closed-loop SNM. R for the pressure estimation was 0.71. In both cases, stimulation was turned on for 15 seconds after a 5 cmH₂O increase was observed in a sliding 4 second window. Spike raster shown for example bladder unit at bottom.

of neuromodulation on DRG signals over time. Preliminary results from a sedated chronic-implant experiment have shown the possibility of closed-loop control (Figure 31a) using chronically implanted electrode arrays. DRG bladder units have been identified in behavioral closed-loop trials, however there was a lower signal-to-noise ratio (SNR) due to motion artifacts (Figure 31 b). A lower SNR might be addressed by common referencing, a more advanced artifact rejection and signal selection algorithm, and hardware improvements to maintain feedback accuracy. Chronic decoding robustness may also be improved by applying information theory. Our collaboration with Imperial College London showed that bladder afferent neurons can be classified into three primary types that contain almost mutually exclusive information in bladder pressure, and that decoding from pooled types and activity clusters is robust against neuron loss [60].

From a translational aspect, the risk of surgery complication associated with interfacing with DRG in addition to the sacral nerve must be minimized. DRG may be accessed percutaneously at the lumbosacral level [100], as opposed to through a laminectomy procedure as done in this study, to minimize surgery invasiveness. In addition, intraneural recording might not be a requirement, as recent research has demonstrated that DRG cell bodies are more likely

to be located near the surface of the DRG [101], and that a thin-film surface electrode can record bladder pressure single units [99]. It may be possible to interface with the DRG through the same or a similar electrode insertion process as SNM lead placement. Further studies are needed to examine this approach, in large animal models. Closed-loop stimulation may reduce unpleasant stimulation sensations that have been reported for some patients receiving standard SNM by reducing the amount of total stimulation time. However, a ramp-up transition between stimulation off and on epochs during adaptive SNM is likely necessary, as repeated stimulation initiation events may be uncomfortable to patients [134].

Signal stability in chronic experiments is crucial to the robustness of the closed-loop system, but it has not been fully demonstrated yet in our animal model due to neural signal loss and electrode migration over time [117]. While penetrating arrays used in this dissertation have yielded high signal selectivity, stable chronic DRG recording across months or even years will require the recording interface to be uniquely tailored to the mechanical and neuroanatomical properties of DRG to minimize tissue scarring and neuronal damage. Initial work in this direction such as high-density thin film electrodes [99], [136] and carbon fiber electrodes [137], [138] have been developed and tested acutely in animal models.

Finally, closed-loop neuromodulation with objective biomarkers is undoubtedly where the field is heading to provide improved, more efficient, and individualized therapy for all patients with varying levels of OAB symptoms. OAB can ultimately be eliminated by identifying the biomarkers that reflect the disease state and dosing electrical stimulation accordingly. The success of this method relies on more advanced hardware and algorithms that will likely be based on this dissertation work.

Bibliography

[1] E. Leron, A. Y. Weintraub, S. A. Mastrolia, and P. Schwarzman, "Overactive Bladder Syndrome: Evaluation and Management," *Current Urology*, vol. 11, no. 3. S. Karger AG, pp. 117–125, Mar. 01, 2018, doi: 10.1159/000447205.

[2] D. Irwin, Z. Kopp, B. Agatep, I. Milsom, and P. Abrams, "Worldwide prevalence estimates of lower urinary tract symptoms, overactive bladder, urinary incontinence and bladder outlet obstruction," *BJU Int.*, vol. 108, no. 7, pp. 1132–1139, 2011, doi: 10.1111/j.1464-410X.2010.09993.x.

[3] M. G. Willis-Gray, A. A. Dieter, and E. J. Geller, "Evaluation and management of overactive bladder: strategies for optimizing care," *Res. Reports Urol.*, vol. 8, pp. 113–122, 2016, doi: 10.2147/RRU.S93636.

[4] J. N. Liberman *et al.*, "Health-related quality of life among adults with symptoms of overactive bladder: Results from a U.S. community-based survey," *Urology*, 2001, doi: 10.1016/S0090-4295(01)00986-4.

[5] B. Rebecca, D. Hebel, S. M. Vouri, and J. M. Pitlick, "Mirabegron: A beta-3 agonist for overactive bladder," *Consult. Pharm.*, 2014, doi: 10.4140/TCP.n.2014.823.

[6] B. Orasanu and S. T. Mahajan, "The use of botulinum toxin for the treatment of overactive bladder syndrome," *Indian J. Urol.*, vol. 29, no. 1, pp. 2–11, Jan. 2013, doi: 10.4103/0970-1591.109975.

[7] M. G. Oefelein, "Safety and tolerability profiles of anticholinergic agents used for the treatment of overactive bladder," *Drug Safety*, vol. 34, no. 9. Springer, pp. 733–754, Nov. 20, 2011, doi: 10.2165/11592790-000000000-00000.

[8] T. A. T. T. Marcelissen, M. S. Rahnama'i, A. Snijkers, B. Schurch, and P. De Vries, "Long-term follow-up of intravesical botulinum toxin-A injections in women with idiopathic overactive bladder symptoms," *World J. Urol.*, vol. 35, no. 2, pp. 307–311, Feb. 2017, doi: 10.1007/s00345-016-1862-y.

[9] J. S. Benner *et al.*, "Patient-reported reasons for discontinuing overactive bladder medication," *BJU Int.*, vol. 105, no. 9, pp. 1276–1282, May 2010, doi: 10.1111/j.1464-410X.2009.09036.x.

[10] J. Yeaw, J. S. Benner, J. G. Walt, S. Sian, and D. B. Smith, "Comparing Adherence and Persistence Across 6 Chronic Medication Classes," *J. Manag. Care Pharm.*, vol. 15, no. 9, pp. 728–740, Nov. 2009, doi: 10.18553/jmcp.2009.15.9.728.

[11] C. A. C. Coupland, T. Hill, T. Dening, R. Morriss, M. Moore, and J. Hippisley-Cox, "Anticholinergic Drug Exposure and the Risk of Dementia," *JAMA Intern. Med.*, vol. 179, no. 8, p. 1084, Aug. 2019, doi: 10.1001/jamainternmed.2019.0677.

[12] C. J. Fowler, D. Griffiths, and W. C. De Groat, "The neural control of micturition," *Nat. Rev. Neurosci.*, vol. 9, no. 6, pp. 453–466, 2008, doi: 10.1038/nrn2401.

[13] O. Yokoyama *et al.*, "Overactive bladder - Experimental aspects," in *Scandinavian Journal of Urology and Nephrology, Supplement*, 2002, vol. 36, no. 210, pp. 59–64, doi:

10.1080/003655902320765980.
[14] S. Siegel *et al.*, “Five-Year Followup Results of a Prospective, Multicenter Study of Patients with Overactive Bladder Treated with Sacral Neuromodulation,” *J. Urol.*, vol. 199, no. 1, pp. 229–236, 2018, doi: 10.1016/j.juro.2017.07.010.
[15] B. Blok *et al.*, “A prospective, multicenter study of a novel, miniaturized rechargeable sacral neuromodulation system: 12-month results from the RELAX-OAB study,” *Neurourol. Urodyn.*, vol. 38, no. 2, pp. 689–695, Feb. 2019, doi: 10.1002/nau.23892.
[16] F. F. Farag, F. M. J. Martens, N. J. M. Rijkhoff, and J. P. F. A. Heesakkers, “Dorsal genital nerve stimulation in patients with detrusor overactivity: A systematic review,” *Current Urology Reports*, vol. 13, no. 5. Springer, pp. 385–388, Oct. 03, 2012, doi: 10.1007/s11934-012-0273-x.
[17] H. M. K. Van Breda, F. F. Farag, F. M. J. Martens, J. P. F. A. Heesakkers, and N. J. M. Rijkhoff, “Subject-Controlled, On-demand, Dorsal Genital Nerve Stimulation to Treat Urgency Urinary Incontinence; A Pilot,” *Front. Neurosci.*, vol. 10, no. FEB, pp. 1–7, 2016, doi: 10.3389/fnins.2016.00024.
[18] H. B. Goldman *et al.*, “Dorsal genital nerve stimulation for the treatment of overactive bladder symptoms,” *Neurourol. Urodyn.*, 2008, doi: 10.1002/nau.20544.
[19] B. Farhan, A. Ahmed, R. Dutta, and G. Ghoniem, “Scient Open Access Exploring the World of Science Percutaneous Tibial Nerve Stimulation in Urology: Overview.” Accessed: Oct. 13, 2020. [Online]. Available: www.scientonline.org.
[20] “Overactive Bladder (OAB) Guideline - American Urological Association.” https://www.auanet.org/guidelines/overactive-bladder-(oab)-guideline (accessed May 05, 2020).
[21] A. N. Herrity, C. S. Williams, C. A. Angeli, S. J. Harkema, and C. H. Hubscher, “Lumbosacral spinal cord epidural stimulation improves voiding function after human spinal cord injury,” *Sci. Rep.*, vol. 8, no. 1, Dec. 2018, doi: 10.1038/s41598-018-26602-2.
[22] S. A. MacDiarmid, M. S. John, and P. B. Yoo, “A pilot feasibility study of treating overactive bladder patients with percutaneous saphenous nerve stimulation,” *Neurourol. Urodyn.*, vol. 37, no. 5, pp. 1815–1820, Jun. 2018, doi: 10.1002/nau.23531.
[23] J. Yamashiro, W. de Riese, and C. de Riese, “New implantable tibial nerve stimulation devices: Review of published clinical results in comparison to established neuromodulation devices,” *Research and Reports in Urology*, vol. 11. Dove Medical Press Ltd., pp. 351–357, 2019, doi: 10.2147/RRU.S231954.
[24] J. Groen and J. L. H. R. Bosch, “Neuromodulation techniques in the treatment of the overactive bladder.”
[25] D. A. W. Janssen, F. M. J. Martens, L. L. de Wall, H. M. K. van Breda, and J. P. F. A. Heesakkers, “Clinical utility of neurostimulation devices in the treatment of overactive bladder: Current perspectives,” *Medical Devices: Evidence and Research*. 2017, doi: 10.2147/mder.s115678.
[26] C. K. Moore, J. J. Rueb, and S. Derisavifard, “What Is New in Neuromodulation?,” *Current Urology Reports*. 2019, doi: 10.1007/s11934-019-0920-6.
[27] L. L. de Wall and J. P. F. A. Heesakkers, “Effectiveness of percutaneous tibial nerve stimulation in the treatment of overactive bladder syndrome,” *Research and Reports in Urology*. 2017, doi: 10.2147/RRU.S124981.
[28] K. M. Peters *et al.*, “Randomized Trial of Percutaneous Tibial Nerve Stimulation Versus Sham Efficacy in the Treatment of Overactive Bladder Syndrome: Results From the

SUmiT Trial," *J. Urol.*, 2010, doi: 10.1016/j.juro.2009.12.036.
[29] K. M. Peters, D. J. Carrico, L. S. Wooldridge, C. J. Miller, and S. A. MacDiarmid, "Percutaneous tibial nerve stimulation for the long-term treatment of overactive bladder: 3-year results of the STEP study," *J. Urol.*, 2013, doi: 10.1016/j.juro.2012.11.175.
[30] J. Salatzki *et al.*, "Factors influencing return for maintenance treatment with percutaneous tibial nerve stimulation for the management of the overactive bladder," *BJU Int.*, 2019, doi: 10.1111/bju.14651.
[31] M. Te Dorsthorst, M. van Balken, and J. Heesakkers, "Tibial nerve stimulation in the treatment of overactive bladder syndrome: technical features of latest applications," *Curr. Opin. Urol.*, 2020, doi: 10.1097/MOU.0000000000000781.
[32] M. Tutolo, E. Ammirati, and F. Van der Aa, "What Is New in Neuromodulation for Overactive Bladder?," *European Urology Focus*, vol. 4, no. 1. Elsevier B.V., pp. 49–53, Jan. 01, 2018, doi: 10.1016/j.euf.2018.04.019.
[33] K. Amin, D. Moskowitz, K. C. Kobashi, U. J. Lee, and A. Lucioni, "Do Patients Discontinue Overactive Bladder Medications after Sacral Neuromodulation?," *J. Urol.*, vol. 201, no. 5, pp. 973–978, 2019, doi: 10.1097/JU.0000000000000035.
[34] A. Yehoshua, B. P. Murray, S. P. Vasavada, and P. K. Sand, "Comparing direct medical costs of onabotulinumtoxina with other common overactive bladder interventions," *Am. J. Pharm. Benefits*, 2018.
[35] C. W. Lo, M. Y. Wu, S. S. D. Yang, F. S. Jaw, and S. J. Chang, "Comparing the efficacy of onabotulinumtoxinA, sacral neuromodulation, and peripheral tibial nerve stimulation as third line treatment for the management of overactive bladder symptoms in adults: Systematic review and network meta-analysis," *Toxins*, vol. 12, no. 2. MDPI AG, 2020, doi: 10.3390/toxins12020128.
[36] L. P. Berthelot *et al.*, "Do failure of posterior tibial nerve stimulation precludes to use sacral neuromodulation in patient with overactive bladder?," *Int. Neurourol. J.*, 2019, doi: 10.5213/inj.1938118.059.
[37] L. Meng *et al.*, "Analysis of the Correlation Between the Clinical Effect of Sacral Neuromodulation and Patient Age: A Retrospective Multicenter Study in China," *Neuromodulation Technol. Neural Interface*, Mar. 2020, doi: 10.1111/ner.13130.
[38] K. M. Peters, P. Kandagatla, K. A. Killinger, C. Wolfert, and J. A. Boura, "Clinical outcomes of sacral neuromodulation in patients with neurologic conditions," *Urology*, vol. 81, no. 4, pp. 738–744, 2013, doi: 10.1016/j.urology.2012.11.073.
[39] S. Siegel *et al.*, "Five-Year Followup Results of a Prospective, Multicenter Study of Patients with Overactive Bladder Treated with Sacral Neuromodulation," *J. Urol.*, vol. 199, no. 1, pp. 229–236, Jan. 2018, doi: 10.1016/j.juro.2017.07.010.
[40] E. L. Graczyk, B. P. Delhaye, M. A. Schiefer, S. J. Bensmaia, and D. J. Tyler, "Sensory adaptation to electrical stimulation of the somatosensory nerves," *J. Neural Eng.*, 2018, doi: 10.1088/1741-2552/aab790.
[41] P. Cariga, M. Catley, C. J. Mathias, and P. H. Ellaway, "Characteristics of habituation of the sympathetic skin response to repeated electrical stimuli in man," *Clin. Neurophysiol.*, vol. 112, no. 10, pp. 1875–1880, 2001, doi: 10.1016/S1388-2457(01)00647-2.
[42] L. M. Harrison, J. A. Norton, and J. A. Stephens, "Habituation of cutaneomuscular reflexes recorded from the first dorsal interosseous and triceps muscle in man," *J. Neurol. Sci.*, vol. 177, no. 1, pp. 32–40, 2000, doi: 10.1016/S0022-510X(00)00326-9.
[43] B. A. Potts *et al.*, "Timing of sacral neurostimulation is important for increasing bladder

capacity in the anesthetized rat," *Am. J. Physiol. Renal Physiol.*, vol. 317, no. 5, pp. F1183–F1188, Aug. 2019, doi: 10.1152/ajprenal.00167.2019.
[44] B. J. Wenzel, J. W. Boggs, K. J. Gustafson, and W. M. Grill, "Closed loop electrical control of urinary continence.," *J. Urol.*, vol. 175, no. 4, pp. 1559–1563, 2006, doi: 10.1016/S0022-5347(05)00657-9.
[45] A. Mendez and M. Sawan, "Chronic monitoring of bladder volume: A critical review and assessment of measurement methods," *Canadian Journal of Urology*. 2011.
[46] K. F. Hunter, A. Bharmal, and K. N. Moore, "Long-term bladder drainage: Suprapubic catheter versus other methods: A scoping review," *Neurourol. Urodyn.*, vol. 32, no. 7, pp. 944–951, Sep. 2013, doi: 10.1002/nau.22356.
[47] E. E. Horvath, P. B. Yoo, C. L. Amundsen, G. D. Webster, and W. M. Grill, "Conditional and continuous electrical stimulation increase cystometric capacity in persons with spinal cord injury," *Neurourol. Urodyn.*, vol. 29, no. 3, pp. 401–407, 2010, doi: 10.1002/nau.20766.
[48] E. Opisso, A. Borau, and N. J. M. Rijkhoff, "Urethral sphincter EMG-controlled dorsal penile/clitoral nerve stimulation to treat neurogenic detrusor overactivity," *J. Neural Eng.*, 2011, doi: 10.1088/1741-2560/8/3/036001.
[49] J. Wright, V. G. Macefield, A. van Schaik, and J. C. Tapson, "A review of control strategies in closed-loop neuroprosthetic systems," *Frontiers in Neuroscience*, vol. 10, no. JUL. Frontiers Media S.A., 2016, doi: 10.3389/fnins.2016.00312.
[50] K. M. PETERS, K. A. KILLINGER, C. JAEGER, and C. CHEN, "Pilot Study Exploring Chronic Pudendal Neuromodulation as a Treatment Option for Pain Associated with Pudendal Neuralgia," *LUTS Low. Urin. Tract Symptoms*, vol. 7, no. 3, pp. 138–142, Sep. 2015, doi: 10.1111/luts.12066.
[51] S. Jezernik, W. M. Grill, and T. Sinkjaer, "Detection and inhibition of hyperreflexia-like bladder contractions in the cat by sacral nerve root recording and electrical stimulation," *Neurourol. Urodyn.*, vol. 20, no. 2, pp. 215–230, Jan. 2001, doi: 10.1002/1520-6777(2001)20:2<215::AID-NAU23>3.0.CO;2-0.
[52] T. M. Bruns, D. J. Weber, and R. A. Gaunt, "Microstimulation of afferents in the sacral dorsal root ganglia can evoke reflex bladder activity," *Neurourol. Urodyn.*, vol. 34, no. 1, pp. 65–71, 2015, doi: 10.1002/nau.22514.
[53] T. M. Bruns, R. A. Gaunt, and D. J. Weber, "Estimating bladder pressure from sacral dorsal root ganglia recordings," in *Proceedings of the Annual International Conference of the IEEE Engineering in Medicine and Biology Society*, Aug. 2011, vol. 2011, pp. 4239–4242, doi: 10.1109/IEMBS.2011.6091052.
[54] T. M. Bruns *et al.*, "Real-time control of hind limb functional electrical stimulation using feedback from dorsal root ganglia recordings," *J. Neural Eng.*, vol. 10, no. 2, p. 026020, Mar. 2013, doi: 10.1088/1741-2560/10/2/026020.
[55] T. P. Zanos *et al.*, "Identification of cytokine-specific sensory neural signals by decoding murine vagus nerve activity," *Proc. Natl. Acad. Sci. U. S. A.*, vol. 115, no. 21, pp. E4843–E4852, May 2018, doi: 10.1073/pnas.1719083115.
[56] J. Rigosa, D. J. Weber, A. Prochazka, R. B. Stein, and S. Micera, "Neuro-fuzzy decoding of sensory information from ensembles of simultaneously recorded dorsal root ganglion neurons for functional electrical stimulation applications," in *Journal of Neural Engineering*, 2011, vol. 8, no. 4, p. 046019, doi: 10.1088/1741-2560/8/4/046019.
[57] K. S. Hong, N. Aziz, and U. Ghafoor, "Motor-commands decoding using peripheral nerve

signals: A review," *Journal of Neural Engineering*. 2018, doi: 10.1088/1741-2552/aab383.
[58] B. P. Christie *et al.*, "Comparison of spike sorting and thresholding of voltage waveforms for intracortical brain-machine interface performance," *J. Neural Eng.*, vol. 12, no. 1, p. 016009, 2015, doi: 10.1088/1741-2560/12/1/016009.
[59] S. R. Nason *et al.*, "A low-power band of neuronal spiking activity dominated by local single units improves the performance of brain–machine interfaces," *Nat. Biomed. Eng.*, 2020, doi: 10.1038/s41551-020-0591-0.
[60] C. Lubba, Z. Ouyang, N. Jones, T. Bruns, and S. Schultz, "Bladder pressure encoding by near-independent fibre subpopulations — implications for decoding," *bioRxiv*, p. 826297, Oct. 2019, doi: 10.1101/826297.
[61] J. P. Cunningham, V. Gilja, S. I. Ryu, and K. V. Shenoy, "Methods for estimating neural firing rates, and their application to brain-machine interfaces," *Neural Networks*, vol. 22, no. 9, pp. 1235–1246, Nov. 2009, doi: 10.1016/j.neunet.2009.02.004.
[62] D. L. Winter, "Receptor characteristics and conduction velocities in bladder afferents," *J. Psychiatr. Res.*, vol. 8, no. 3–4, pp. 225–235, Aug. 1971, doi: 10.1016/0022-3956(71)90021-5.
[63] S. E. Ross, Z. J. Sperry, C. M. Mahar, and T. M. Bruns, "Hysteretic behavior of bladder afferent neurons in response to changes in bladder pressure," *BMC Neurosci.*, vol. 17, no. 1, p. 57, Dec. 2016, doi: 10.1186/s12868-016-0292-5.
[64] W. Wu, Y. Gao, E. Bienenstock, J. P. Donoghue, and M. J. Black, "Bayesian population decoding of motor cortical activity using a Kalman filter," *Neural Comput.*, vol. 18, no. 1, pp. 80–118, 2006, doi: 10.1162/089976606774841585.
[65] C. H. Fry *et al.*, "Animal models and their use in understanding lower urinary tract dysfunction," *Neurourol. Urodyn.*, vol. 29, no. 4, pp. 603–608, Apr. 2010, doi: 10.1002/nau.20903.
[66] V. W. Nitti, "The prevalence of urinary incontinence.," *Rev. Urol.*, vol. 3 Suppl 1, pp. S2-6, 2001, Accessed: Sep. 15, 2019. [Online]. Available: http://www.ncbi.nlm.nih.gov/pubmed/16985992.
[67] S. J. A. Majerus, P. C. Fletter, E. K. Ferry, H. Zhu, K. J. Gustafson, and M. S. Damaser, "Suburothelial bladder contraction detection with implanted pressure sensor," *PLoS One*, vol. 12, no. 1, p. e0168375, 2017, doi: 10.1371/journal.pone.0168375.
[68] J. Melgaard and N. J. M. Rijkhoff, "Detecting Urinary Bladder Contractions: Methods and Devices," *J. Sens. Technol.*, vol. 04, no. 04, pp. 165–176, 2014, doi: 10.4236/jst.2014.44016.
[69] R. Karam *et al.*, "Real-time classification of bladder events for effective diagnosis and treatment of urinary incontinence," *IEEE Trans. Biomed. Eng.*, vol. 63, no. 4, pp. 721–729, 2016, doi: 10.1109/TBME.2015.2469604.
[70] Y. T. Lin *et al.*, "Dual-Channel neuromodulation of pudendal nerve with closed-loop control strategy to improve bladder functions," *J. Med. Biol. Eng.*, vol. 34, no. 1, pp. 82–89, 2014, doi: 10.5405/jmbe.1247.
[71] D. J. Chew *et al.*, "A microchannel neuroprosthesis for bladder control after spinal cord injury in rat," *Sci. Transl. Med.*, vol. 5, no. 210, p. 210ra155, Nov. 2013, doi: 10.1126/scitranslmed.3007186.
[72] R. Tibshirani, "Regression Shrinkage and Selection Via the Lasso," *J. R. Stat. Soc. Ser. B*, vol. 58, no. 1, pp. 267–288, 1996, doi: 10.1111/j.2517-6161.1996.tb02080.x.

[73] A. Mendez, M. Sawan, T. Minagawa, and J. J. Wyndaele, “Estimation of bladder volume from afferent neural activity,” *IEEE Trans. Neural Syst. Rehabil. Eng.*, vol. 21, no. 5, pp. 704–715, Sep. 2013, doi: 10.1109/TNSRE.2013.2266899.

[74] T. M. Bruns, R. A. Gaunt, and D. J. Weber, “Multielectrode array recordings of bladder and perineal primary afferent activity from the sacral dorsal root ganglia,” *J. Neural Eng.*, vol. 8, no. 5, p. 056010, Aug. 2011, doi: 10.1088/1741-2560/8/5/056010.

[75] A. Khurram *et al.*, “Chronic monitoring of lower urinary tract activity via a sacral dorsal root ganglia interface,” *J. Neural Eng.*, vol. 14, no. 3, p. 036027, Jun. 2017, doi: 10.1088/1741-2552/aa6801.

[76] M. Rizk and P. D. Wolf, “Optimizing the automatic selection of spike detection thresholds using a multiple of the noise level,” *Med. Biol. Eng. Comput.*, vol. 47, no. 9, pp. 955–966, Sep. 2009, doi: 10.1007/s11517-009-0451-2.

[77] D. J. Weber, R. B. Stein, D. G. Everaert, and A. Prochazka, “Limb-state feedback from ensembles of simultaneously recorded dorsal root ganglion neurons,” in *Journal of Neural Engineering*, 2007, vol. 4, no. 3, pp. S168–S180, doi: 10.1088/1741-2560/4/3/S04.

[78] J. C. Kao, P. Nuyujukian, S. Stavisky, S. I. Ryu, S. Ganguli, and K. V Shenoy, “Investigating the role of firing-rate normalization and dimensionality reduction in brain-machine interface robustness,” in *Proceedings of the Annual International Conference of the IEEE Engineering in Medicine and Biology Society, EMBS*, 2013, pp. 293–298, doi: 10.1109/EMBC.2013.6609495.

[79] A. Geramipour, S. Makki, and A. Erfanian, “Neural network based forward prediction of bladder pressure using pudendal nerve electrical activity,” in *Proceedings of the Annual International Conference of the IEEE Engineering in Medicine and Biology Society*, Aug. 2015, vol. 2015, pp. 4745–4748, doi: 10.1109/EMBC.2015.7319454.

[80] S. Perel *et al.*, “Single-unit activity, threshold crossings, and local field potentials in motor cortex differentially encode reach kinematics,” *J. Neurophysiol.*, vol. 114, no. 3, pp. 1500–1512, Sep. 2015, doi: 10.1152/jn.00293.2014.

[81] J. H. Park *et al.*, “Detecting bladder fullness through the ensemble activity patterns of the spinal cord unit population in a somatovisceral convergence environment,” *J. Neural Eng.*, vol. 10, no. 5, pp. 56009–7, Oct. 2013, doi: 10.1088/1741-2560/10/5/056009.

[82] W. Wu, a Shaikhouni, J. P. Donoghue, and M. J. Black, “Closed-loop neural control of cursor motion using a Kalman filter.,” *Conf. Proc. IEEE Eng. Med. Biol. Soc.*, vol. 6, pp. 4126–9, 2004, doi: 10.1109/IEMBS.2004.1404151.

[83] D. C. Baptiste, M. Elkelini, M. Hassouna, and M. G. Fehlings, “The dysfunctional bladder following spinal cord injury: From concept to clinic,” *Curr. Bladder Dysfunct. Rep.*, 2009, doi: 10.1007/s11884-009-0028-9.

[84] W. C. de Groat and N. Yoshimura, “Plasticity in reflex pathways to the lower urinary tract following spinal cord injury,” *Experimental Neurology*. 2012, doi: 10.1016/j.expneurol.2011.05.003.

[85] W. C. De Groat and N. Yoshimura, “Changes in afferent activity after spinal cord injury,” *Neurourology and Urodynamics*. 2010, doi: 10.1002/nau.20761.

[86] N. Yoshimura, “Bladder afferent pathway and spinal cord injury: Possible mechanisms inducing hyperreflexia of the urinary bladder,” *Progress in Neurobiology*. 1999, doi: 10.1016/S0301-0082(98)00070-7.

[87] A. J. Wein and E. S. Rovner, “Definition and epidemiology of overactive bladder.,” *Urology*, vol. 60, no. 5 Suppl 1, pp. 7–12, Nov. 2002, Accessed: Apr. 09, 2019. [Online].

Available: http://www.ncbi.nlm.nih.gov/pubmed/12493342.
[88] J. M. Latini and A. Giannantoni, “Pharmacotherapy of overactive bladder: epidemiology and pathophysiology of overactive bladder.,” *Expert Opin. Pharmacother.*, vol. 12, no. 7, pp. 1017–1027, 2011, doi: 10.1517/14656566.2011.554396.
[89] C. Lubba, E. Mitrani, J. Hokanson, W. M. Grill, and S. R. Schultz, “Real-time decoding of bladder pressure from pelvic nerve activity,” in *International IEEE/EMBS Conference on Neural Engineering, NER*, 2017, pp. 617–620, doi: 10.1109/NER.2017.8008427.
[90] C. Im *et al.*, “Decoding intravesical pressure from local field potentials in rat lumbosacral spinal cord,” *J. Neural Eng.*, vol. 13, no. 5, p. 056005, Oct. 2016, doi: 10.1088/1741-2560/13/5/056005.
[91] S. E. Ross, Z. Ouyang, S. Rajagopalan, and T. M. Bruns, “Evaluation of Decoding Algorithms for Estimating Bladder Pressure from Dorsal Root Ganglia Neural Recordings,” *Ann. Biomed. Eng.*, vol. 46, no. 2, pp. 233–246, Nov. 2018, doi: 10.1007/s10439-017-1966-6.
[92] S. Jezernik, J. G. Wen, N. J. M. Rijkhoff, J. C. Djurhuus, and T. Sinkjær, “Analysis of bladder related nerve cuff electrode recordings from preganglionic pelvic nerve and sacral roots in pigs,” *J. Urol.*, vol. 163, no. 4, pp. 1309–1314, 2000, doi: 10.1016/S0022-5347(05)67769-5.
[93] Z. Wang, L. Liao, H. Deng, X. Li, and G. Chen, “The inhibitory effect of sacral dorsal root ganglion stimulation on nociceptive and nonnociceptive bladder reflexes in cats,” *World Journal of Urology*, vol. 36, no. 5, pp. 829–836, May 27, 2018.
[94] M. Choudhary, E. van Asselt, R. van Mastrigt, and F. Clavica, “Neurophysiological modeling of bladder afferent activity in the rat overactive bladder model,” *J. Physiol. Sci.*, vol. 65, no. 4, pp. 329–338, 2015, doi: 10.1007/s12576-015-0370-y.
[95] J. W. Downie, J. A. Champion, and D. M. Nance, “A quantitative analysis of the afferent and extrinsic efferent innervation of specific regions of the bladder and urethra in the cat,” *Brain Res. Bull.*, vol. 12, no. 6, pp. 735–740, 1984, doi: 10.1016/0361-9230(84)90154-0.
[96] F. A. Kullmann, G. I. Wells, C. L. Langdale, J. Zheng, and K. B. Thor, “Stability of the Acetic Acid-Induced Bladder Irritation Model in Alpha Chloralose-Anesthetized Female Cats,” *PLoS One*, vol. 8, no. 9, p. e73771, 2013, doi: 10.1371/journal.pone.0073771.
[97] A. E. Snellings and W. M. Grill, “Effects of stimulation site and stimulation parameters on bladder inhibition by electrical nerve stimulation,” *BJU Int.*, vol. 110, no. 1, pp. 136–143, Jan. 2012, doi: 10.1111/j.1464-410X.2011.10789.x.
[98] B. J. B. J. Wenzel, J. W. J. W. J. W. Boggs, K. J. K. J. Gustafson, and W. M. W. M. W. M. Grill, “Detecting the onset of hyper-reflexive bladder contractions from the electrical activity of the pudendal nerve,” *IEEE Trans. Neural Syst. Rehabil. Eng.*, vol. 13, no. 3, pp. 428–435, Sep. 2005, doi: 10.1109/TNSRE.2005.848355.
[99] Z. J. Sperry *et al.*, “Flexible microelectrode array for interfacing with the surface of neural ganglia,” *J. Neural Eng.*, vol. 15, no. 3, p. 036027, 2018, doi: 10.1088/1741-2552/aab55f.
[100] L. Liem *et al.*, “One-Year Outcomes of Spinal Cord Stimulation of the Dorsal Root Ganglion in the Treatment of Chronic Neuropathic Pain,” *Neuromodulation Technol. Neural Interface*, vol. 18, no. 1, pp. 41–49, Jan. 2015, doi: 10.1111/ner.12228.
[101] A. K. Ostrowski, Z. J. Sperry, G. Kulik, and T. M. Bruns, “Quantitative models of feline lumbosacral dorsal root ganglia neuronal cell density,” *J. Neurosci. Methods*, vol. 290, pp. 116–124, 2017, doi: 10.1016/j.jneumeth.2017.07.018.
[102] J. A. Hokanson, C. L. Langdale, A. Sridhar, and W. M. Grill, “OAB without an overactive

bladder in the acute prostaglandin E2 rat model," *Am. J. Physiol. - Ren. Physiol.*, vol. 313, no. 5, pp. F1169–F1177, Nov. 2017, doi: 10.1152/ajprenal.00270.2017.
[103] J. D. Redshaw *et al.*, "Protocol for a randomized clinical trial investigating early sacral nerve stimulation as an adjunct to standard neurogenic bladder management following acute spinal cord injury," *BMC Urol.*, vol. 18, no. 1, p. 72, Dec. 2018, doi: 10.1186/s12894-018-0383-y.
[104] C. W. Lo, M. Y. Wu, S. S. D. Yang, F. S. Jaw, and S. J. Chang, "Comparing the efficacy of onabotulinumtoxinA, sacral neuromodulation, and peripheral tibial nerve stimulation as third line treatment for the management of overactive bladder symptoms in adults: Systematic review and network meta-analysis," *Toxins*, vol. 12, no. 2. MDPI AG, p. 128, 2020, doi: 10.3390/toxins12020128.
[105] Z. Ouyang, Z. J. Sperry, N. D. Barrera, and T. M. Bruns, "Real-Time Bladder Pressure Estimation for Closed-Loop Control in a Detrusor Overactivity Model," *IEEE Trans. Neural Syst. Rehabil. Eng.*, vol. 27, no. 6, pp. 1209–1216, 2019, doi: 10.1109/TNSRE.2019.2912374.
[106] N. C. Swann *et al.*, "Adaptive deep brain stimulation for Parkinson's disease using motor cortex sensing," *J. Neural Eng.*, 2018, doi: 10.1088/1741-2552/aabc9b.
[107] B. Blok *et al.*, "Three month clinical results with a rechargeable sacral neuromodulation system for the treatment of overactive bladder," *Neurourol. Urodyn.*, vol. 37, pp. S9–S16, 2018, doi: 10.1002/nau.23465.
[108] A. Zhou *et al.*, "A wireless and artefact-free 128-channel neuromodulation device for closed-loop stimulation and recording in non-human primates," *Nat. Biomed. Eng.*, 2019, doi: 10.1038/s41551-018-0323-x.
[109] S. Luan *et al.*, "Compact standalone platform for neural recording with real-time spike sorting and data logging," *J. Neural Eng.*, 2018, doi: 10.1088/1741-2552/aabc23.
[110] F. Zhang *et al.*, "Neural pathways involved in sacral Neuromodulation of reflex bladder activity in cats," *Am. J. Physiol. - Ren. Physiol.*, vol. 304, no. 6, pp. F710–F717, 2013, doi: 10.1152/ajprenal.00334.2012.
[111] A. Goebel, S. Lewis, R. Phillip, and M. Sharma, "Dorsal Root Ganglion Stimulation for Complex Regional Pain Syndrome (CRPS) Recurrence after Amputation for CRPS, and Failure of Conventional Spinal Cord Stimulation," *Pain Pract.*, vol. 18, no. 1, pp. 104–108, Jan. 2018, doi: 10.1111/papr.12582.
[112] Z. A. Ouyang *et al.*, "Behavioral Monitoring and Neuromodulation of Feline Voiding Function," in *International IEEE/EMBS Conference on Neural Engineering, NER*, 2019, vol. 2019-March, pp. 1058–1061, doi: 10.1109/NER.2019.8717187.
[113] D. Markle Price and K. Noblett, "Prospective Randomized Crossover Trial Comparing Continuous and Cyclic Stimulation in InterStim Therapy," *Female Pelvic Med. Reconstr. Surg.*, vol. 21, no. 6, pp. 355–358, Nov. 2015, doi: 10.1097/SPV.0000000000000188.
[114] T. S. Brink, P. L. Zimmerman, M. A. Mattson, X. Su, and D. E. Nelson, "A chronic, conscious large animal platform to quantify therapeutic effects of sacral neuromodulation on bladder function," *J. Urol.*, vol. 194, no. 1, pp. 252–258, 2015, doi: 10.1016/j.juro.2015.01.109.
[115] W. W. Leng and M. B. Chancellor, "How sacral nerve stimulation neuromodulation works," *Urol. Clin. North Am.*, vol. 32, no. 1, pp. 11–18, Feb. 2005, doi: 10.1016/j.ucl.2004.09.004.
[116] Z. J. Sperry, R. D. Graham, N. Peck-Dimit, S. F. Lempka, and T. M. Bruns, "Spatial

models of cell distribution in human lumbar dorsal root ganglia," *J. Comp. Neurol.*, p. cne.24848, Jan. 2020, doi: 10.1002/cne.24848.
[117] A. Khurram *et al.*, "Chronic monitoring of lower urinary tract activity via a sacral dorsal root ganglia interface," *J. Neural Eng.*, vol. 14, no. 3, p. 036027, Jun. 2017, doi: 10.1088/1741-2552/aa6801.
[118] T. M. Bruns, N. Bhadra, and K. J. Gustafson, "Variable patterned pudendal nerve stimuli improves reflex bladder activation," *IEEE Trans. Neural Syst. Rehabil. Eng.*, vol. 16, no. 2, pp. 140–8, 2008.
[119] H. A. C. Wark, S. R. Black, K. S. Mathews, P. C. Cartwright, K. J. Gustafson, and R. A. Normann, "Restoration From Acute Urinary Dysfunction Using Utah Electrode Arrays Implanted Into the Feline Pudendal Nerve.," *Neuromodulation*, vol. 18, no. 4, pp. 317–323, Nov. 2015, doi: 10.1111/ner.12259.
[120] Z. Xiao *et al.*, "Somatic Modulation of Spinal Reflex Bladder Activity Mediated by Nociceptive Bladder Afferent Nerve Fibers in Cats.," *Am. J. Physiol. Renal Physiol.*, vol. 307, pp. F673–F679, 2014, doi: 10.1152/ajprenal.00308.2014.
[121] S. Matsuura and J. W. Downie, "Effect of anesthetics on reflex micturition in the chronic cannula-implanted rat," *Neurourol. Urodyn.*, vol. 19, no. 1, pp. 87–99, Jan. 2000.
[122] T. W. Cannon and M. S. Damaser, "Effects of anesthesia on cystometry and leak point pressure of the female rat," *Life Sci.*, vol. 69, no. 10, pp. 1193–1202, 2001, doi: 10.1016/S0024-3205(01)01182-1.
[123] C. Ozkurkcugil and L. Ozkan, "Effects of anesthetics on cystometric parameters in female rats," *Int. Urol. Nephrol.*, vol. 42, no. 4, pp. 909–913, 2010, doi: 10.1007/s11255-010-9745-4.
[124] J. Wang *et al.*, "Bladder inhibition or excitation by electrical perianal stimulation in a cat model of chronic spinal cord injury," *BJU Int.*, vol. 103, no. 4, pp. 530–536, 2009, doi: 10.1111/j.1464-410X.2008.08029.x.
[125] C. Tai, B. Shen, J. Wang, M. B. Chancellor, J. R. Roppolo, and W. C. De Groat, "Inhibitory and excitatory perigenital-to-bladder spinal reflexes in the cat," *Am. J. Physiol. - Ren. Physiol.*, vol. 294, no. 3, 2008, doi: 10.1152/ajprenal.00443.2007.
[126] T.-H. H. Hsieh, Y.-T. T. Lin, S.-C. C. Chen, and C.-W. W. Peng, "Chronic pudendal neuromodulation using an implantable microstimulator improves voiding function in diabetic rats," *J. Neural Eng.*, vol. 13, no. 4, p. 046001, 2016, doi: 10.1088/1741-2560/13/4/046001.
[127] C. V. Comiter, "Conscious neuromodulation of the bladder before clinical use," *J. Urol.*, vol. 194, no. 1, pp. 16–17, 2015, doi: 10.1016/j.juro.2015.04.015.
[128] B. B. Klevmark, "Volume Threshold for Micturition. Influence of Filling Rate on Sensory and Motor Bladder Function," *Scand. J. Urol. Nephrol.*, vol. 36, no. 4, pp. 6–10, Jan. 2002, doi: 10.1080/003655902320765890.
[129] P. P. Vu *et al.*, "A regenerative peripheral nerve interface allows real-time control of an artificial hand in upper limb amputees," *Sci. Transl. Med.*, vol. 12, no. 533, Mar. 2020, doi: 10.1126/scitranslmed.aay2857.
[130] M. Jabbari and A. Erfanian, "Estimation of Bladder Pressure and Volume from the Neural Activity of Lumbosacral Dorsal Horn Using a Long-Short-Term-Memory-based Deep Neural Network," *Sci. Rep.*, vol. 9, no. 1, pp. 1–15, Dec. 2019, doi: 10.1038/s41598-019-54144-8.
[131] A. P. S. S. Kirkham, N. C. Shah, S. L. Knight, P. J. R. R. Shah, and M. D. Craggs, "The

acute effects of continuous and conditional neuromodulation on the bladder in spinal cord injury," *Spinal Cord*, vol. 39, no. 8, pp. 420–428, Aug. 2001, doi: 10.1038/sj.sc.3101177.
[132] A. L. Dalmose, N. J. M. Rijkhoff, H. J. Kirkeby, M. Nohr, T. Sinkjaer, and J. C. Djurhuus, "Conditional stimulatzion of the dorsal penile/clitoral nerve may increase cystometric capacity in patients with spinal cord injury," *Neurourol. Urodyn.*, vol. 22, no. 2, pp. 130–137, 2003, doi: 10.1002/nau.10031.
[133] Z. Ouyang *et al.*, "Closed-loop sacral neuromodulation for bladder function using dorsal root ganglia sensory feedback in an acute feline model," *bioRxiv*. Cold Spring Harbor Laboratory, p. 2020.05.02.074484, May 03, 2020, doi: 10.1101/2020.05.02.074484.
[134] D. J. A. J. Oerlemans, A. C. van Voskuilen, T. Marcelissen, E. H. J. Weil, R. A. de Bie, and P. E. V. Van Kerrebroeck, "Is on-demand sacral neuromodulation in patients with OAB syndrome a feasible therapy regime?," *Neurourol. Urodyn.*, vol. 30, no. 8, pp. 1493–1496, Nov. 2011, doi: 10.1002/nau.21070.
[135] J. Bandari *et al.*, "Neurotransmitter Mechanisms Underlying Sacral Neuromodulation of Bladder Overactivity in Cats," *Neuromodulation*, vol. 20, no. 1, pp. 81–87, Jan. 2017, doi: 10.1111/ner.12534.
[136] Z. Sperry *et al.*, "High-density Neural Recordings from Feline Sacral Dorsal Root Ganglia with Thin-film Array," *bioRxiv*, p. 2020.07.14.199653, Sep. 2020, doi: 10.1101/2020.07.14.199653.
[137] A. A. Jiman *et al.*, "Multi-channel intraneural vagus nerve recordings with a novel high-density carbon fiber microelectrode array," *Sci. Rep.*, vol. 10, no. 1, pp. 1–13, Dec. 2020, doi: 10.1038/s41598-020-72512-7.
[138] E. C. Bottorff *et al.*, "Acute intraganglia recordings of single-unit neural activity with a novel microelectrode array," *Society for Neuroscience Annual Meeting*, Oct. 22, 2019. https://www.abstractsonline.com/pp8/#!/7883/presentation/59071 (accessed Oct. 14, 2020).
[139] "St George Urology | Interstim Device – Sacral Neuromodulation." https://www.stgeorgeurology.com.au/sacral-neuromodulation (accessed May 05, 2020).